

UNIVERSITY OF KWAZULU-NATAL (HOWARD COLLEGE)

MASTERS THESIS

A Fluorescent Image Segmentation Model Based on Improved Discrete Active Contours

Author:
Ryan NAIDOO

Supervisor:
Dr. Jules-Raymond TAPAMO

*A thesis submitted in fulfillment of the requirements
for the degree of Master of Science in Engineering
in the*

Department of Electrical, Electronic and Computer Engineering
School of Engineering

November 7, 2016

Declaration of Authorship

I, Ryan NAIDOO, declare that this thesis titled, "A Fluorescent Image Segmentation Model Based on Improved Discrete Active Contours" and the work presented in it are my own. I confirm that:

- This work was done wholly or mainly while in candidature for a research degree at this University.
- Where any part of this thesis has previously been submitted for a degree or any other qualification at this University or any other institution, this has been clearly stated.
- Where I have consulted the published work of others, this is always clearly attributed.
- Where I have quoted from the work of others, the source is always given. With the exception of such quotations, this thesis is entirely my own work.
- I have acknowledged all main sources of help.
- Where the thesis is based on work done by myself jointly with others, I have made clear exactly what was done by others and what I have contributed myself.

Signed:

Date:

“Thanks to my solid academic training, today I can write hundreds of words on virtually any topic without possessing a shred of information, which is how I got a good job in journalism.”

Dave Barry

UNIVERSITY OF KWAZULU-NATAL (HOWARD COLLEGE)

Abstract

Faculty of Engineering
School of Engineering

Master of Science in Engineering

A Fluorescent Image Segmentation Model Based on Improved Discrete Active Contours

by Ryan NAIDOO

The Thesis Abstract is written here (and usually kept to just this page). The page is kept centered vertically so can expand into the blank space above the title too...

Acknowledgements

The acknowledgments and the people to thank go here, don't forget to include your project advisor...

Contents

Declaration of Authorship	iii
Abstract	vii
Acknowledgements	ix
List of Figures	xiii
List of Tables	xv
List of Abbreviations	xix
1 Parameter Estimation for ACWE Chan-Vese Segmentation	1
1.1 Graph Cut Model for Chan-Vese Segmentation	1
1.2 Modified Weighting and Parameter Estimation	4
1.2.1 Graph Weighting	5
1.2.2 Analysis of Weighting System and Parameter Relationships	5
1.2.3 Tuning Parameters for Fluorescence Microscopy	10
1.3 Experimental Results	26
1.4 Discussion	60
A Cell Images Dataset	63
A.1 Sample Set	63
A.2 Test Set	64
Bibliography	69

List of Figures

1.1	(a) Cauchy-Crofton length approximation. (b) 8-connected neighbourhood system.	3
1.2	CAPTION MISSING HERE.	4
1.3	CAPTION MISSING HERE.	5
1.4	Fully connected single node.	6
1.5	Data energy functions plot.	8
1.6	Relationship between α and p_e .	8
1.7	Image 1 from sample set Figure A.1 initial masks.	12
1.8	Segmented output for various combination of α and λ_1 for Image 1 in the sample set.	12
1.9	Image 2 from sample set Figure A.1 initial masks.	13
1.10	Segmented output for various combination of α and λ_1 for Image 2 in the sample set.	13
1.11	Image 3 from sample set Figure A.1 initial masks.	14
1.12	Segmented output for various combination of α and λ_1 for Image 3 in the sample set.	14
1.13	Image 4 from sample set Figure A.1 initial masks.	15
1.14	Segmented output for various combination of α and λ_1 for Image 4 in the sample set.	15
1.15	Image 5 from sample set Figure A.1 initial masks.	16
1.16	Segmented output for various combination of α and λ_1 for Image 5 in the sample set.	16
1.17	Image 6 from sample set Figure A.1 initial masks.	17
1.18	Segmented output for various combination of α and λ_1 for Image 6 in the sample set.	17
1.19	p_e as a fraction of the distance between c_0 and c_1 .	18
1.20	h as a fraction of the distance between c_0 and c_1 .	19
1.21	Image 1 from test set Appendix A initial masks.	28
1.22	Image 1 from test set Appendix A segmentation results.	28
1.23	Image 2 from test set Appendix A initial masks.	29
1.24	Image 2 from test set Appendix A segmentation results.	29
1.25	Image 3 from test set Appendix A initial masks.	30
1.26	Image 3 from test set Appendix A segmentation results.	30
1.27	Image 4 from test set Appendix A initial masks.	31
1.28	Image 4 from test set Appendix A segmentation results.	31
1.29	Image 5 from test set Appendix A initial masks.	32
1.30	Image 5 from test set Appendix A segmentation results.	32
1.31	Image 6 from test set Appendix A initial masks.	33
1.32	Image 6 from test set Appendix A segmentation results.	33
1.33	Image 7 from test set Appendix A initial masks.	34

1.34	Image 7 from test set Appendix A segmentation results	34
1.35	Image 8 from test set Appendix A initial masks.	35
1.36	Image 8 from test set Appendix A segmentation results.	35
1.37	Image 9 from test set Appendix A initial masks.	36
1.38	Image 9 from test set Appendix A segmentation results.	36
1.39	Image 10 from test set Appendix A initial masks.	37
1.40	Image 10 from test set Appendix A segmentation results.	37
1.41	Image 11 from test set Appendix A initial masks.	38
1.42	Image 11 from test set Appendix A segmentation results.	38
1.43	Image 12 from test set Appendix A initial masks.	39
1.44	Image 12 from test set Appendix A segmentation results.	39
1.45	Image 13 from test set Appendix A initial masks.	40
1.46	Image 13 from test set Appendix A segmentation results.	40
1.47	Image 14 from test set Appendix A initial masks.	41
1.48	Image 14 from test set Appendix A segmentation results.	41
1.49	Image 15 from test set Appendix A initial masks.	42
1.50	Image 15 from test set Appendix A segmentation results.	42
1.51	Image 16 from test set Appendix A initial masks.	43
1.52	Image 16 from test set Appendix A segmentation results.	43
1.53	Image 17 from test set Appendix A initial masks.	44
1.54	Image 17 from test set Appendix A segmentation results.	44
1.55	Image 18 from test set Appendix A initial masks.	45
1.56	Image 18 from test set Appendix A segmentation results.	45
1.57	Image 19 from test set Appendix A initial masks.	46
1.58	Image 19 from test set Appendix A segmentation results.	46
1.59	Image 20 from test set Appendix A initial masks.	47
1.60	Image 20 from test set Appendix A segmentation results.	47
1.61	Image 21 from test set Appendix A initial masks.	48
1.62	Image 21 from test set Appendix A segmentation results.	48
1.63	Image 22 from test set Appendix A initial masks.	49
1.64	Image 22 from test set Appendix A segmentation results.	49
1.65	Image 23 from test set Appendix A initial masks.	50
1.66	Image 23 from test set Appendix A segmentation results.	50
1.67	Image 24 from test set Appendix A initial masks.	51
1.68	Image 24 from test set Appendix A segmentation results.	51
1.69	Image 25 from test set Appendix A initial masks.	52
1.70	Image 25 from test set Appendix A segmentation results.	52
1.71	Precision vs Recall over test set.	60
1.72	Accuracy over test set.	61
A.1	Sample set.	63
A.2	Uneven Illumination	64
A.3	High cell density	64
A.4	Multi-modal (non-bi-modal)	65
A.5	Hazy/Glowing Edges	66
A.6	Thin Tentacles	66
A.7	Bright Spots and Speckles	67

List of Tables

1.1	Initial means and standard deviations for all images in the sample set for Otsu, K-means and EMGMM clustering	18
1.2	Results from manual tuning	19
1.3	Average of final means for good segmentations	22
1.4	Dilation after Otsu binarization	22
1.5	Dilation after K-means clustering	23
1.6	Dilation after EM-GMM clustering	24
1.7	Parameter Settings and Segmentation Results	53
1.8	Segmentation Efficiency	56
1.9	Overall Segmentation Efficiency	60

List of Algorithms

List of Abbreviations

ACWE	Active Contours Without Edges
AOD	Average Optical Density
BCC	Boundary Chain Code
BFS	Breadth First Search
BP	Belief Propagation
CCD	Charge-Coupled Device
CED	Coherence Enhancing Diffusion
CLSM	Confocal Laser Scanning Microscopy
CRF	Conditional Random Field
DCC	Differential Chain Code
DFS	Depth First Search
DNA	Deoxyribonucleic Acid
DP	Dynamic Programming
DT	Delaunay Triangulation
EGFP	Enhanced Green Fluorescent Protein
EM	Expectation Maximisation
FCS	Fluorescence Correlation Spectroscopy
FIFO	First-In First-Out
FISH	Fluorescence in-situ Hybridisation
FLIM	Fluorescence Lifetime Imaging Microscopy
FRAP	Fluorescence Recovery After Photobleaching
FRET	Fluorescence Resonance Energy Transfer
GA	Genetic Algorithm
GCBLS	Graph Cut Based Level Set
GFP	Green Fluorescent Protein
GLCM	Gray Level Co-occurrence Matrix
GMM	Guassian Mixture Modelling
GRF	Gibbs Random Field
HLF	Highest Level First
ICC	Immunocytochemistry
ICF	Immunocytofluorescence
ICM	Iterated Conditional Modes
IHC	Immunohistochemistry
IHF	Immunohistofluorescence
IOD	Integrated Optical Density
Laser	Light Amplification by Stimulated Emission of Radiation
LBP	Loopy Belief Propagation
LED	Light Emitting Diode
LoG	Laplacian of Gaussian
MAP	Maximum A Posteriori
MCC	Matthews Correlation Coefficient

MIS	Medical Image Segmentation
MLP	Multi-Layered Perceptron
MRF	Markov Random Field
MST	Minimum Spanning Tree
NA	Numerical Aperture
ORI	Optimised Rotational Invariance
OTF	Optical Transfer Function
PSF	Point Spread Function
RF	Random Field
RNA	Ribonucleic Acid
SNR	Signal-to-Noise Ratio
TV	Total Variation
UV	Ultraviolet

For/Dedicated to/To my...

Chapter 1

Parameter Estimation for ACWE Chan-Vese Segmentation

[Introduction] What is special about the Chan-Vese formulation to the Mumford-Shah evolution energy function. Advantages, disadvantages (parameter estimation). Course of the chapter.

1.1 Graph Cut Model for Chan-Vese Segmentation

Chan-Vese formulation of the Mumford-Shah formulation. Length approximation using discrete representations (cut-metrics). Discrete representation of Chan-Vese formulation. Graph representation and sub-modularity constraint. Insensitivity to initialisation. What do the parameters mean and how do they influence the final result. In this section we briefly reintroduce the graph cut formulation for the Chan-Vese formulation of the Mumford-Shah evolution energy function for image segmentation. The Mumford-Shah model uses gradient descent techniques to obtain a minimum but as previously discussed, ??, they usually terminate at local minima. By reformulating the energy function in a discrete form that allows for appropriate graph representability, we can use graph cuts, which are able to terminate at a global minimum, to iteratively converge to the optimal solution. For an in-depth exposition into this technique, look to [124, 147, 175].

The level set representation of the Mumford-Shah energy function is

$$\begin{aligned} F(c_1, c_2, \phi) = & \mu \int_{\Omega} \delta(\phi(x, y)) |\nabla \phi(x, y)| dx dy \\ & + \nu \int_{\Omega} H(\phi(x, y)) dx dy \\ & + \lambda_1 \int_{\Omega} |u(x, y) - c_1|^2 H(\phi(x, y)) dx dy \\ & + \lambda_2 \int_{\Omega} |u(x, y) - c_2|^2 (1 - H(\phi(x, y))) dx dy, \end{aligned} \tag{1.1}$$

where $u(x, y)$ is the image, $H(\cdot)$ is the Heaviside step function, $\delta(\cdot)$ is the Dirac delta function, $\phi : \Omega \rightarrow \mathbb{R}$ is the level set function, such that:

$$\begin{aligned} \omega &= \{(x, y) \in \Omega | \Phi(x_p) > 0\} \text{ Inside the boundary} \\ \bar{\omega} &= \{(x, y) \in \Omega | \Phi(x_p) < 0\} \text{ Outside the boundary} \\ C &= \partial\omega = \{(x, y) \in \Omega | \Phi(x_p) = 0\} \text{ Along the boundary,} \end{aligned} \tag{1.2}$$

c_1 and c_2 are the arithmetic means given by:

$$c_1(\phi) = \frac{\int_{\Omega} u(x, y) H(\phi(x, y)) dx dy}{\int_{\Omega} H(\phi(x, y)) dx dy}, \quad (1.3)$$

$$c_2(\phi) = \frac{\int_{\Omega} u(x, y)(1 - H(\phi(x, y))) dx dy}{\int_{\Omega} (1 - H(\phi(x, y))) dx dy}. \quad (1.4)$$

The piecewise smooth approximation of the image is then

$$u(x, y) = c_1 H(\phi(x, y)) + c_2(1 - H(\phi(x, y))). \quad (1.5)$$

Discrete Approximation of Contour Length For the energy function to be represented as a graph, one of the requirements is that it must be in a discrete representation. This means that the length of the contour, the first term in Equation (1.1), must be approximated discretely and be graph representable. This work has already been done by Kolmogorov and Boykov in [176, 177] where they used the Cauchy-Crofton theorem. The theorem states that the length of a curve can be approximated by drawing a large number of straight lines from 0 to 2π and counting the number of intersections between the lines and the contour. The mathematical representation is

$$\int_L n_L dL = \int_0^\pi \int_{-\infty}^\infty n_L d\rho d\theta = 2\|C\|_E, \quad (1.6)$$

where n_L is the number of intersections between the contour C and the line L , $\|C\|_E$ is the Euclidean length of the contour, $0 < \rho < \infty$ and $0 < \theta < 2\pi$. From this the discrete approximation used by Boykov and Zabih is

$$\|C\|_E = \frac{1}{2} \sum_k n_k \frac{\delta^2 \Delta \theta_k}{|e_k|} = \frac{1}{2} \sum_k n_k w_k \quad (1.7)$$

An example of approximating the contour by two grids is illustrated in Figure 1.1(a) using four families of parallel lines which are 45° apart.

Discrete Representation of Mumford-Shah Function With the exception of the second term in Equation (1.1), the remaining terms are represented easily discretely. For each pixel $p \in \Omega$, let x_p be a binary variable such that

$$x_p = \begin{cases} 0 & \phi(p) \leq 0 \\ 1 & \phi(p) > 0 \end{cases} \quad (1.8)$$

The means can now be calculated using

$$c_1 = \frac{\sum_p u(x, y)x_p}{\sum_p x_p}, \quad (1.9)$$

$$c_2 = \frac{\sum_p u(x, y)(1 - x_p)}{\sum_p (1 - x_p)}. \quad (1.10)$$

For simplification, $\nu = 0$. To determine contour length using an 8-neighbourhood system, as illustrated in Figure 1.1(b), we set $\Delta\rho = 1$. The weight w_k is assigned to its corresponding edge e_k . The Euclidean length of the edges is $|e_1| = |e_3| = 1$ and $|e_2| = |e_4| = \sqrt{2}$, therefore

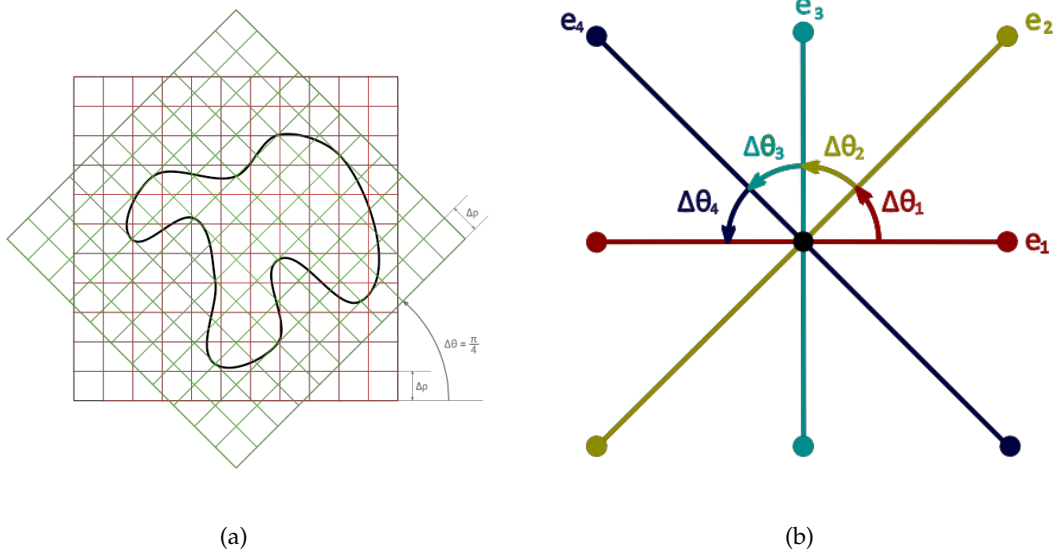


FIGURE 1.1: (a) Cauchy-Crofton length approximation. (b) 8-connected neighbourhood system.

the corresponding weights, which are determined using Equation (1.7), is $w_1 = w_3 = \frac{\pi}{8}$ and $w_2 = w_4 = \frac{\pi}{8\sqrt{2}}$. To calculate n_k we need to count the intersections between the lines and the contour. An intersection between two pixels p and q exists if and only if x_p and x_q have different labels.

$$n_k = x_p(1 - x_q) + x_q(1 - x_p); k = (pq) \in \mathcal{N}_p. \quad (1.11)$$

The contour length can now fully be expressed discretely as

$$\|C\|_E = \sum_{p,q \in e_k} w_k(x_p(1 - x_q) + x_q(1 - x_p)). \quad (1.12)$$

The discrete representation of Equation (1.1) is

$$\begin{aligned} F(x_1, \dots, x_n) &= \mu \sum_{p,q \in e_k} w_k(x_p(1 - x_q) + x_q(1 - x_p)) \\ &\quad + \lambda_1 \sum_p |u(x, y) - c_1|^2 x_p \\ &\quad + \lambda_2 \sum_p |u(x, y) - c_2|^2 (1 - x_p) \end{aligned} \quad (1.13)$$

Graph Representation The discrete energy function Equation (1.13) has been shown that it obey the submodularity constraint for graph representability. Therefore the data energy and regularisation energy is

$$E^p(x_p) = \lambda_1 |u(x, y) - c_1|^2 x_p + \lambda_2 |u(x, y) - c_2|^2 (1 - x_p) \quad (1.14)$$

$$E^{pq}(x_p, x_q) = (x_p + x_q - 2x_p x_q) w_{pq} \quad (1.15)$$

The graph for the energy function is constructed as in [151].

1.2 Modified Weighting and Parameter Estimation

What is wrong with the previously described graph weighting. What would we expect from a better weighting system. Problem images are multi-modal and extremely low contrast. In this section we introduce a novel idea to weighting a graph for image segmentation based on the Chan-Vese formulation of the Mumford-Shah evolution function. Previous parameter estimation schemes focused very specifically on a certain image and this resulted in hard-coded. In [175], where this method was first devised, they used the parameter settings $\mu = 0.1 \times 255^2$, $\lambda_1 = \lambda_2 = 1$. This worked very well on their synthetic images proving a strong resilience to noise and initial conditions. However, for fluorescence microscopy images, the results to be a bit too over-segmented for practical use. These parameters were used to segment the images in the sample set, Figure A.1, the segmentation result is shown in Figure 1.2.

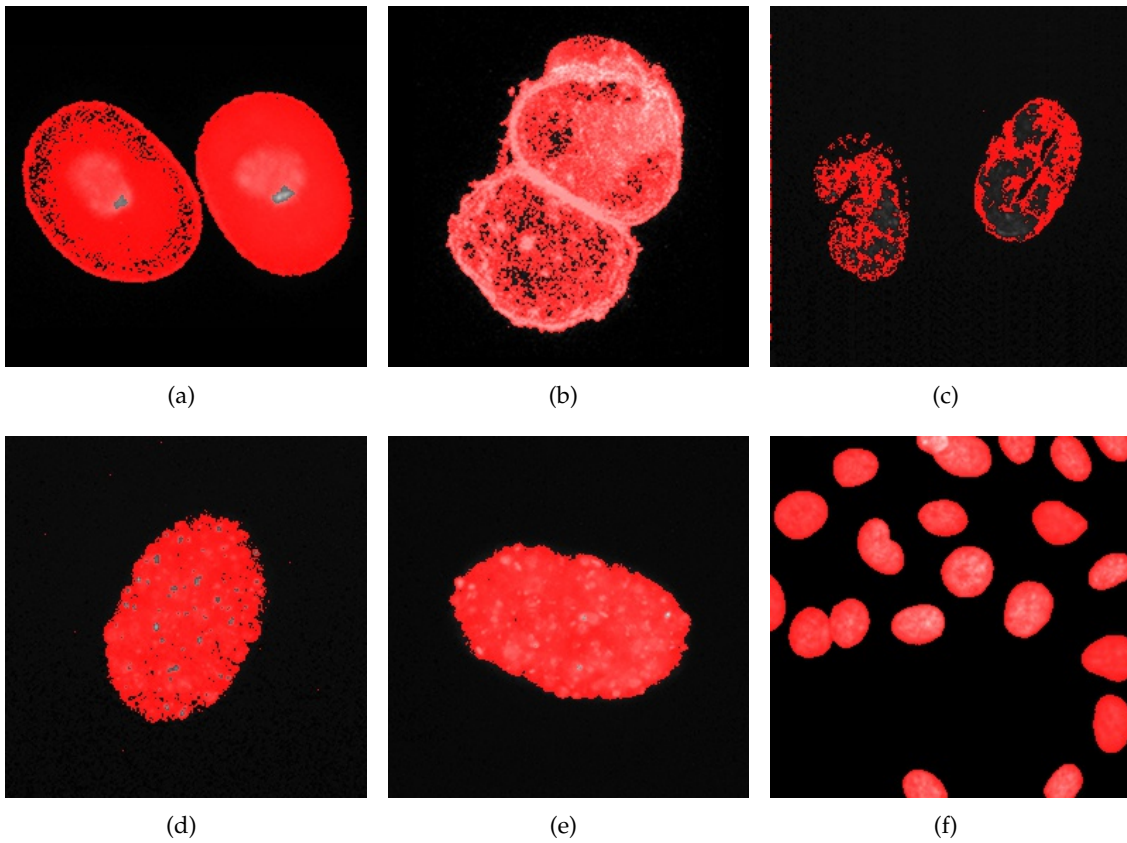


FIGURE 1.2: CAPTION MISSING HERE.

In [178], the authors proposed a segmentation and tracking scheme for whole fluorescent cells in a timelapse series. The result was another set of hard-coded parameters which were based on maximising the Jaccard coefficient of the automatically segmented cells in each frame of the timelapse series which was also manually segmented. The optimal parameter settings were $\mu = 0.01$, $\lambda_1 = 1$ and $\lambda_2 = 85$. These parameters were used on the sample set in Figure A.1 and the results proved to be less useful as shown in Figure 1.3. It can be deduced that the parameters were specifically tuned to the image type that was studied.

It can be seen that hard-coded parameter values do not produce very consistent results over a large range of image types as that found in fluorescence microscopy imaging. In the next

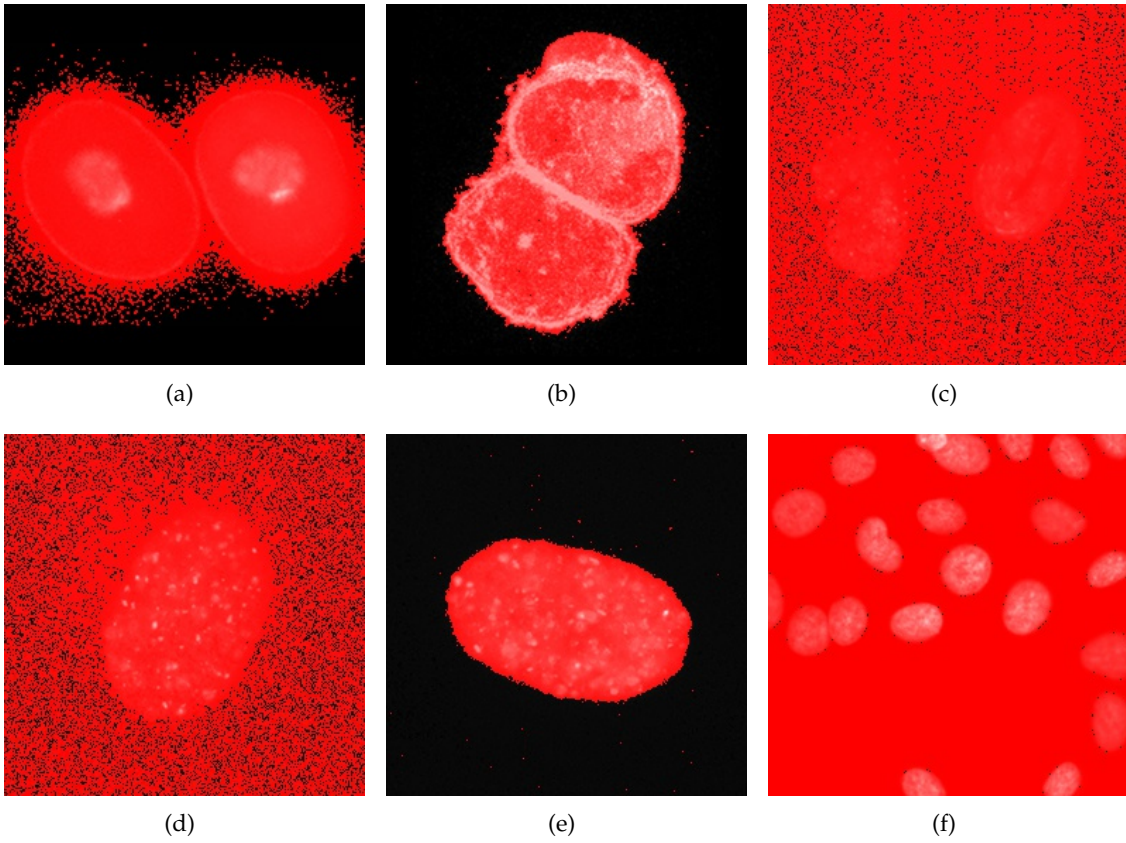


FIGURE 1.3: CAPTION MISSING HERE.

section, Section 1.2.1 we devise a novel weighting scheme, parameter estimation as well as a new way to think of the parameters involved, in terms of *proxy parameters*. We then specifically focus on tuning these parameter for fluorescence images in Section 1.2.3.

1.2.1 Graph Weighting

The first thing we do is normalise the weighting for both the data and smoothing connections. For the weighting of the neighbourhood connections we use the Euclidean distance between adjacent nodes. This results in neighbourhood connections as illustrated in Figure 1.4. The range of pixel intensities is also normalised i.e. $p \in [0, 1]$. The weight of the connection from the source to the node p is given by $E^i(0)|_{i=p} = \lambda_0|p - c_0|^2$. This is seen as how far away the pixel is from c_0 . Similarly, the weight of the connection from the node to the sink is given by $E^i(1)|_{i=p} = \lambda_1|p - c_1|^2$, i.e. how far away the pixel is from c_1 . The fully connected graph for a single node in the 8-connected neighbourhood system is illustrated in Figure 1.4.

Describe the modified weighting and parameter relations.

1.2.2 Analysis of Weighting System and Parameter Relationships

Describe the relationship between various parameters including their limits and ranges.

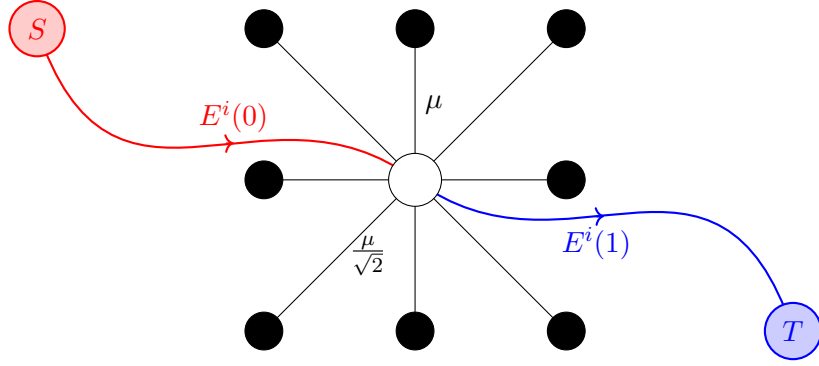


FIGURE 1.4: Fully connected single node.

To better understand the relationship between λ_0 and λ_1 and its impact on the final solution we explicitly formalise the dependency and set

$$\lambda_0 = \alpha \lambda_1. \quad (1.16)$$

Forcing this relation between λ_0 and λ_1 makes further analysis simpler and more intuitive. We can immediately see a constraint on α . Since, we require data connections to be positive, i.e. $E^i(0), E^i(1) \geq 0$ (SEE SECTION??), this gives us a lowerbound on α for positive concavity of the energy functions

$$\alpha > 0 \text{ lowerbound on } \alpha \quad (1.17)$$

We will now analyse the flow through a single node. We use Figure 1.4 to facilitate our explanation. From the neighbourhood connections, in an 8-connected neighbourhood construction, the maximum flow into or out of a node to its neighbours is

$$f_{max} = 4\mu + 4\frac{\mu}{\sqrt{2}} = \mu(2\sqrt{2} + 4). \quad (1.18)$$

To guarantee that a node p will be placed in the source set, $p \in S$, we know that the incoming flow from the source must completely saturate all flow outlets, this can be expressed as

$$E^i(0) > E^i(1) + \mu(2\sqrt{2} + 4). \quad (1.19)$$

This can be read as "*The source saturates the sink and all neighbourhood connections*". Similarly to guarantee the node will be in the sink set, $p \in T$

$$E^i(1) > E^i(0) + \mu(2\sqrt{2} + 4). \quad (1.20)$$

This can be read as "*The sink is larger than the source and all neighbourhood connections*". To aid in understanding the energies we use Figure 1.5.

For quadratic energies with $0 < c_0 < c_1 < 1$, there is a point, between c_0 and c_1 , where the incoming flow from the source is completely saturates the sink with no excess remaining. This point, where the energies are equal, we call p_e , i.e. $E_0(p_e) = E_1(p_e)$. This point of zero net flow

can be found as follows

$$\begin{aligned} E^{i=p_e}(1) &= E^{i=p_e}(0) \\ \lambda_1(p_e - c_1)^2 &= \lambda_0(p_e - c_0)^2 \\ \frac{(p_e - c_0)^2}{(p_e - c_1)^2} &= \frac{\lambda_1}{\lambda_0} \\ \frac{p_e - c_0}{p_e - c_1} &= \sqrt{\frac{\lambda_1}{\lambda_0}} \quad \text{or} \quad \frac{p_e - c_0}{p_e - c_1} = -\sqrt{\frac{\lambda_1}{\lambda_0}} \end{aligned}$$

We know that

$$\begin{aligned} c_0 < p_e < c_1 \\ \therefore p_e - c_0 > 0 \quad \text{and} \quad p_e - c_1 < 0 \end{aligned}$$

It follows directly that

$$\begin{aligned} \frac{p_e - c_1}{p_e - c_0} &= -\sqrt{\frac{\lambda_1}{\lambda_0}} \\ \frac{(p_e - c_0) + (c_0 - c_1)}{p_e - c_0} &= -\sqrt{\frac{\lambda_1}{\lambda_0}} \\ \frac{c_0 - c_1}{p_e - c_0} &= -\left(\sqrt{\frac{\lambda_1}{\lambda_0}} + 1\right) \\ p_e &= c_0 + \frac{c_1 - c_0}{\sqrt{\frac{\lambda_1}{\lambda_0}} + 1} \end{aligned}$$

After substituting the relation in Equation (1.16) we get

$$p_e = c_0 + \frac{c_1 - c_0}{\sqrt{\alpha} + 1} \quad (1.21)$$

The point where the energies are equal, p_e , is shown in Figure 1.5.

Analysis of the relationship between p_e and α From Equation (1.21) we note that there is one tunable parameter, i.e. α . We can see that p_e and α are inversely related. This is expressed mathematically as

$$\begin{aligned} \text{if } \alpha = 1, p_e &= c_0 + \frac{c_1 - c_0}{1 + \sqrt{1}} = \frac{c_0 + c_1}{2} && \text{(midpoint between } c_0 \text{ and } c_1) \\ \lim_{\alpha \rightarrow \infty} p_e &= \lim_{\alpha \rightarrow \infty} c_0 + \frac{c_1 - c_0}{1 + \sqrt{\infty}} = c_0 && \text{(maximum } \alpha \text{ yields lowerbound on } p_e) \\ \lim_{\alpha \rightarrow 0} p_e &= \lim_{\alpha \rightarrow 0} c_0 + \frac{c_1 - c_0}{1 + \sqrt{0}} = c_1 && \text{(minimum } \alpha \text{ yields upperbound on } p_e) \end{aligned}$$

The relationship between p_e and α is illustrated in Figure 1.6.

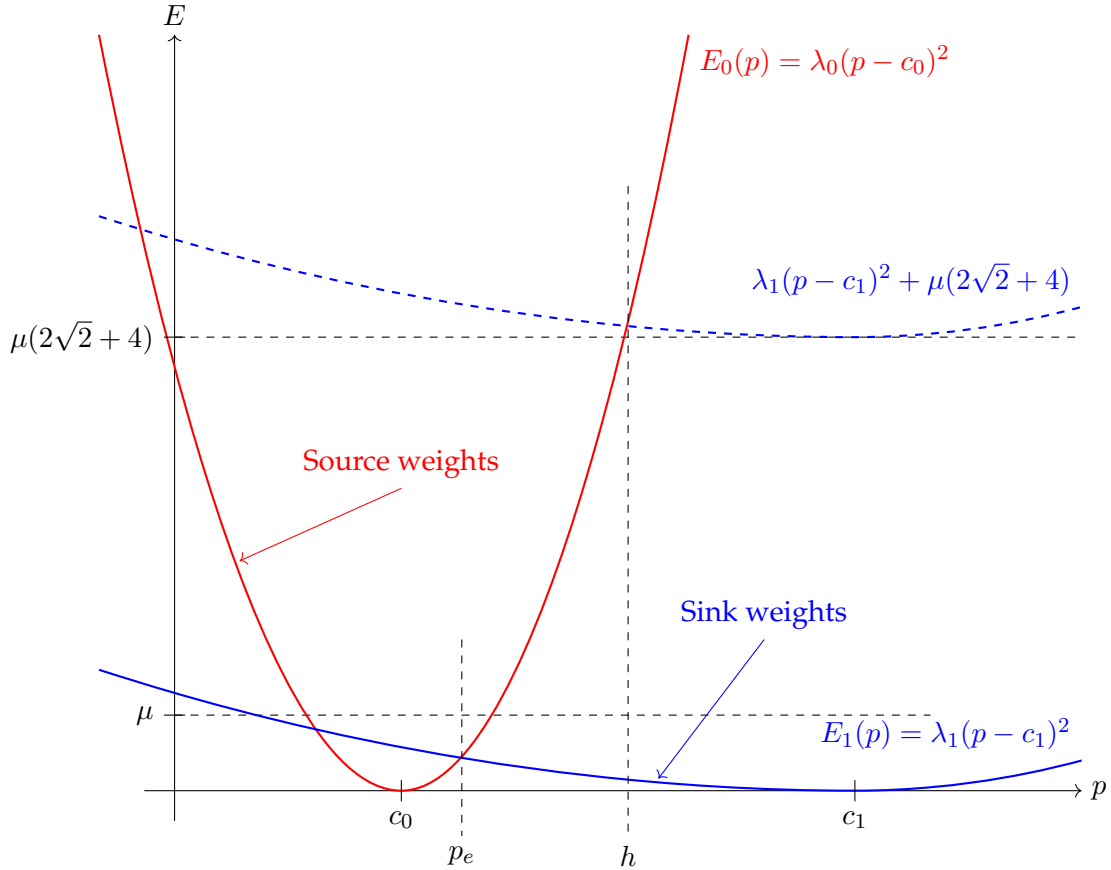
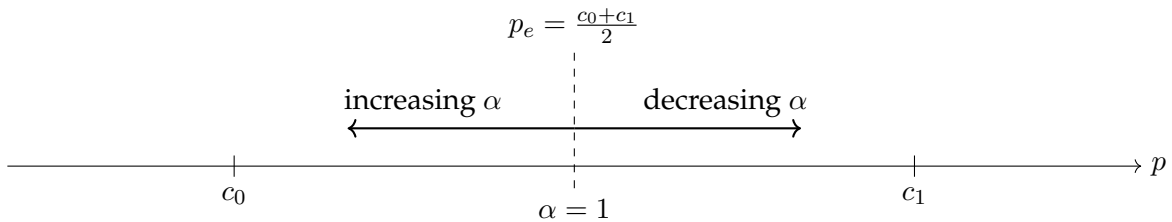


FIGURE 1.5: Data energy functions plot.

FIGURE 1.6: Relationship between α and p_e .

Figuring α If we are able to make good estimates on p_e , c_0 and c_1 for the final segmented image, then it is possible to calculate α as follows:

$$\begin{aligned}
 p_e &= c_0 + \frac{c_1 - c_0}{\sqrt{\alpha} + 1} \\
 1 + \sqrt{\alpha} &= \frac{c_1 - c_0}{p_e - c_0} \\
 \alpha &= \left(\frac{c_1 - c_0}{p_e - c_0} - 1 \right)^2
 \end{aligned} \tag{1.22}$$

Lowerbound on μ When we found the point, p_e , where the energies are equal in Equation (1.21), we ignored the other solution as it was not within the range from c_0 to c_1 . Let this point be

p_{e^*} . If this point is positive and $0 < p_{e^*} < c_0$ then we must ensure that at no point within this range that the source flow saturates all the outgoing edges. This force a limit on how low μ can be. This is only of significant concern when $\alpha > 1$. We only need to concern ourselves with the point $p = 0$ as this is the point where the difference $E^i(0) - E^i(1)$ is the largest. The lowerbound on μ can be obtained as follows

$$\begin{aligned} E^i(0)|_{p_i=0} &< E^i(1)|_{p_i=0} + \mu (2\sqrt{2} + 4) \\ \lambda_0 c_0^2 &< \lambda_1 c_1^2 + \mu (2\sqrt{2} + 4) \\ \therefore \mu (2\sqrt{2} + 4) &> \lambda_0 c_0^2 - \lambda_1 c_1^2 \\ \mu &> \frac{\lambda_0 c_0^2 - \lambda_1 c_1^2}{(2\sqrt{2} + 4)} \end{aligned}$$

Taking into account the relation in Equation (1.16) this becomes

$$\mu > \frac{\lambda_1 (\alpha c_0^2 - c_1^2)}{(2\sqrt{2} + 4)} \quad (1.23)$$

Absolutely in the source set From Equation (1.19) we can see that there is a point beyond which all nodes which correspond to pixel value higher than that point will be saturated and have excess flow which means that they will be in the source set. We will call this point the *saturation point* and denote it by h . This is shown in Figure 1.5. This point can be determined as follows:

$$\begin{aligned} \lambda_0 (h - c_0)^2 &> \lambda_1 (h - c_1)^2 + f_{max} \\ \lambda_0 (h - c_0)^2 - \lambda_1 (h - c_1)^2 &> f_{max} \\ (\lambda_0 - \lambda_1) h^2 + (-2\lambda_0 c_0 + 2\lambda_1 c_1) h + (\lambda_0 c_0^2 - \lambda_1 c_1^2 - f_{max}) &> 0 \end{aligned}$$

The solutions to h are

$$h = \frac{(2\lambda_0 c_0 - 2\lambda_1 c_1) \pm \sqrt{(-2\lambda_0 c_0 + 2\lambda_1 c_1)^2 - 4(\lambda_0 - \lambda_1)(\lambda_0 c_0^2 - \lambda_1 c_1^2 - f_{max})}}{2(\lambda_0 - \lambda_1)}$$

Substituting the relation in Equation (1.16)

$$\begin{aligned} h &= \frac{(\alpha c_0 - c_1) \pm \sqrt{(\alpha c_0 - c_1)^2 - (\alpha - 1)(\alpha c_0^2 - c_1^2 - \frac{f_{max}}{\lambda_1})}}{\alpha - 1} \\ &= \frac{(\alpha c_0 - c_1) \pm \sqrt{\alpha(c_0 - c_1)^2 + \frac{f_{max}}{\lambda_1}(\alpha - 1)}}{\alpha - 1} \end{aligned}$$

If the μ is greater than the lowerbound in Equation (1.23) then there is only one solution to h which is of importance. This is the positive solution for h which is

$$h = \frac{(\alpha c_0 - c_1) + \sqrt{\alpha(c_0 - c_1)^2 + \frac{\mu(2\sqrt{2}+4)}{\lambda_1}(\alpha - 1)}}{\alpha - 1} \quad (1.24)$$

This point is marked off in Figure 1.5.

Determining λ_1 Given good approximations for c_0, c_1, α, h and μ , we can calculate the appropriate value for λ_1 . We proceed from Equation (1.19) as follows

$$\begin{aligned}\lambda_0(h - c_0)^2 &= \lambda_1(h - c_1)^2 + \mu(2\sqrt{2} + 4) \\ \lambda_1(\alpha(h - c_0)^2 - (h - c_1)^2) &= \mu(2\sqrt{2} + 4) \\ \lambda_1 &= \frac{\mu(2\sqrt{2} + 4)}{\alpha(h - c_0)^2 - (h - c_1)^2}\end{aligned}\tag{1.25}$$

Parameter estimation process The parameter estimation is based on the assumption that sufficiently good approximations for c_0, c_1, p_e and h can be obtained. By sufficiently good we are referring to the closeness to the values these parameters would take for an ideal segmentation. From these approximations, we calculate the approximation for α using Equation (1.22). The parameters μ and λ_1 are related and aren't separable, therefore we set choose to set μ . We can then calculate λ_1 using Equation (1.25). For the chosen μ we can calculate the upperbound on λ_1 to ensure that the constraint Equation (1.23) is met. The constraint on λ_1 is calculated as follows

$$\begin{aligned}\mu(2\sqrt{2} + 4) &> \lambda_1(\alpha c_0^2 - c_1^2) \\ \lambda_1 &< \frac{\mu(2\sqrt{2} + 4)}{\alpha c_0^2 - c_1^2}\end{aligned}\tag{1.26}$$

Finally λ_0 can be calculated using Equation (1.16).

1.2.3 Tuning Parameters for Fluorescence Microscopy

What sort of image properties are we tuning for? E.g. dark bg, low contrast, etc. Parameters limits and ranges. The properties of the images obtained in fluorescence microscopy imaging can be used to guide the parameter estimation process. We focus, specifically, on black background images. Due to the fact that the predominant form of noise in the imaging system is Poisson distributed, we can further assume that the darker the background, the less noise that is present therein. The Poisson process also tells us that brighter regions exhibit a greater intensity variation due to the sampling process. Therefore, the curve for $E^i(1)$ is less convex than $E^i(0)$ as in Figure 1.5 and, resultantly, the value for p_e , in Figure 1.6, is shifted to the left. This places a new lowerbound on α for fluorescence images

$$\alpha \geq 1.\tag{1.27}$$

Manual Tuning Before moving further into analysis of the relationships between the parameters, we first perform a manual tuning of parameters and observing the effect on the segmented results. This allows us to understand how strongly correlated the parameter is to the final result. We note that the curves, $E^i(0)$ and $E^i(1)$, can be tuned relative to a fixed value for μ and this wouldn't impact significantly on the range of possible solution sets. Therefore, we set $\mu = 1$ in all our manual parameter tuning. We use a stopping criterion of $\epsilon = 1 \times 10^{-3}$.

We cover a relatively wide range of parameter settings and note the output, i.e. over-segmented, under-segmented, almost ideal, etc. At this point, categorising the segmented output is largely subjective. We also use various initial conditions. Specifically, we use the segmented output from Otsu binarization, K-means ($k = 2$) and Expectation-Maximisation

for Gaussian Mixture Modelling (EMGMM) with ($k = 2$). The initial and final means are of significant important in this study.

For Figure A.1(a), we used show the output for the following combinations of α and λ_1 . $(\alpha, \lambda_1) = \{(30, 150), (40, 50), (40, 100), (40, 150), (40, 200), (45, 150), (50, 150)\}$. The initial segmentation masks are shown in Figure 1.7. The segmented output for the combinations are shown in Figure 1.8.

For Figure A.1(b), we used show the output for the following combinations of α and λ_1 . $(\alpha, \lambda_1) = \{(30, 150), (40, 50), (40, 100), (40, 150), (40, 200), (45, 150), (50, 150)\}$. The initial segmentation masks are shown in Figure 1.9. The segmented output for the combinations are shown in Figure 1.10.

For Figure A.1(c), we used show the output for the following combinations of α and λ_1 . $(\alpha, \lambda_1) = \{(1, 150), (10, 150), (10, 200), (10, 400), (10, 800), (20, 150), (30, 150), (40, 150), (50, 150)\}$. The initial segmentation masks are shown in Figure 1.11. The segmented output for the combinations are shown in Figure 1.12.

For Figure A.1(d), we used show the output for the following combinations of α and λ_1 . $(\alpha, \lambda_1) = \{(30, 50), (30, 100), (30, 150), (40, 100), (40, 150), (50, 150)\}$. The initial segmentation masks are shown in Figure 1.13. The segmented output for the combinations are shown in Figure 1.14.

For Figure A.1(e), we used show the output for the following combinations of α and λ_1 . $(\alpha, \lambda_1) = \{(30, 50), (30, 100), (30, 150), (40, 100), (40, 150), (50, 150)\}$. The initial segmentation masks are shown in Figure 1.15. The segmented output for the combinations are shown in Figure 1.16.

For Figure A.1(f), we used show the output for the following combinations of α and λ_1 . $(\alpha, \lambda_1) = \{(20, 20), (20, 150), (30, 150), (40, 50), (40, 150), (50, 150)\}$. The initial segmentation masks are shown in Figure 1.17. The segmented output for the combinations are shown in Figure 1.18.

The means and standard deviations for the initial masks obtained are shown in Table 1.1.

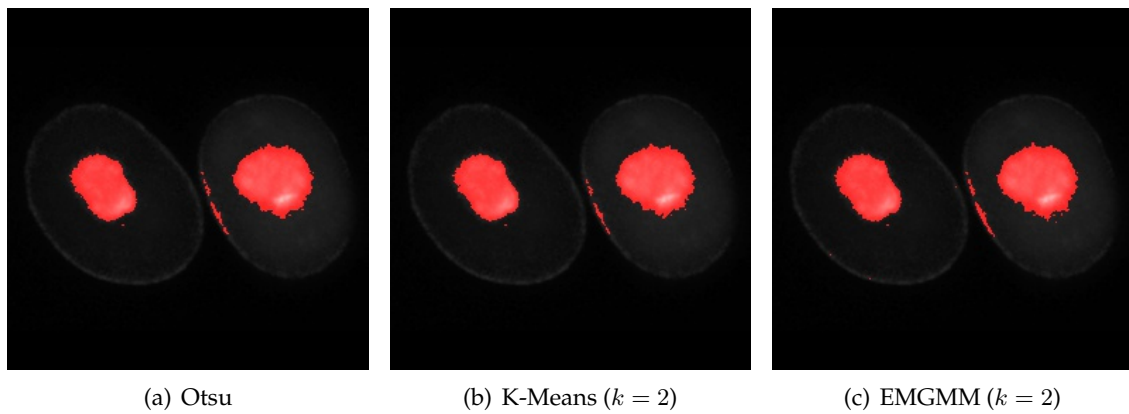


FIGURE 1.7: Image 1 from sample set Figure A.1 initial masks.

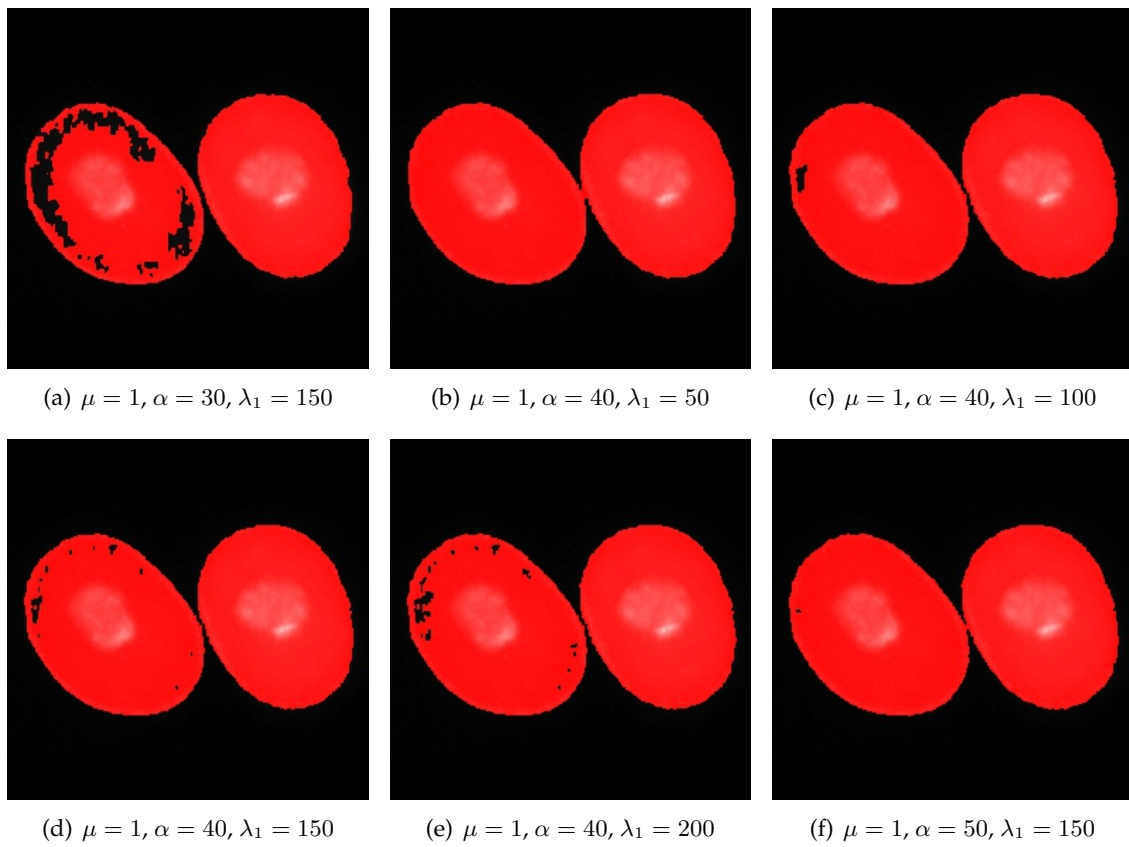


FIGURE 1.8: Segmented output for various combination of α and λ_1 for Image 1 in the sample set.

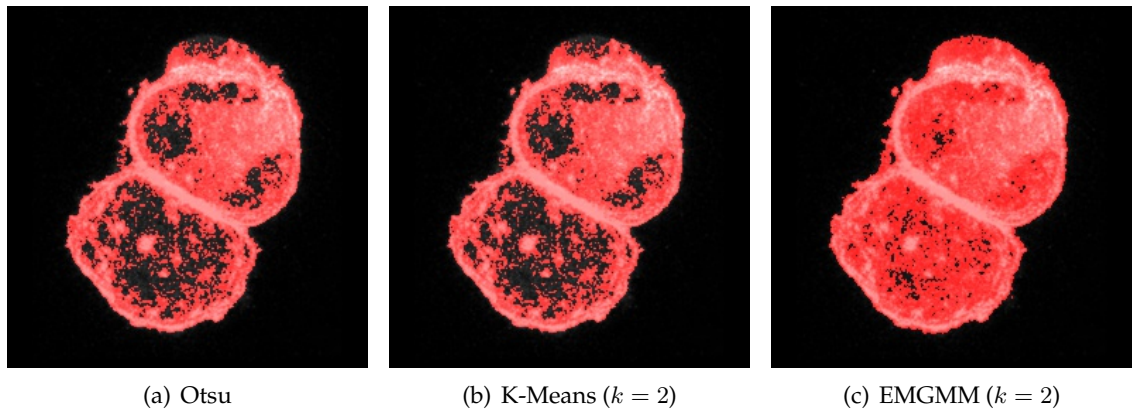
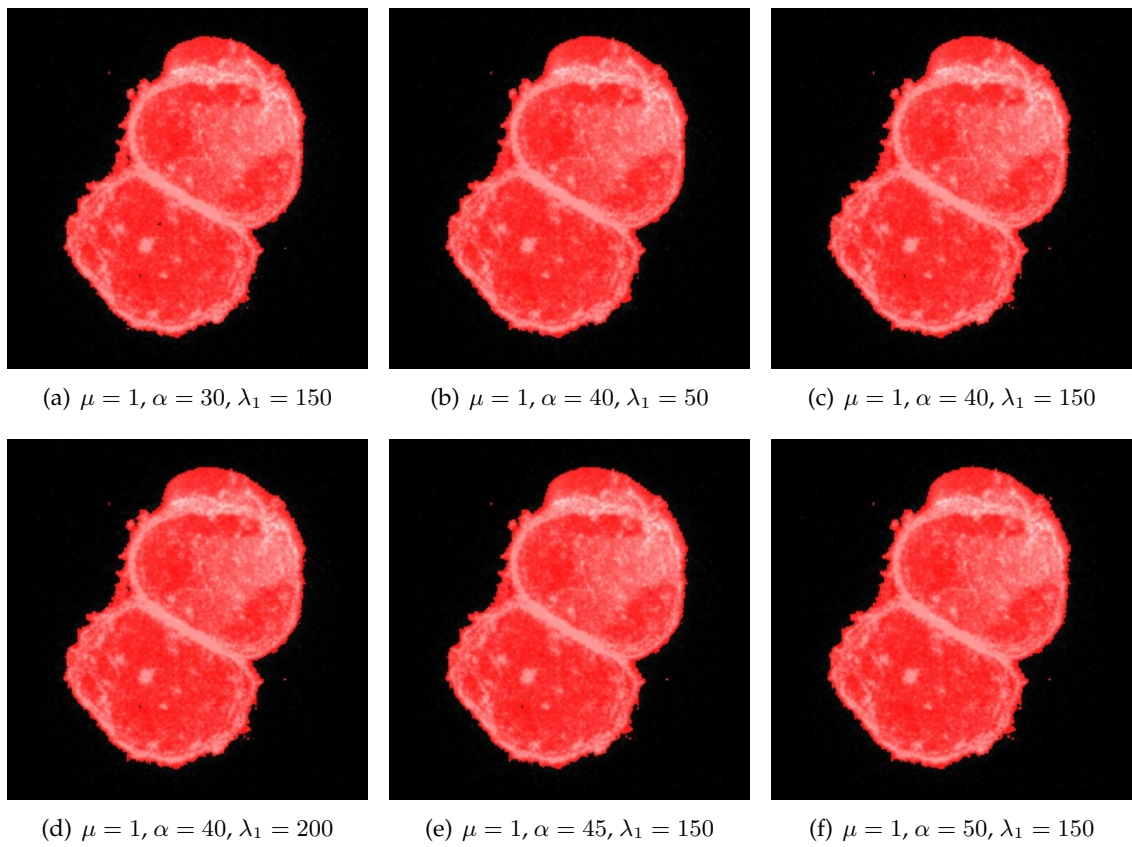


FIGURE 1.9: Image 2 from sample set Figure A.1 initial masks.

FIGURE 1.10: Segmented output for various combination of α and λ_1 for Image 2 in the sample set.

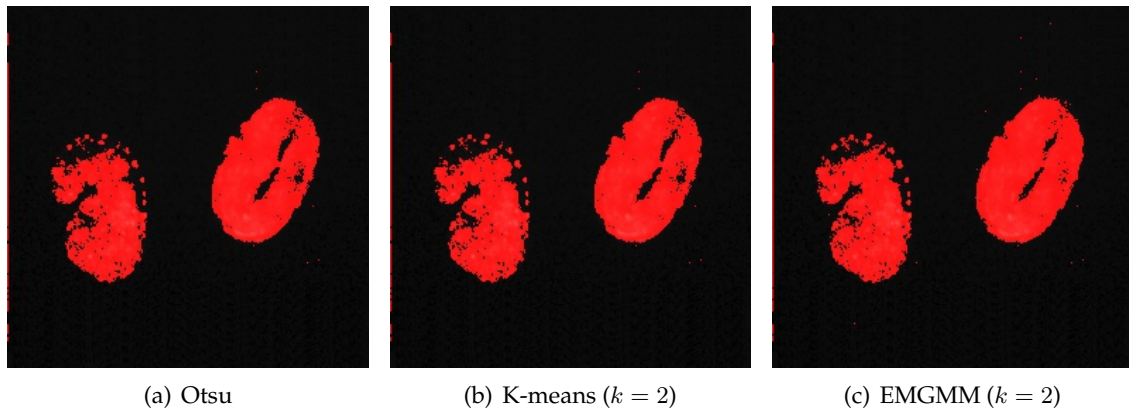


FIGURE 1.11: Image 3 from sample set Figure A.1 initial masks.

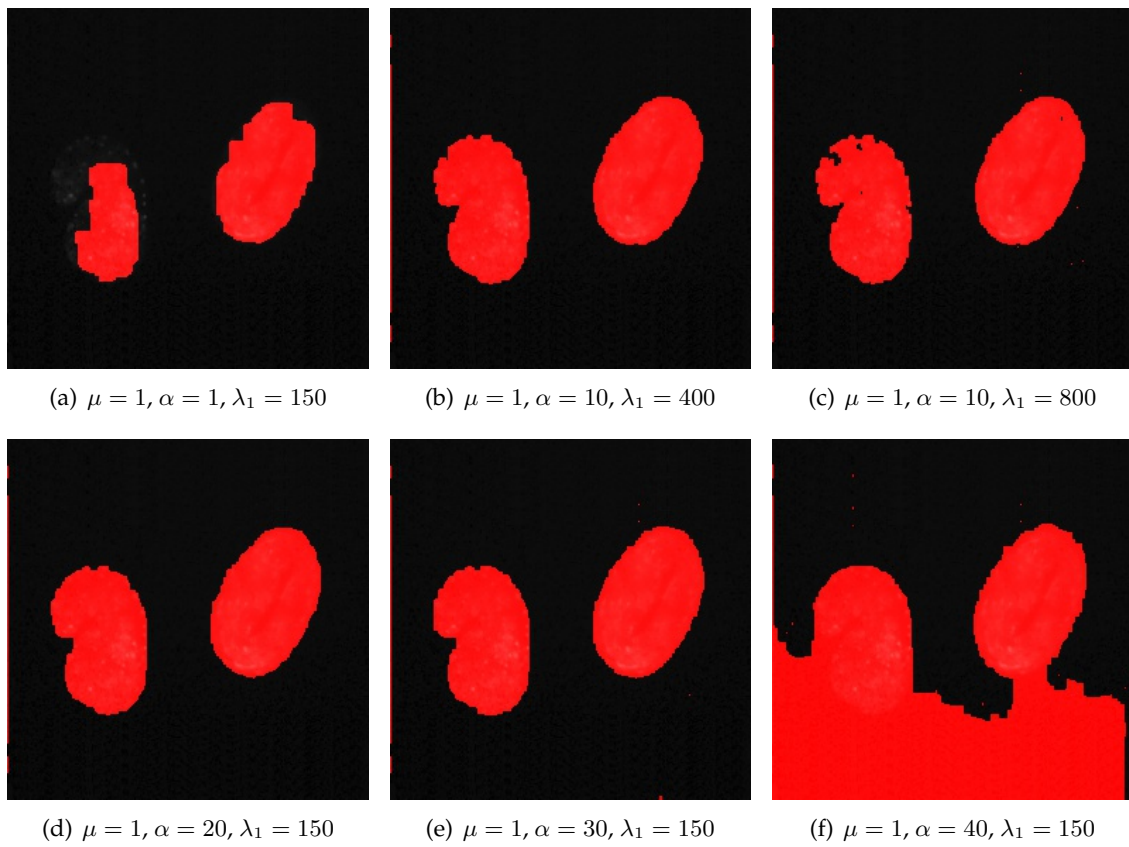


FIGURE 1.12: Segmented output for various combination of α and λ_1 for Image 3 in the sample set.

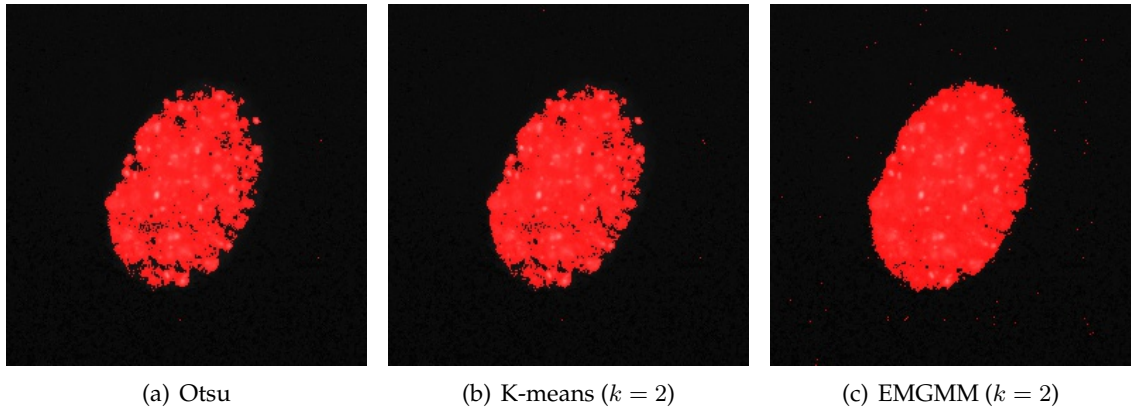
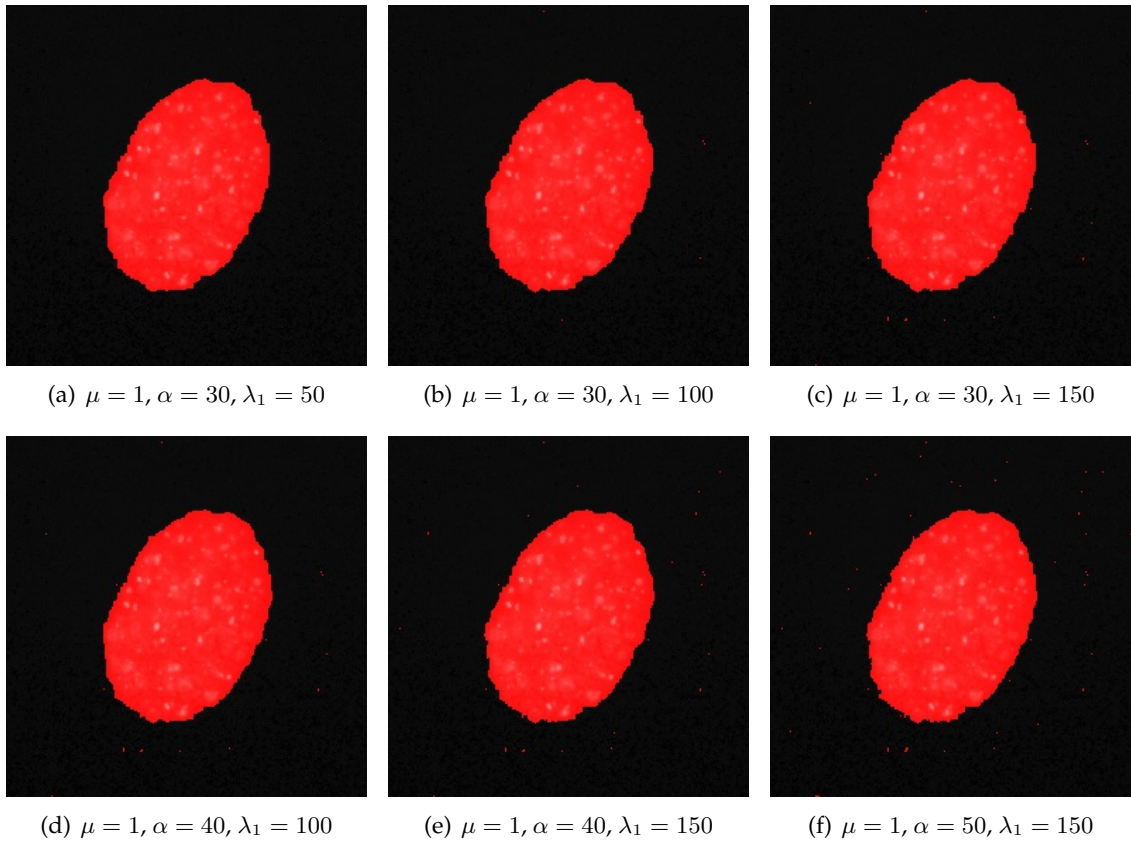


FIGURE 1.13: Image 4 from sample set Figure A.1 initial masks.

FIGURE 1.14: Segmented output for various combination of α and λ_1 for Image 4 in the sample set.

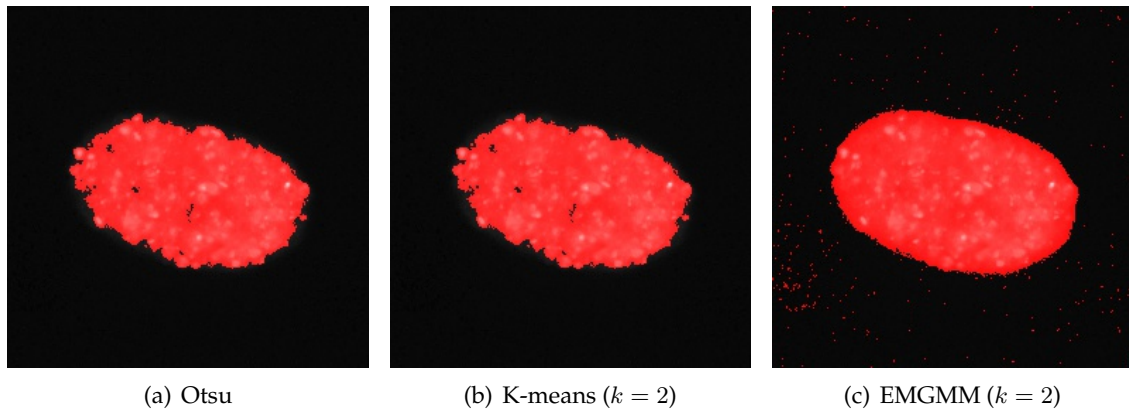


FIGURE 1.15: Image 5 from sample set Figure A.1 initial masks.

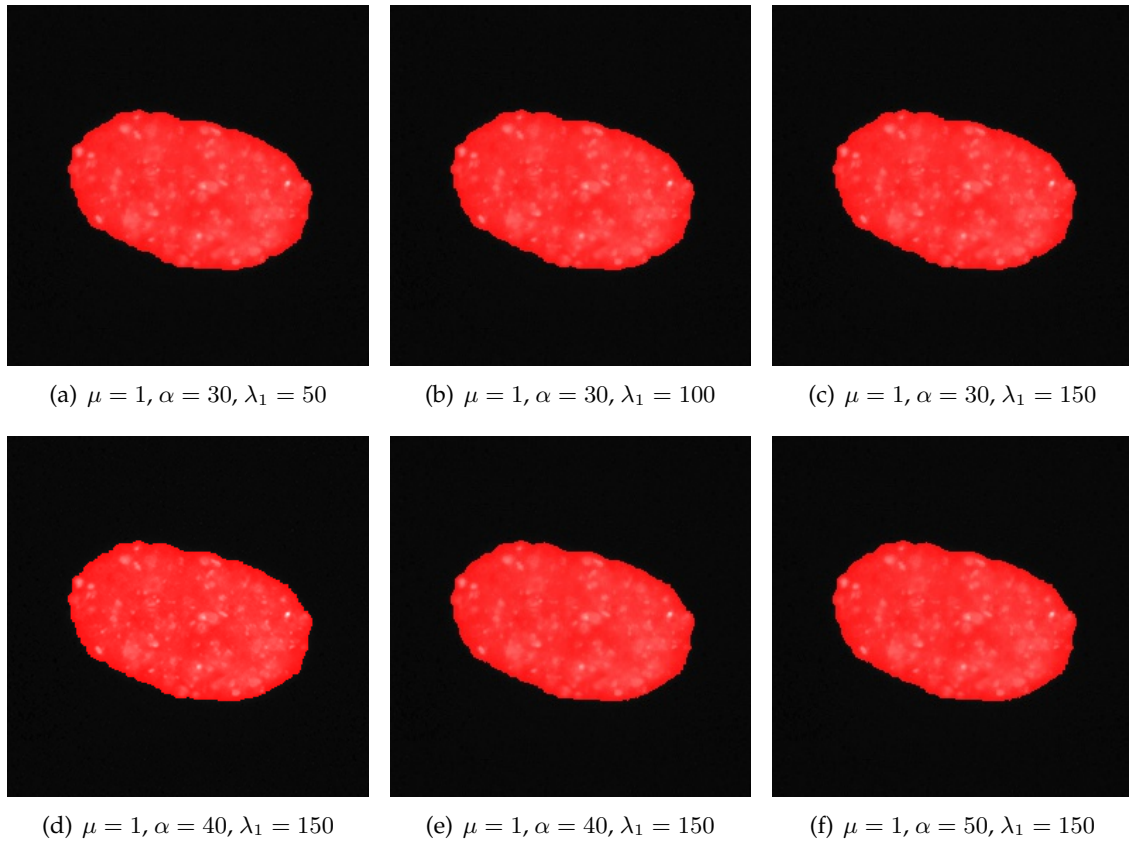


FIGURE 1.16: Segmented output for various combination of α and λ_1 for Image 5 in the sample set.

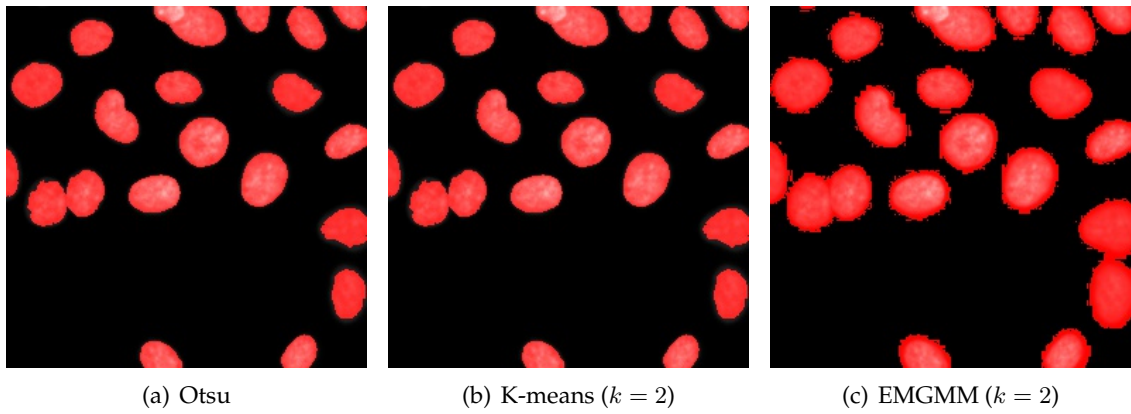


FIGURE 1.17: Image 6 from sample set Figure A.1 initial masks.

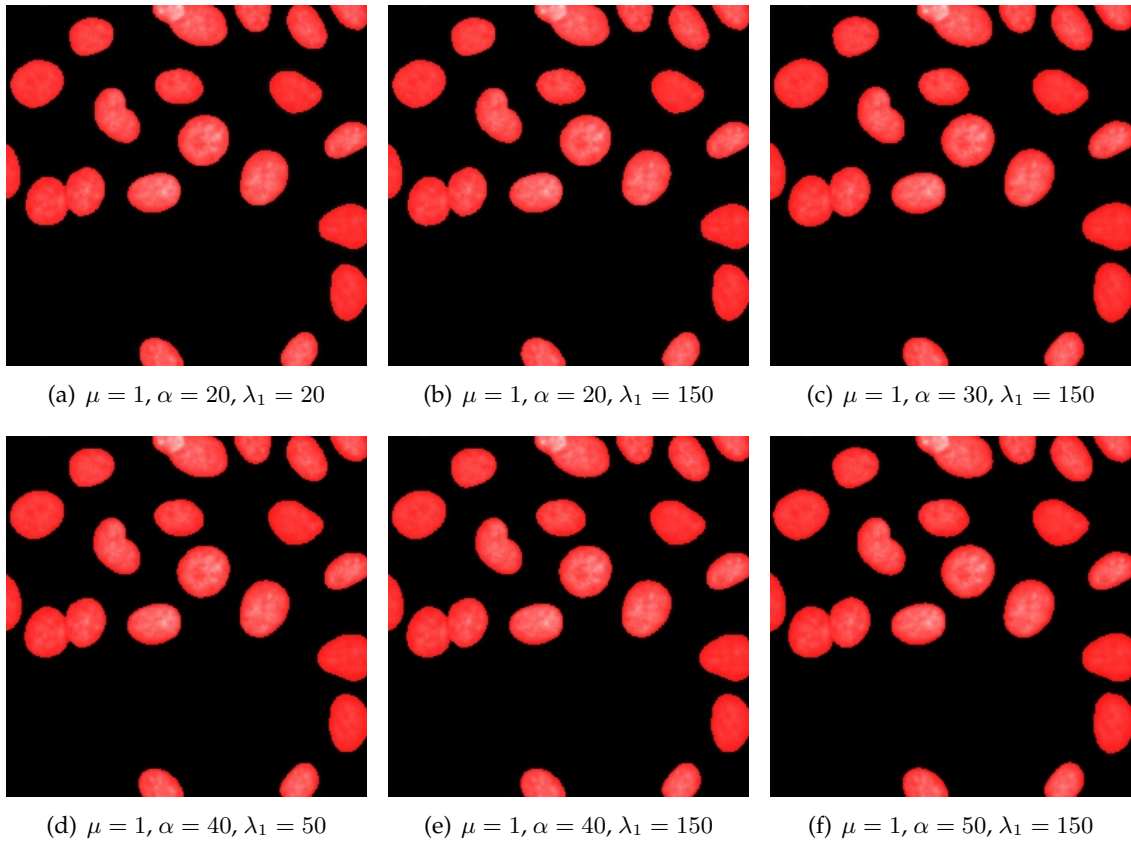
FIGURE 1.18: Segmented output for various combination of α and λ_1 for Image 6 in the sample set.

TABLE 1.1: Initial means and standard deviations for all images in the sample set for Otsu, K-means and EMGMM clustering.

	c_0	c_1	s_0	s_1
Image 1				
Otsu	0.0307515	0.26466	0.0385001	0,0803506
K-means($k = 2$)	0.0308984	0.267192	0.0387009	0.0793621
EMGMM ($k = 2$)	0.0305648	0.261392	0.0382529	0.081608
Image 2				
Otsu	0.0293218	0.373293	0.054652	0.124376
K-means($k = 2$)	0.0293218	0.373293	0.054652	0.124376
EMGMM ($k = 2$)	0.010789	0.321058	0.0211362	0.140498
Image 3				
Otsu	0.0422978	0.105043	0.0104066	0.0269333
K-means($k = 2$)	0.0422978	0.105043	0.0104066	0.0269333
EMGMM ($k = 2$)	0.042026	0.103124	0.0100784	0.0273395
Image 4				
Otsu	0.0424602	0.147303	0.0133024	0.0513289
K-means($k = 2$)	0.0420671	0.145145	0.0125633	0.0513602
EMGMM ($k = 2$)	0.0407566	0.136167	0.0102742	0.052472
Image 5				
Otsu	0.037086	0.216513	0.0138978	0.0626164
K-means($k = 2$)	—	—	—	—
EMGMM ($k = 2$)	0.0343141	0.190501	0.00456055	0.0782783
Image 6				
Otsu	0.270483	0.00657006	0.0228327	0.0916426
K-means($k = 2$)	0.270483	0.00657006	0.0228327	0.0916426
EMGMM ($k = 2$)	0	0.187883	0	0.133022

The final values for the segmentation results are shown in Table 1.2. The table shows for each image, given the values for the input parameters, whether the degree of acceptance of the output. We take the final results are the means of object and the background. From the final results, we calculate the values for p_e , Equation (1.21), and h , Equation (1.24). The means for each image can vary greatly. To put the values of p_e and h into a relative perspective, they are also shown as a fraction of the distance between c_0 and c_1 . Let $k_p \in (0, 1)$ be the fraction of the distance $p_e - c_0$ and $c_1 - c_0$ as illustrated in Figure 1.19. Let $k_h \in (k_p, 1)$ be the fraction of the distance $h - c_0$ and $c_1 - c_0$ as illustrated in Figure 1.20. The following relation holds $0 < k_p < k_h$.



FIGURE 1.19: p_e as a fraction of the distance between c_0 and c_1 .

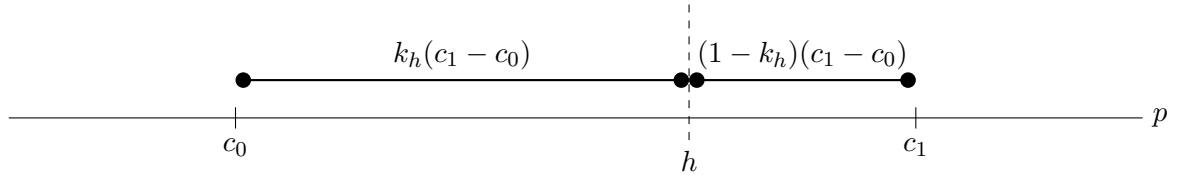
FIGURE 1.20: h as a fraction of the distance between c_0 and c_1 .

TABLE 1.2: Results from manual tuning.

Image	α	λ_1	c_0	c_1	p_e	h	k_p	k_h
1-O	30	100	0.009171	0.117209	0.025851	0.058086	0.154387	0.452755
1-O	40	100	0.006909	0.110953	0.021114	0.049359	0.136527	0.407996
1-O	40	50	0.006803	0.110618	0.020976	0.065665	0.136527	0.566987
1-O	40	150	0.006953	0.111119	0.021175	0.042396	0.136527	0.340248
1-O	40	200	0.007093	0.111541	0.021353	0.038508	0.136527	0.300772
1-O	45	150	0.006832	0.110758	0.020314	0.040326	0.129732	0.322287
1-O	50	150	0.006681	0.110301	0.019519	0.038516	0.123899	0.307235
1-K	30	100	0.009557	0.118306	0.026346	0.058499	0.154387	0.450049
1-K	40	100	0.006928	0.111013	0.021138	0.049379	0.136527	0.407847
1-K	40	50	0.006818	0.110658	0.020995	0.065680	0.136527	0.566856
1-K	40	150	0.007063	0.111430	0.021312	0.042514	0.136527	0.339679
1-K	40	200	0.007176	0.111789	0.021459	0.038600	0.136527	0.300384
1-K	45	150	0.006852	0.110824	0.020340	0.040348	0.129732	0.322165
1-K	50	150	0.006685	0.110311	0.019524	0.038521	0.123899	0.307219
1-E	30	150	0.008876	0.116478	0.025489	0.049694	0.154387	0.379343
1-E	40	100	0.006687	0.110890	0.020913	0.049142	0.136527	0.407426
1-E	40	50	0.006788	0.110583	0.020959	0.065649	0.136527	0.567093
1-E	40	150	0.006944	0.111087	0.021163	0.042385	0.136527	0.340313
1-E	40	200	0.007058	0.111434	0.021308	0.038469	0.136527	0.300940
1-E	45	150	0.006800	0.110654	0.020273	0.040291	0.129732	0.322481
1-E	50	150	0.006676	0.110283	0.019512	0.038510	0.123899	0.307268
2-O	30	150	0.007640	0.309246	0.054204	0.066628	0.154387	0.195579
2-O	40	50	0.007449	0.308057	0.048489	0.076410	0.136527	0.229407
2-O	40	100	0.007428	0.307890	0.048449	0.063950	0.136527	0.188118
2-O	40	150	0.007424	0.307975	0.048457	0.059239	0.136527	0.172400
2-O	40	200	0.007441	0.308094	0.048488	0.056764	0.136527	0.164052
2-O	45	150	0.007423	0.307976	0.046415	0.056577	0.129732	0.163545
2-O	50	150	0.007297	0.307166	0.044450	0.054107	0.123899	0.156103
2-K	30	150	0.007640	0.309246	0.054204	0.066628	0.154387	0.195579
2-K	40	50	0.007449	0.308057	0.048489	0.076410	0.136527	0.229407
2-K	40	100	0.007428	0.307890	0.048449	0.063950	0.136527	0.188118
2-K	40	150	0.007424	0.307975	0.048457	0.059239	0.136527	0.172400
2-K	40	200	0.007441	0.308094	0.048488	0.056764	0.136527	0.164052
2-K	45	150	0.007423	0.307976	0.046415	0.056577	0.129732	0.163545
2-K	50	150	0.007297	0.307166	0.044450	0.054107	0.123899	0.156103
2-E	30	150	0.007556	0.308779	0.054061	0.066498	0.154387	0.195674

2-E	40	50	0.007568	0.308796	0.048694	0.076578	0.136527	0.229095
2-E	40	100	0.007564	0.308815	0.048693	0.064163	0.136527	0.187881
2-E	40	150	0.007566	0.308838	0.048697	0.059458	0.136527	0.172244
2-E	40	200	0.007558	0.308800	0.048686	0.056948	0.136527	0.163952
2-E	45	150	0.007467	0.308260	0.046489	0.056646	0.129732	0.163496
2-E	50	150	0.007343	0.307470	0.044528	0.054178	0.123899	0.156053
3-O	10	150	0.041366	0.096327	0.054571	0.108955	0.240253	1.229755
3-O	10	200	0.041364	0.096323	0.054568	0.099806	0.240253	1.063370
3-O	10	400	0.041359	0.096339	0.054568	0.082894	0.240253	0.755457
3-O	10	800	0.041371	0.096708	0.054666	0.071643	0.240253	0.547049
3-O	20	150	0.041323	0.095848	0.051287	0.089056	0.182743	0.875426
3-O	30	150	0.041267	0.094999	0.049563	0.080313	0.154387	0.726674
3-O	40	150	0.044802	0.057616	0.046551	0.078701	0.136527	2.645434
3-K	10	150	0.041366	0.096327	0.054571	0.108955	0.240253	1.229755
3-K	10	200	0.041364	0.096323	0.054568	0.099806	0.240253	1.063370
3-K	10	400	0.041359	0.096339	0.054568	0.082894	0.240253	0.755457
3-K	10	800	0.041371	0.096708	0.054666	0.071643	0.240253	0.547049
3-K	20	150	0.041323	0.095848	0.051287	0.089056	0.182744	0.875426
3-K	30	150	0.041267	0.094999	0.049563	0.080313	0.154387	0.726674
3-K	40	150	0.044802	0.057616	0.046551	0.078701	0.136527	2.645434
3-E	10	150	0.041362	0.096283	0.054557	0.108952	0.240253	1.230667
3-E	10	200	0.041357	0.096260	0.054548	0.099799	0.240253	1.064463
3-E	10	400	0.041356	0.096309	0.054559	0.082890	0.240253	0.755812
3-E	10	800	0.041367	0.096932	0.054717	0.071656	0.240253	0.545117
3-E	20	150	0.041321	0.095836	0.051284	0.089054	0.182744	0.875599
3-E	30	150	0.041262	0.094923	0.049545	0.080307	0.154387	0.727635
3-E	40	150	0.044849	0.057396	0.046562	0.078753	0.136527	2.702195
4-O	30	50	0.040339	0.131121	0.054355	0.107943	0.154387	0.744683
4-O	30	100	0.040328	0.131038	0.054332	0.088659	0.154387	0.532819
4-O	30	150	0.040319	0.130976	0.054315	0.080354	0.154387	0.441615
4-O	40	100	0.040240	0.129694	0.052453	0.082233	0.136527	0.469438
4-O	40	150	0.040264	0.130244	0.052549	0.075108	0.136527	0.387237
4-O	50	150	0.040232	0.129761	0.051324	0.071509	0.123899	0.349362
4-K	30	50	0.040356	0.131362	0.054406	0.107962	0.154387	0.742875
4-K	30	100	0.040343	0.131304	0.054386	0.088682	0.154387	0.531430
4-K	30	150	0.040339	0.131307	0.054383	0.080387	0.154387	0.440244
4-K	40	100	0.040233	0.129556	0.052428	0.082222	0.136527	0.470084
4-K	40	150	0.040260	0.130177	0.052536	0.075101	0.136527	0.387482
4-K	50	150	0.040223	0.129553	0.051291	0.071494	0.123899	0.350061
4-E	30	50	0.040262	0.129873	0.054097	0.107852	0.154387	0.754261
4-E	30	100	0.040254	0.129884	0.054091	0.088555	0.154387	0.538901
4-E	30	150	0.040237	0.129708	0.054049	0.080225	0.154387	0.446937
4-E	40	100	0.040236	0.129624	0.052439	0.082227	0.136527	0.469763
4-E	40	150	0.040225	0.129532	0.052418	0.075043	0.136527	0.389868
4-E	50	150	0.040201	0.129085	0.051213	0.071456	0.123899	0.351638
5-O	30	50	0.034756	0.201631	0.060519	0.104517	0.154387	0.418045

5-O	30	150	0.034757	0.201659	0.060525	0.079633	0.154387	0.268872
5-O	40	150	0.034675	0.200630	0.057333	0.073912	0.136527	0.236429
5-O	50	150	0.034487	0.197806	0.054722	0.069683	0.123899	0.215506
5-K	30	50	0.034756	0.201631	0.060519	0.104517	0.154387	0.418045
5-K	30	150	0.034757	0.201659	0.060525	0.079633	0.154387	0.268872
5-K	40	150	0.034675	0.200630	0.057333	0.073912	0.136527	0.236429
5-K	50	150	0.034487	0.197806	0.054722	0.069683	0.123899	0.215506
5-E	30	50	0.034683	0.200718	0.060316	0.104407	0.154387	0.419937
5-E	30	150	0.034681	0.200701	0.060313	0.079483	0.154387	0.269859
5-E	40	150	0.034582	0.199297	0.057069	0.073726	0.136527	0.237648
5-E	50	150	0.034580	0.199280	0.054986	0.069870	0.123899	0.214269
6-O	20	20	0.002964	0.251959	0.048466	0.136161	0.182744	0.534939
6-O	20	150	0.002932	0.251781	0.048407	0.066168	0.182744	0.254113
6-O	30	50	0.001533	0.228802	0.036620	0.074639	0.154387	0.321672
6-O	30	150	0.001521	0.238690	0.038137	0.053144	0.154387	0.217666
6-O	40	50	0.001817	0.242106	0.034623	0.066509	0.136527	0.269226
6-O	40	150	0.001815	0.242097	0.034619	0.047477	0.136527	0.190034
6-O	50	50	0.001259	0.235130	0.030236	0.059146	0.123899	0.247513
6-O	50	150	0.001239	0.234857	0.030184	0.041921	0.123899	0.174135
6-K	20	20	0.002964	0.251959	0.048466	0.136161	0.182744	0.534939
6-K	20	150	0.002932	0.251781	0.048407	0.066168	0.182744	0.254113
6-K	30	50	0.001533	0.228802	0.036620	0.074639	0.154387	0.321672
6-K	30	150	0.001521	0.238690	0.038137	0.053144	0.154387	0.217666
6-K	40	50	0.001817	0.242106	0.034623	0.066509	0.136527	0.269226
6-K	40	150	0.001814	0.242097	0.034619	0.047476	0.136527	0.190034
6-K	50	50	0.001259	0.235130	0.030236	0.059146	0.123899	0.247513
6-K	50	150	0.001239	0.234857	0.030185	0.041921	0.123899	0.174135
6-E	20	20	0.002643	0.249529	0.047759	0.135753	0.182744	0.539155
6-E	20	150	0.002584	0.249164	0.047645	0.065530	0.182744	0.255277
6-E	30	50	0.002252	0.246370	0.039940	0.076508	0.154387	0.304183
6-E	30	150	0.002246	0.246324	0.039928	0.054615	0.154387	0.214558
6-E	40	50	0.001527	0.238746	0.033914	0.066025	0.136527	0.271893
6-E	40	150	0.001519	0.238667	0.033896	0.046879	0.136527	0.191277
6-E	50	50	0.001655	0.240298	0.031222	0.059817	0.123899	0.243720
6-E	50	150	0.001645	0.240193	0.031201	0.042755	0.123899	0.172337

Upon comparing the initial means in Table 1.1 and final means for the acceptable and good segmentation results in Table 1.2, the values of the initial means are larger. This is due to over-segmentation produced by Otsu, K-means and EMGMM clustering. A naïve approach to shifting the initial means closer to the final means is to dilate the initial mask. This pushes the boundaries of the contour for the object to accept the lower intensity neighbouring pixels as well as removes these relatively higher values from the background mask.

Dilated table results and final radius for dilation. To determine the optimal dilation size, we compare the difference of the mean values for each image in Table 1.2, for the good segmentation results only. These values are shown in Table 1.3. We use an elliptical element for

TABLE 1.3: Average of final means for good segmentations.

Image	\bar{c}_0	\bar{c}_1
1	0,006824	0,110693
2	0,007468	0,308217
3	0,041334	0,095952
4	0,040282	0,130360
5	0,034656	0,200287
6	0,001926	0,241672

dilation. The results of the dilation and the difference from the respective final means is shown in Table 1.4, Table 1.5 and Table 1.6 for the initial masks obtained from Otsu binarization, K-means and EMGMM clustering respectively. The closest values to the average final mean is highlighted in blue. From the tables it can be seen that a dilation size of 3 for a elliptical dilation element results in mean values that are closest to the average final means.

TABLE 1.4: Dilation after Otsu binarization.

Image	Size	c_0	c_1	$ c_0 - \bar{c}_0 $	$ c_1 - \bar{c}_1 $	$\sum_i c_i - \bar{c}_i $
1	3	0.027716	0.205161	0.020892	0.094468	0.115360
1	5	0.026188	0.173038	0.019364	0.062345	0.081709
1	7	0.024682	0.151369	0.017858	0.040676	0.058534
1	9	0.023158	0.136273	0.016334	0.025580	0.041914
1	11	0.021564	0.124931	0.014739	0.014238	0.028978
1	13	0.019981	0.116536	0.013157	0.005843	0.018999
1	15	0.018341	0.109705	0.011517	0.000988	0.012505
2	3	0.007563	0.301761	9.47e-05	0.006456	0.006551
2	5	0.006025	0.286271	0.001443	0.021946	0.023389
2	7	0.005386	0.273472	0.002082	0.034745	0.036827
2	9	0.004936	0.262053	0.002532	0.046164	0.048696
2	11	0.004587	0.250695	0.002881	0.057522	0.060403
2	13	0.004277	0.240651	0.003191	0.067566	0.070757
2	15	0.004041	0.231146	0.003428	0.077071	0.080498
3	3	0.041796	0.090729	0.000462	0.005223	0.005685
3	5	0.041641	0.084544	0.000307	0.011408	0.011715
3	7	0.041535	0.080118	0.000201	0.015834	0.016034
3	9	0.042983	0.076541	0.001649	0.019411	0.021059
3	11	0.041439	0.073293	0.000105	0.022659	0.022764
3	13	0.041397	0.070676	6.27e-05	0.025276	0.025339
3	15	0.041369	0.068354	3.48e-05	0.027599	0.027633
4	3	0.041060	0.133918	0.000778	0.003558	0.004336
4	5	0.040715	0.128101	0.000433	0.002259	0.002692
4	7	0.040534	0.122898	0.000252	0.007462	0.007714
4	9	0.040429	0.118341	0.000147	0.012019	0.012166
4	11	0.040354	0.113853	7.17e-05	0.016507	0.016579
4	13	0.040297	0.109960	1.53e-05	0.020400	0.020415
4	15	0.040235	0.106414	4.70e-05	0.023946	0.023993

5	3	0.035322	0.203137	0.000666	0.002850	0.003516
5	5	0.034726	0.193711	7.02e-05	0.006576	0.006646
5	7	0.034434	0.184644	0.000222	0.015643	0.015865
5	9	0.034281	0.176477	0.000375	0.023810	0.024185
5	11	0.034188	0.168599	0.000468	0.031688	0.032156
5	13	0.034120	0.161732	0.000536	0.038555	0.039091
5	15	0.034056	0.155296	0.000600	0.044991	0.045591
6	3	0.000457	0.209125	0.001469	0.032547	0.034016
6	5	7.29e-05	0.171123	0.001853	0.070549	0.072402
6	7	1.84e-05	0.144280	0.001908	0.097392	0.099299
6	9	1.08e-05	0.125501	0.001915	0.116171	0.118086
6	11	1.15e-05	0.110706	0.001914	0.130966	0.132880
6	13	1.27e-05	0.100486	0.001913	0.141186	0.143099
6	15	1.44e-05	0.092725	0.001912	0.148947	0.150858

TABLE 1.5: Dilation after K-means clustering.

Image	Size	c_0	c_1	$ c_0 - \bar{c}_0 $	$ c_1 - \bar{c}_1 $	$\sum_i c_i - \bar{c}_i $
1	3	0.027716	0.205161	0.020892	0.094468	0.115360
1	5	0.026188	0.173038	0.019364	0.062345	0.081709
1	7	0.024682	0.151369	0.017858	0.040676	0.058534
1	9	0.023158	0.136273	0.016334	0.025580	0.041914
1	11	0.021564	0.124931	0.014739	0.014238	0.028978
1	13	0.019981	0.116536	0.013157	0.005843	0.018999
1	15	0.018341	0.109705	0.011517	0.000988	0.012505
2	3	0.007563	0.301761	9.47e-05	0.006456	0.006551
2	5	0.006025	0.286271	0.001443	0.021946	0.023389
2	7	0.005386	0.273472	0.002082	0.034745	0.036827
2	9	0.004936	0.262053	0.002532	0.046164	0.048696
2	11	0.004587	0.250695	0.002881	0.057522	0.060403
2	13	0.004277	0.240651	0.003191	0.067566	0.070757
2	15	0.004041	0.231146	0.003427	0.077071	0.080499
3	3	0.041796	0.090729	0.000462	0.005223	0.005685
3	5	0.041641	0.084544	0.000307	0.011408	0.011715
3	7	0.041535	0.080118	0.000201	0.015834	0.016034
3	9	0.041480	0.076541	0.000146	0.019411	0.019557
3	11	0.041439	0.073293	0.000105	0.022659	0.022764
3	13	0.041397	0.070676	6.27e-05	0.025276	0.025339
3	15	0.041369	0.068354	3.48e-05	0.027599	0.027633
4	3	0.041060	0.133918	0.000778	0.003558	0.004336
4	5	0.040715	0.128101	0.000433	0.002259	0.002692
4	7	0.040534	0.122898	0.000252	0.007462	0.007714
4	9	0.040429	0.118341	0.000147	0.012019	0.012166
4	11	0.040354	0.113853	7.17e-05	0.016507	0.016579
4	13	0.040297	0.109960	1.53e-05	0.020400	0.020415
4	15	0.040235	0.106414	4.70e-05	0.023946	0.023993

5	3	0.035322	0.203137	0.000666	0.002850	0.003516
5	5	0.034726	0.193711	7.02e-05	0.006576	0.006646
5	7	0.034434	0.184644	0.000222	0.015643	0.015865
5	9	0.034281	0.176477	0.000375	0.023810	0.024185
5	11	0.034188	0.168599	0.000468	0.031688	0.032156
5	13	0.034120	0.161732	0.000536	0.038555	0.039091
5	15	0.034056	0.155296	0.000600	0.044991	0.045591
6	3	0.000457	0.209125	0.001469	0.032547	0.034016
6	5	7.29e-05	0.171123	0.001853	0.070549	0.072402
6	7	1.84e-05	0.144280	0.001908	0.097392	0.099299
6	9	1.08e-05	0.125501	0.001915	0.116171	0.118086
6	11	1.15e-05	0.110706	0.001914	0.130966	0.132880
6	13	1.27e-05	0.100486	0.001913	0.141186	0.143099
6	15	1.44e-05	0.092725	0.001912	0.148947	0.150858

TABLE 1.6: Dilation after EM-GMM clustering.

Image	Size	c_0	c_1	$ c_0 - \bar{c}_0 $	$ c_1 - \bar{c}_1 $	$\sum_i c_i - \bar{c}_i $
1	3	0.027251	0.198511	0.020427	0.087818	0.108245
1	5	0.025597	0.166707	0.018773	0.056014	0.074787
1	7	0.023968	0.146071	0.017144	0.035378	0.052522
1	9	0.022313	0.131983	0.015489	0.021290	0.036779
1	11	0.020595	0.121338	0.013771	0.010645	0.024416
1	13	0.018866	0.113441	0.012042	0.002748	0.014789
1	15	0.017084	0.107025	0.010260	0.003668	0.013928
2	3	0.006516	0.294763	0.000952	0.013454	0.014406
2	5	0.005719	0.280590	0.001748	0.027627	0.029375
2	7	0.005165	0.268079	0.002303	0.040138	0.042441
2	9	0.004774	0.256867	0.002694	0.051350	0.054044
2	11	0.004438	0.245779	0.003030	0.062438	0.065468
2	13	0.004165	0.235995	0.003303	0.072222	0.075525
2	15	0.003947	0.226736	0.003521	0.081481	0.085002
3	3	0.041729	0.089955	0.000395	0.005997	0.006392
3	5	0.041603	0.083968	0.000269	0.011984	0.012252
3	7	0.041502	0.079529	0.000168	0.016423	0.016590
3	9	0.041435	0.075914	0.000101	0.020038	0.020138
3	11	0.041384	0.072717	5.00e-05	0.023236	0.023285
3	13	0.041335	0.070134	1.30e-06	0.025819	0.025819
3	15	0.041299	0.067855	3.52e-05	0.028097	0.028132
4	3	0.040788	0.114645	0.000506	0.015715	0.016221
4	5	0.040886	0.099155	0.000604	0.031205	0.031809
4	7	0.041119	0.087943	0.000838	0.042417	0.043255
4	9	0.041369	0.080176	0.001087	0.050184	0.051271
4	11	0.041665	0.074350	0.001383	0.056010	0.057393
4	13	0.042029	0.070365	0.001747	0.059995	0.061742
4	15	0.042324	0.067586	0.002042	0.062774	0.064816

5	3	0.034368	0.147707	0.000288	0.052580	0.052868
5	5	0.034298	0.119630	0.000358	0.080657	0.081015
5	7	0.034222	0.102563	0.000434	0.097724	0.098158
5	9	0.034181	0.092259	0.000475	0.108028	0.108504
5	11	0.034143	0.085251	0.000513	0.115036	0.115549
5	13	0.034105	0.080911	0.000551	0.119377	0.119928
5	15	0.034075	0.077899	0.000581	0.122388	0.122969
6	3	0.000000	0.136655	0.001926	0.105017	0.106943
6	5	0.000000	0.116893	0.001926	0.124779	0.126705
6	7	0.000000	0.103734	0.001926	0.137938	0.139864
6	9	0.000000	0.094463	0.001926	0.147209	0.149135
6	11	0.000000	0.087325	0.001926	0.154347	0.156273
6	13	0.000000	0.082486	0.001926	0.159186	0.161112
6	15	0.000000	0.079177	0.001926	0.162495	0.164421

Updated equations taking into account k_p and k_h . When defining the values for p_e and h implicitly and k_p and k_h respectively, we can find the updated equation for determining α following from Equation (1.22)

$$\begin{aligned}\alpha &= \left(\frac{c_1 - c_0}{p_e - c_0} - 1 \right)^2 \\ &= \left(\frac{c_1 - c_0 - p_e + c_0}{p_e - c_0} \right)^2 \\ &= \left(\frac{c_1 - c_0 - c_0 - k_p(c_1 - c_0) + c_0}{c_0 + k_p(c_1 - c_0) - c_0} \right)^2 \\ &= \left(\frac{c_1 - c_0 - k_p(c_1 - c_0)}{k_p(c_1 - c_0)} \right)^2 \\ &= \left(\frac{(1 - k_p)(c_1 - c_0)}{k_p(c_1 - c_0)} \right)^2\end{aligned}$$

Therefore, given k_p , the equation to calculate α is

$$\alpha = \left(\frac{1 - k_p}{k_p} \right)^2 \quad (1.28)$$

$$\alpha - 1 = \frac{1 - 2k_p + k_p^2 - k_p^2}{k_p^2} = \frac{1 - 2k_p}{k_p^2} \quad (1.29)$$

Following from Equation (1.25)...

$$h = c_0 + k_h(c_1 - c_0) = c_1 - (1 - k_h)(c_1 - c_0)$$

$$\begin{aligned}
& \alpha(c_0 + k_h(c_1 - c_0) - c_0)^2 - (c_1 - (1 - k_h)(c_1 - c_0) - c_1)^2 \\
&= \alpha k_h^2(c_1 - c_0)^2 + (k_h - 1)^2(c_1 - c_0)^2 \\
&= \alpha k_h^2(c_1 - c_0)^2 - (k_h - 1)^2(c_1 - c_0)^2 \\
&= (c_1 - c_0)^2(\alpha k_h^2 - (k_h - 1)^2) \\
&= (c_1 - c_0)^2(\alpha k_h^2 - k_h^2 + 2k_h - 1) \\
&= (c_1 - c_0)^2(k_h^2(\alpha - 1) + 2k_h - 1) \\
&= (c_1 - c_0)^2\left(\left(\frac{1 - 2k_p}{k_p^2}\right)k_h^2 + 2k_h - 1\right) \\
\lambda_1 &= \frac{\mu(2\sqrt{2} + 4)}{(c_1 - c_0)^2\left(\left(\frac{1 - 2k_p}{k_p^2}\right)k_h^2 + 2k_h - 1\right)}
\end{aligned} \tag{1.30}$$

1.3 Experimental Results

Present and analyse the experimental results. The parameters α and λ_1 , in the proposed parameter estimation method, depend greatly on predicting good final means, c_0 and c_1 , for the ideal segmentation. It is rarely the case where this is known or can be calculated, if ever at all. Instead, we use the results from three popular unsupervised clustering algorithms and compare the final segmented result against a ground truth. The algorithms chosen to generate an initial mask, from which we calculate c_0 and c_1 are: *Otsu* [cite otsu here], *k*-means with $k = 2$ [cite k-means here] and Expectation Maximisation Gaussian Mixture Modelling (**EMGMM**) [cite EMGMM here]. From observations we see that these algorithms tend to generate over-segmented results. In light of this, we generate a fourth mask which is an EMGMM output with dilation. For dilation we used an elliptical shape with a radius of $3px$. We also compare our results to two previously published parameter settings. The first is the parameter settings used in [175], by El Zehiry *et al.*, which is where this technique was first published. Their results showed excellent segmentation ouptput on synthetic images and mammography images with very high robustness against noise. They do not specify the noise type. The second parameter setting which we test against is presented in [178], by Masaka *et al.*. Their parameter setting where based on a timelapse series of fluorescence images. Their scheme is a hybrid of algorithms design to segment whole fluorescent cells, however, we use the parameters settings they've presented for segmentation only. Their parameters were obtained by minimising the Jaccard coefficient over the timelapse series. Their results show a greater area of cell detection and smoother boundaries. Although, the smoother contours are a result of CED-ORI [cite cedorl] which is part of the scheme before segmentation.

The initial masks used in subsequent parameter estimation is shown in Figures 1.21, 1.23, 1.25, 1.27, 1.29, 1.31, 1.33, 1.35, 1.37, 1.39, 1.41, 1.43, 1.45, 1.47, 1.49, 1.51, 1.53, 1.55, 1.57, 1.59, 1.61, 1.63, 1.65, 1.67 and 1.69.

The segmented outputs are shown in Figures 1.22, 1.24, 1.26, 1.28, 1.30, 1.32, 1.34, 1.36, 1.38, 1.40, 1.42, 1.44, 1.46, 1.48, 1.50, 1.52, 1.54, 1.56, 1.58, 1.60, 1.62, 1.64, 1.66, 1.68 and 1.70.

The parameter settings and corresponding resutls are summarised in Table 1.7. The last column, labelled "*Diff*", is a measure of how far off the final means are from the ideal. It is calculated as

$$Diff = |c_0^{Final} - c_0^{Ideal}| + |c_1^{Final} - c_1^{Ideal}|.$$

In Table 1.7 differentiate between methods on the same image as follows:

[imageno]-[method],

where *imageno* goes from 1 to 25 and *method* is defined as follows:

n - using parameter setting presented in [175].

m - using parameter setting presented in [178].

o - Proposed method with parameters estimated from an initial Otsu segmentation.

k - Proposed method with parameters estimated from an initial K-means segmentation with $k = 2$.

e - Proposed method with parameters estimated from an initial EMGMM segmentation with $k = 2$.

d - Proposed method with parameters estimated from an initial EMGMM segmentation with $k = 2$ and an elliptical dilation of $3px$.

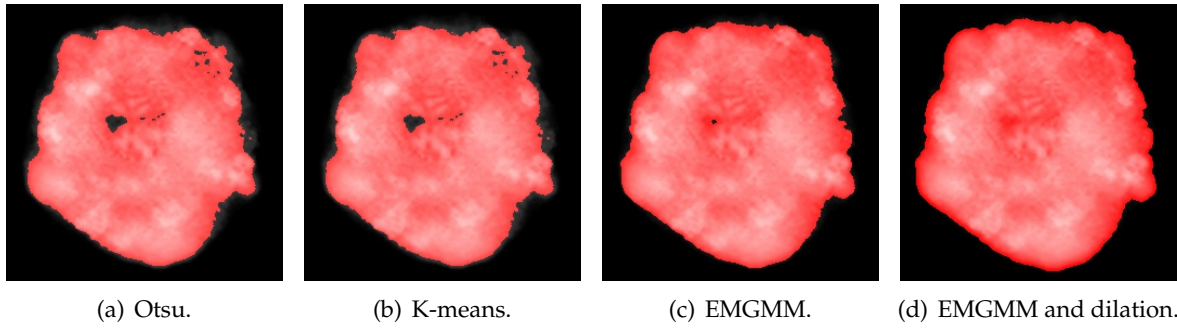


FIGURE 1.21: Image 1 from test set Appendix A initial masks.

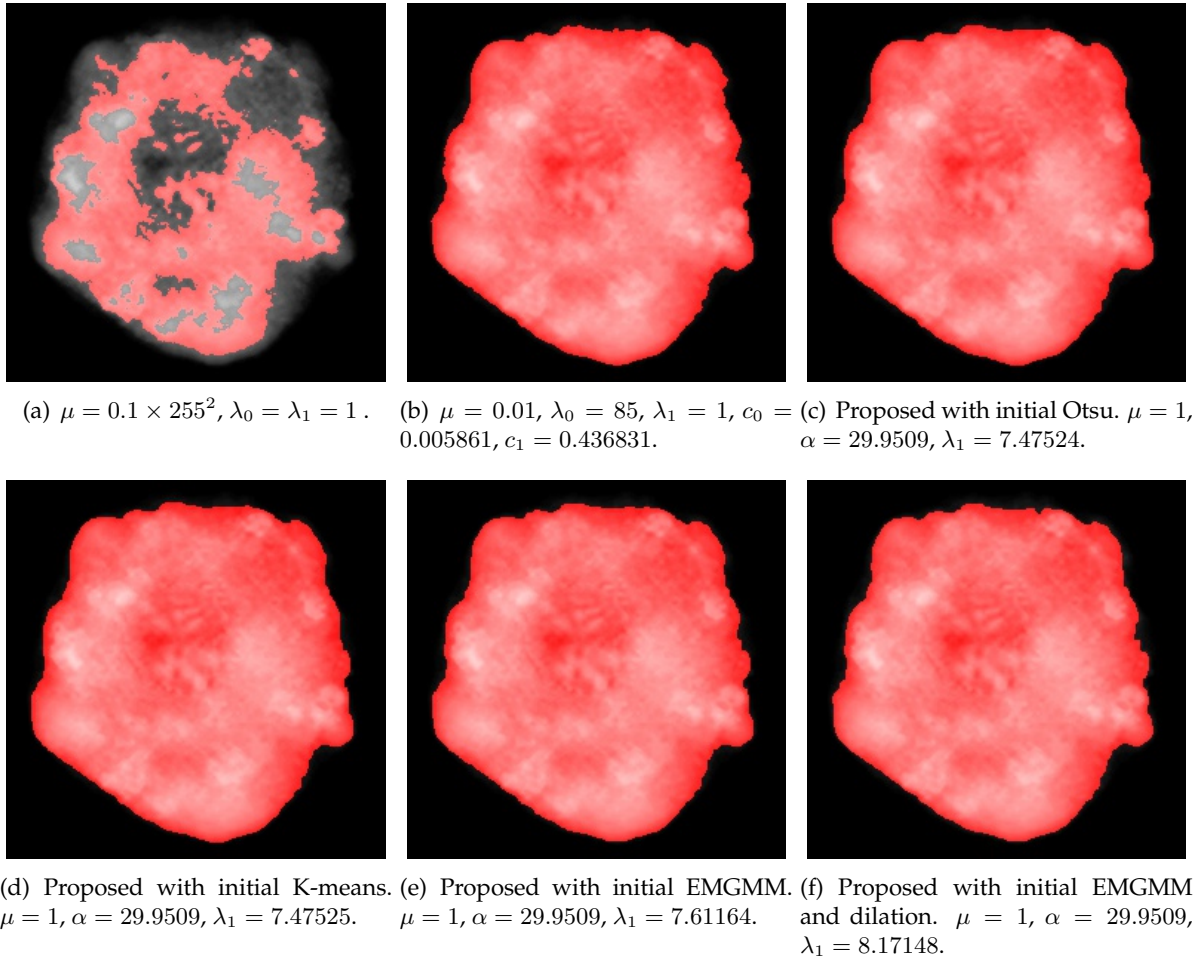


FIGURE 1.22: Image 1 from test set Appendix A segmentation results.

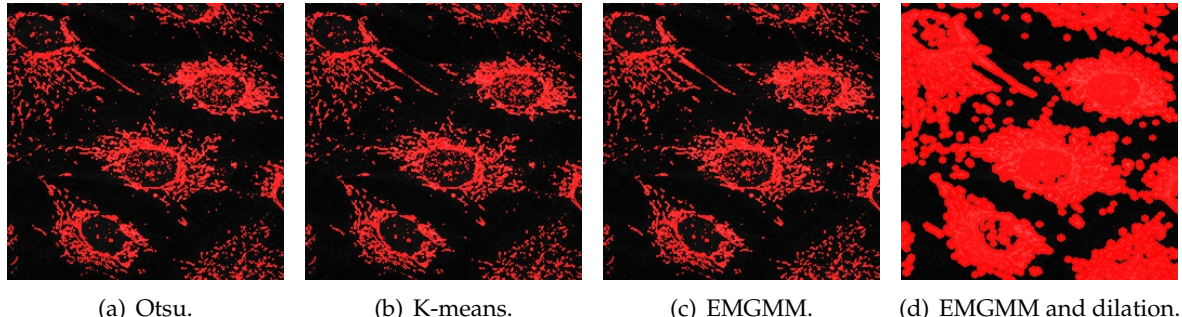


FIGURE 1.23: Image 2 from test set Appendix A initial masks.

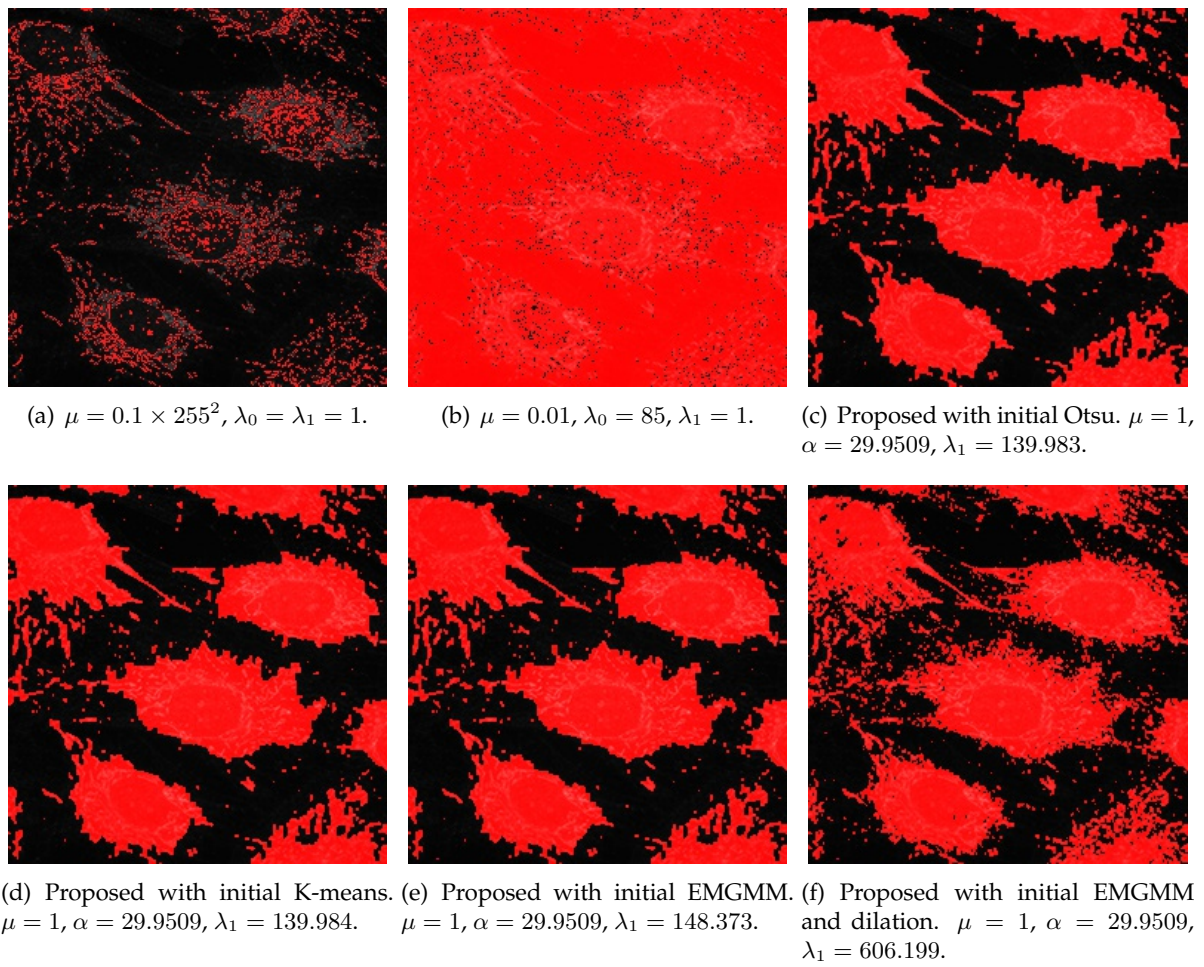


FIGURE 1.24: Image 2 from test set Appendix A segmentation results.

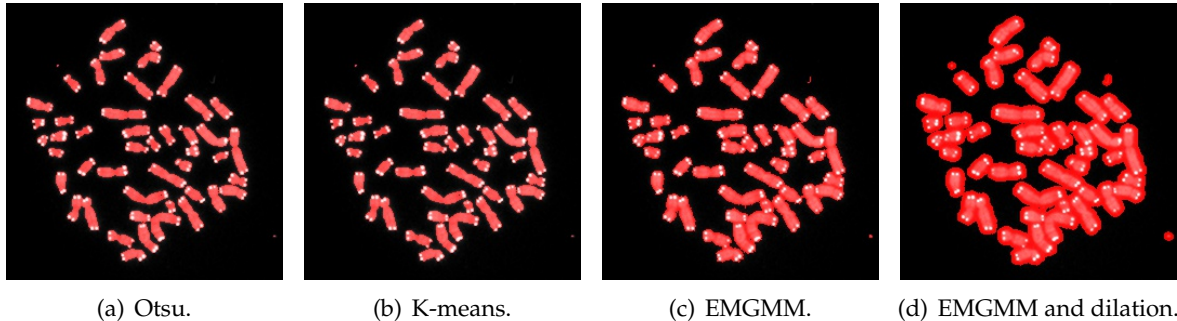


FIGURE 1.25: Image 3 from test set Appendix A initial masks.

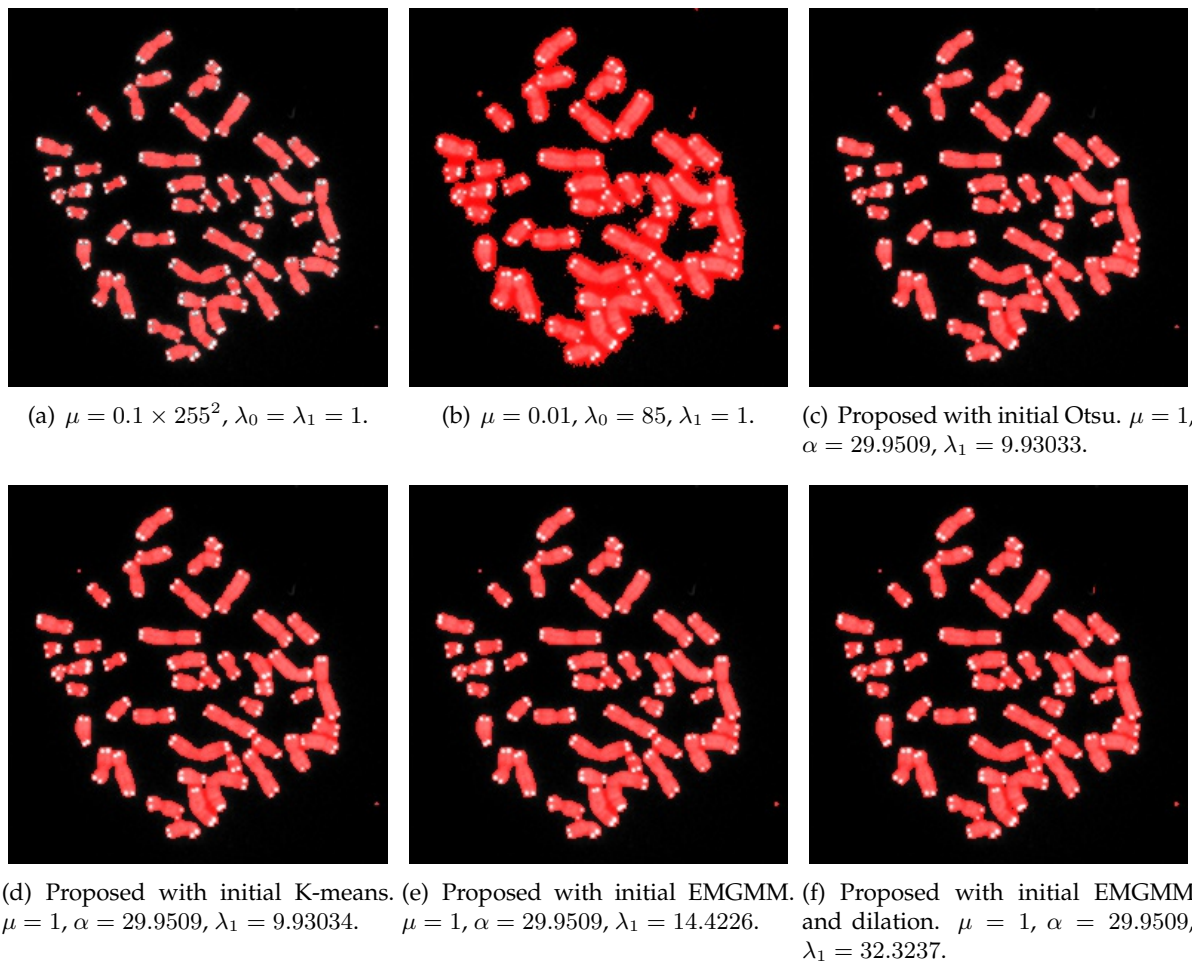


FIGURE 1.26: Image 3 from test set Appendix A segmentation results.

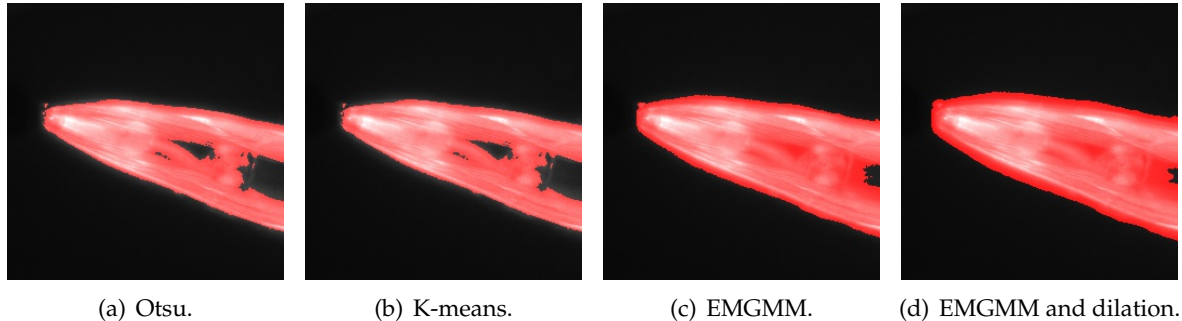


FIGURE 1.27: Image 4 from test set Appendix A initial masks.

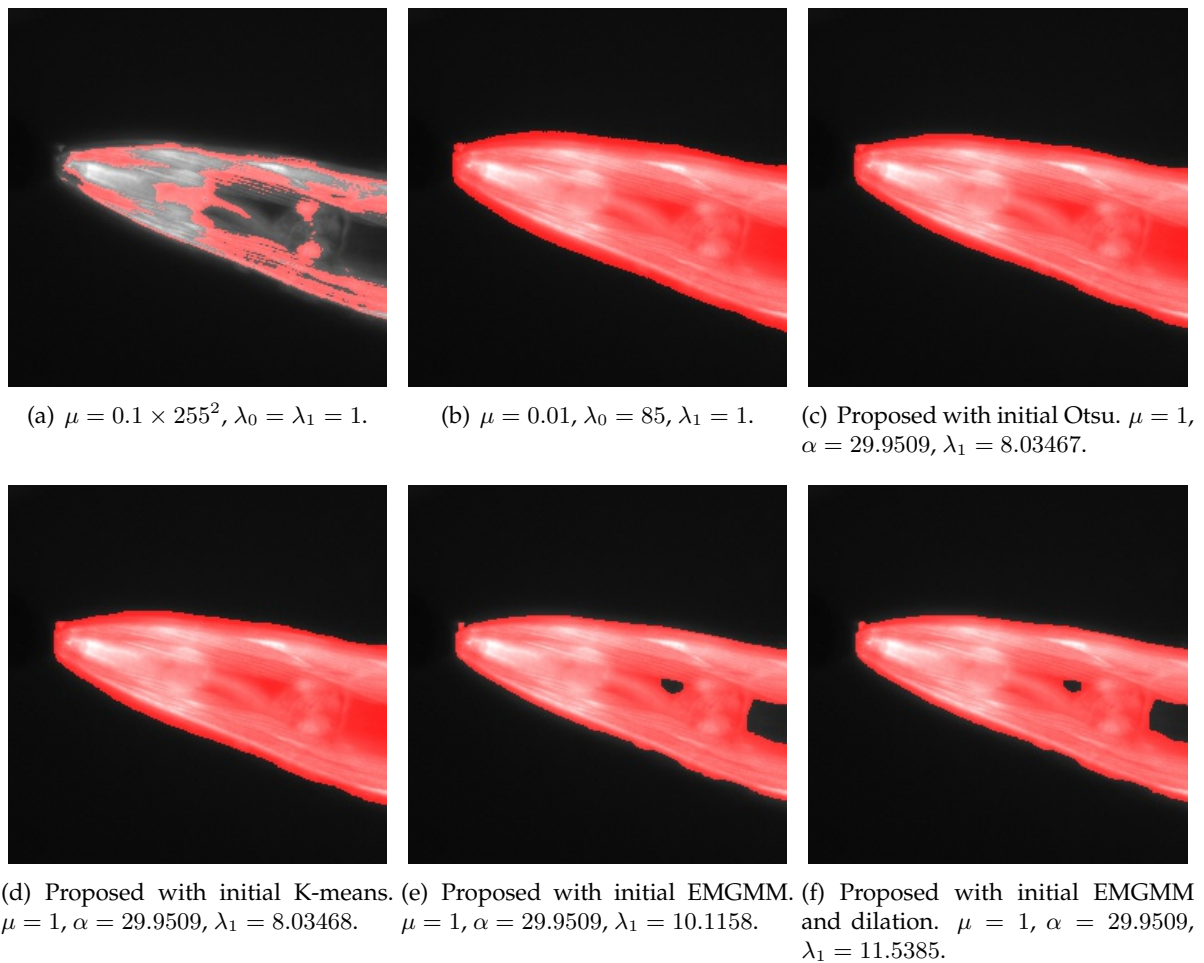


FIGURE 1.28: Image 4 from test set Appendix A segmentation results.

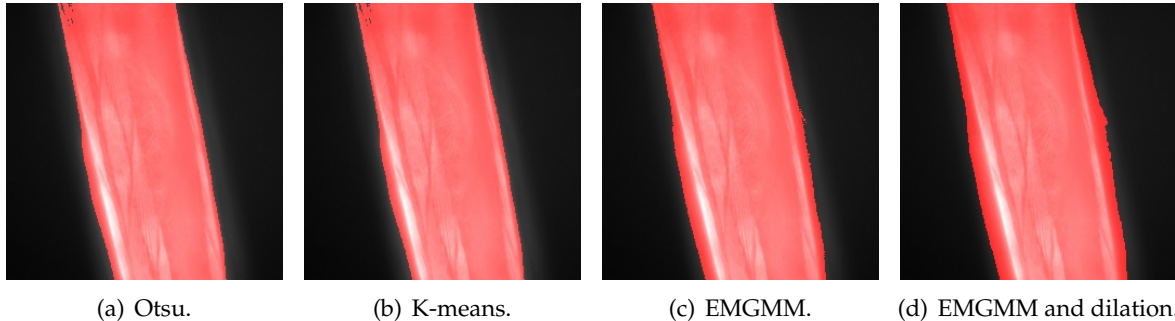


FIGURE 1.29: Image 5 from test set Appendix A initial masks.

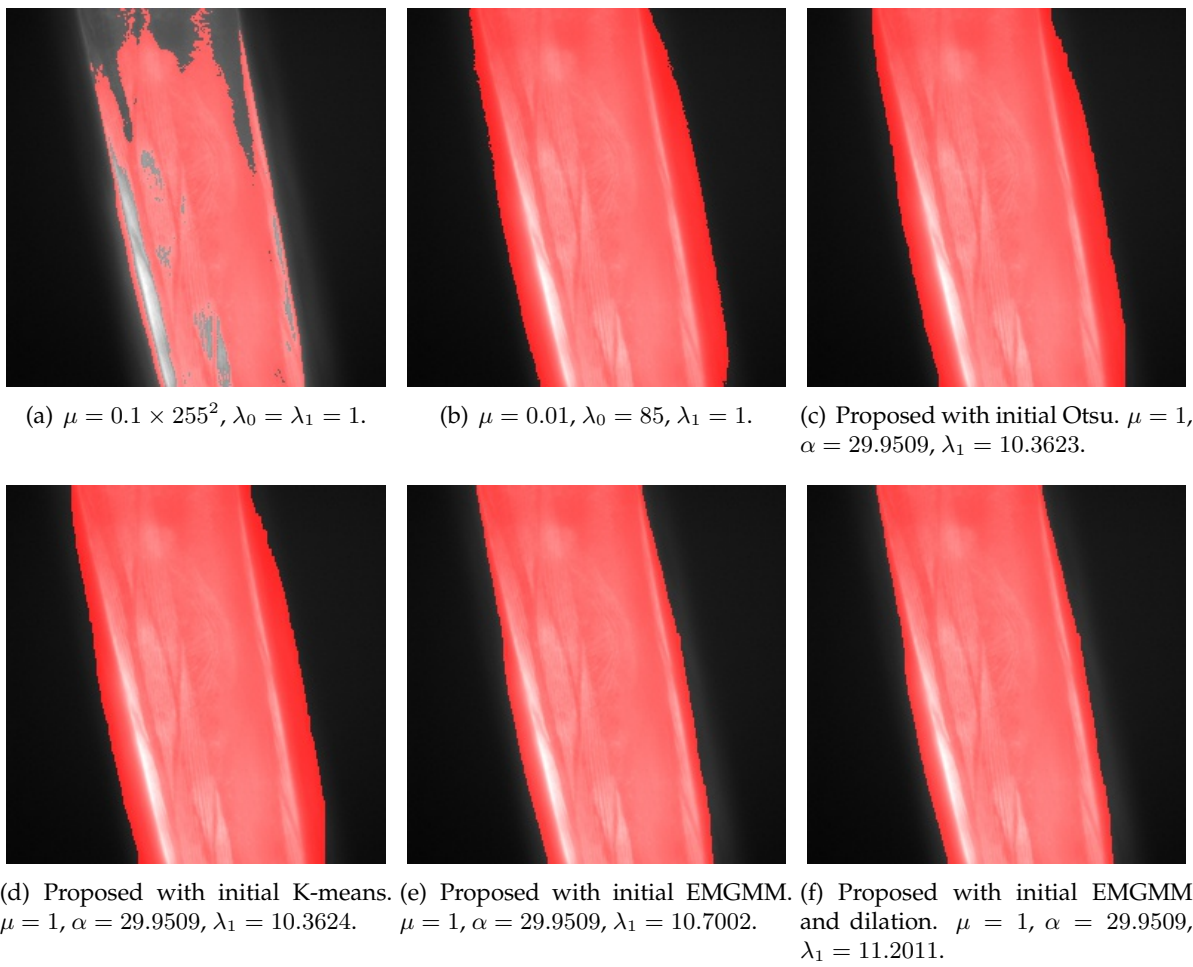


FIGURE 1.30: Image 5 from test set Appendix A segmentation results.

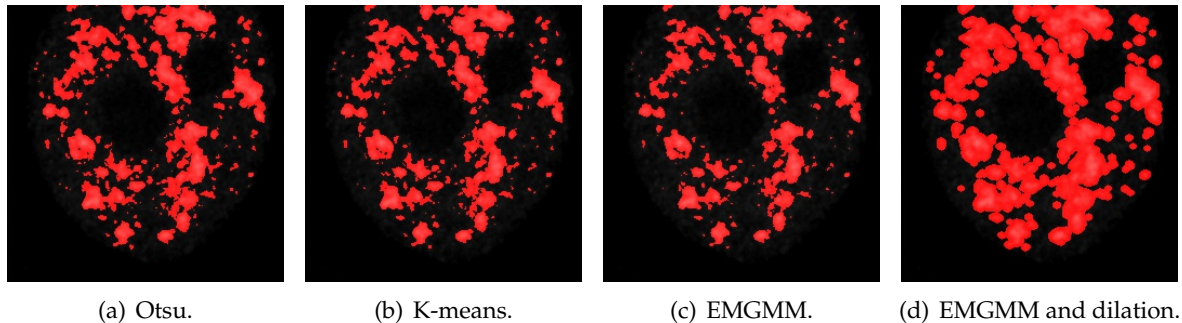


FIGURE 1.31: Image 6 from test set Appendix A initial masks.

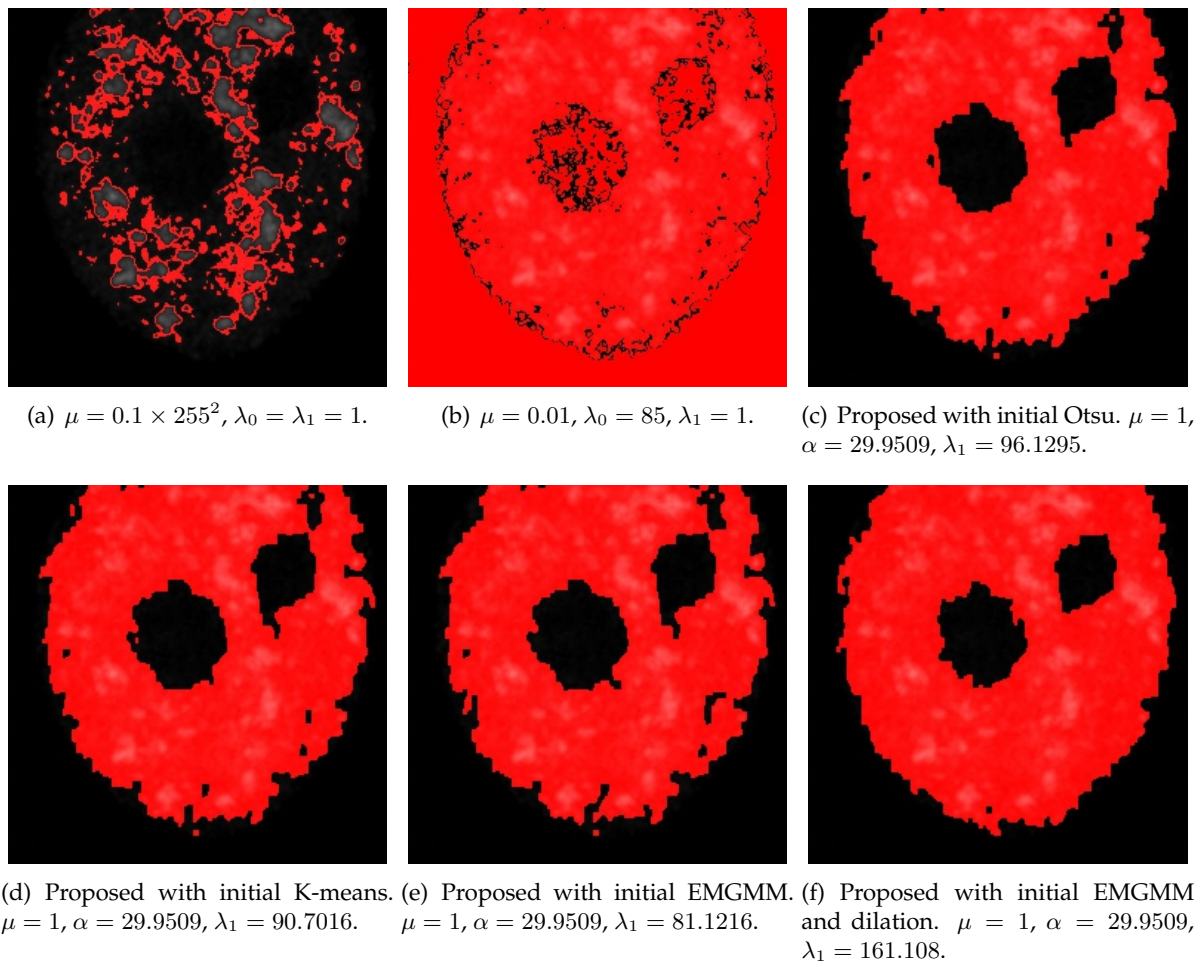


FIGURE 1.32: Image 6 from test set Appendix A segmentation results.

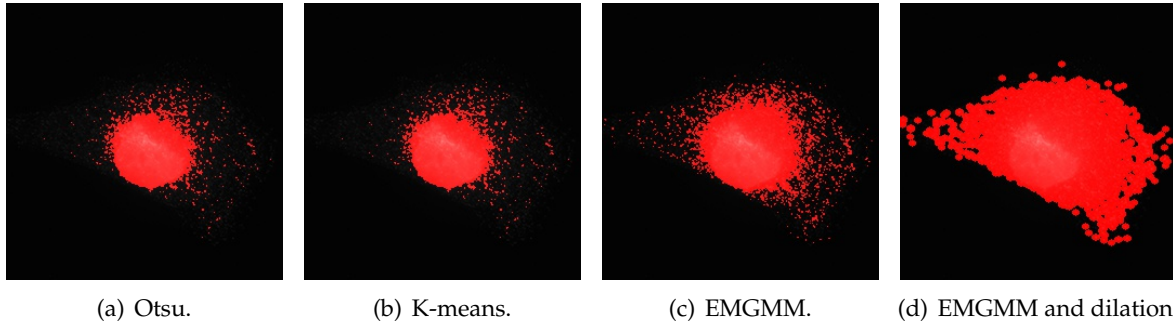


FIGURE 1.33: Image 7 from test set Appendix A initial masks.

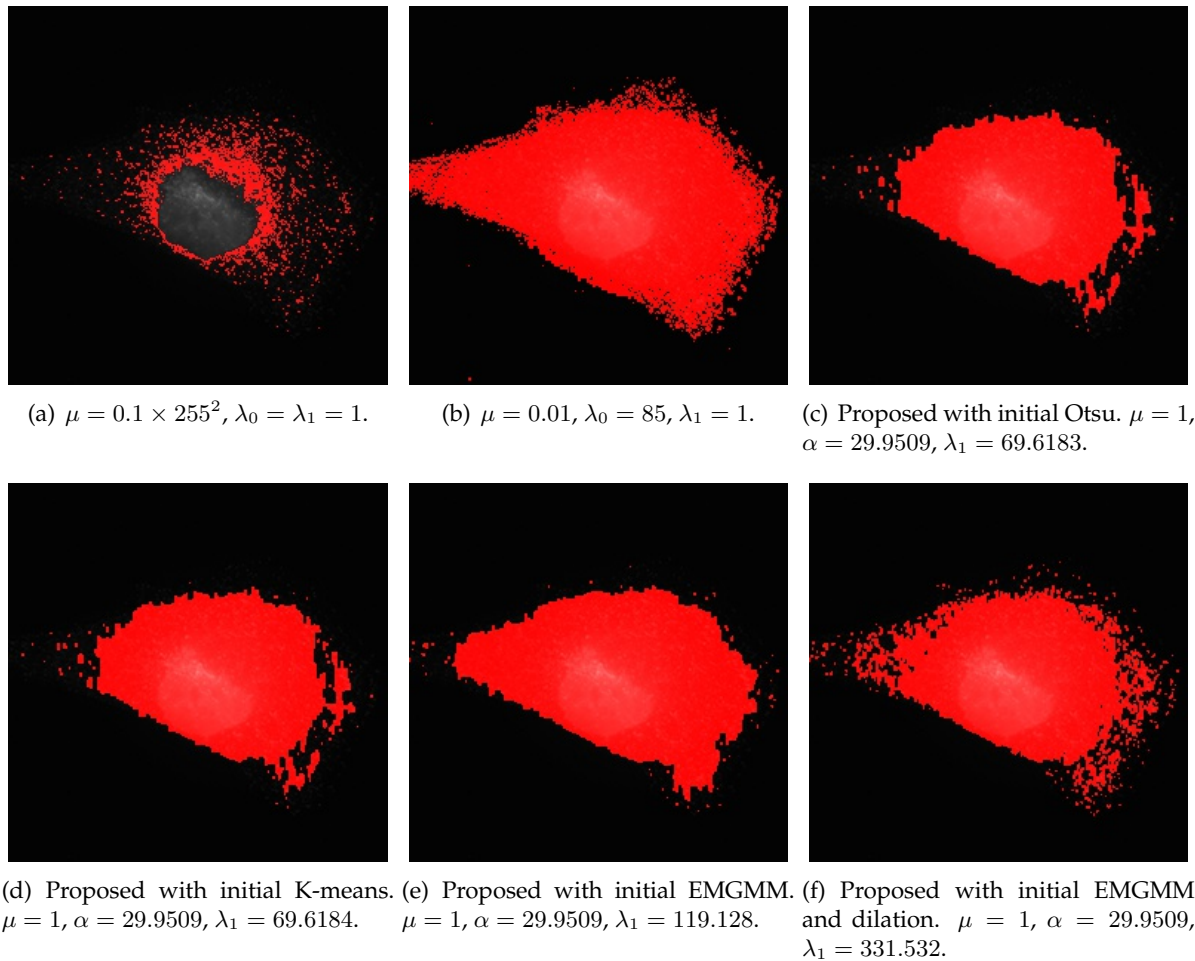


FIGURE 1.34: Image 7 from test set Appendix A segmentation results.

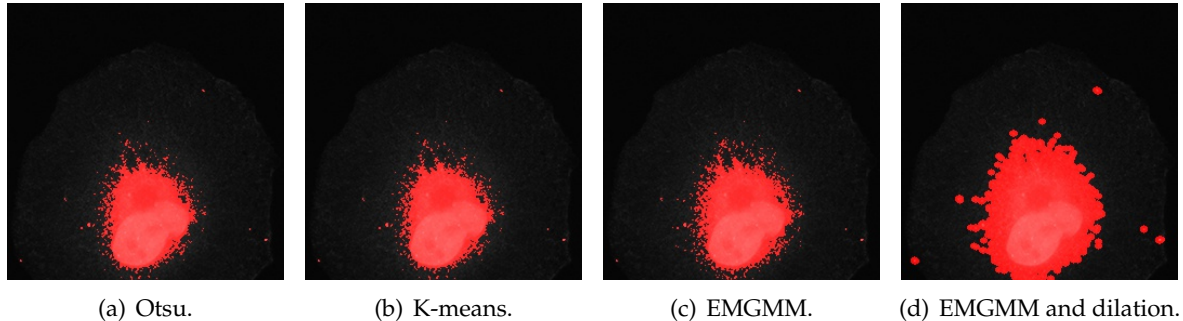


FIGURE 1.35: Image 8 from test set Appendix A initial masks.

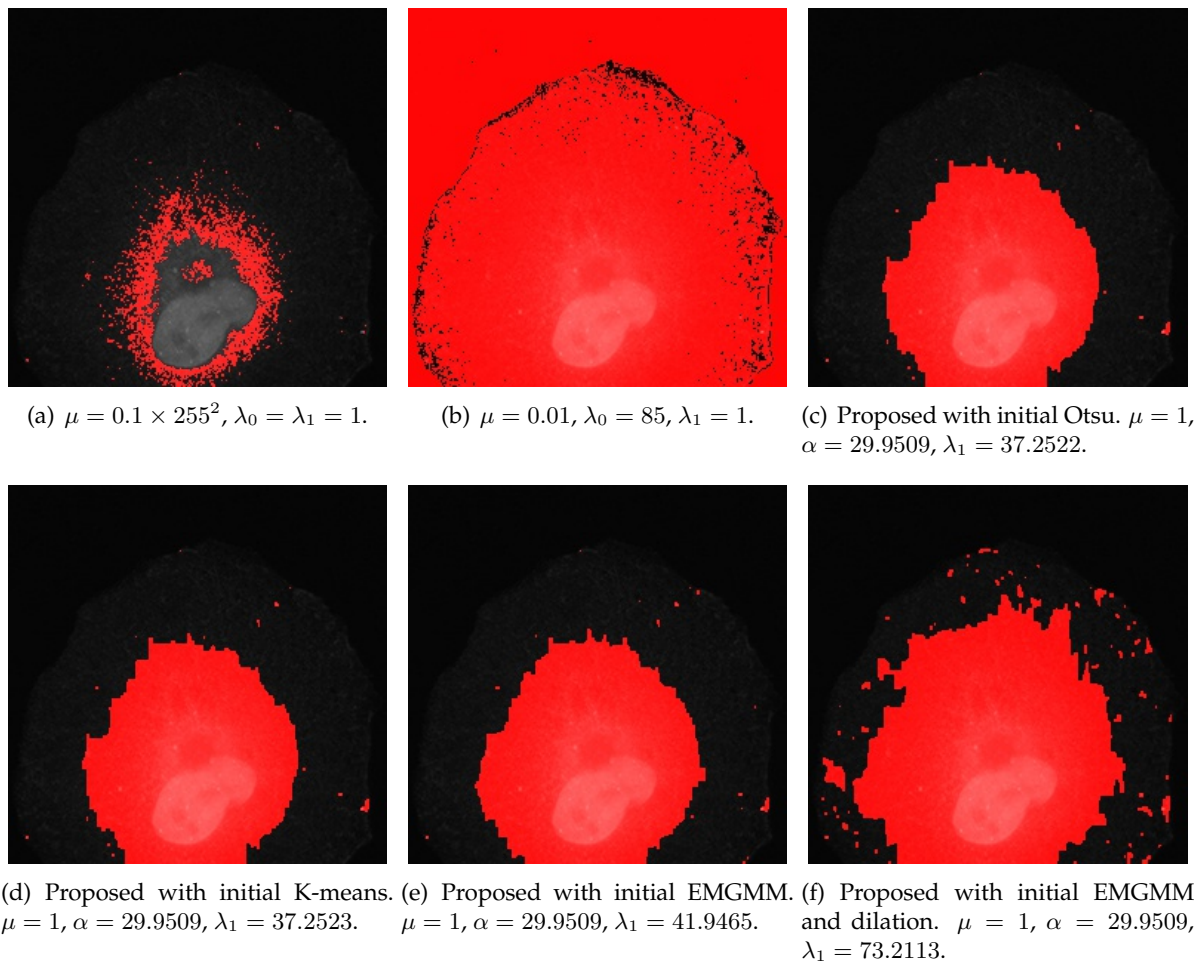


FIGURE 1.36: Image 8 from test set Appendix A segmentation results.

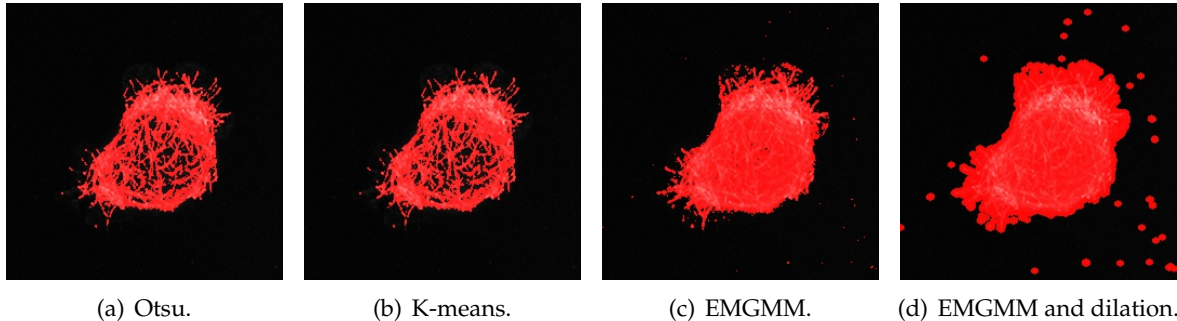


FIGURE 1.37: Image 9 from test set Appendix A initial masks.

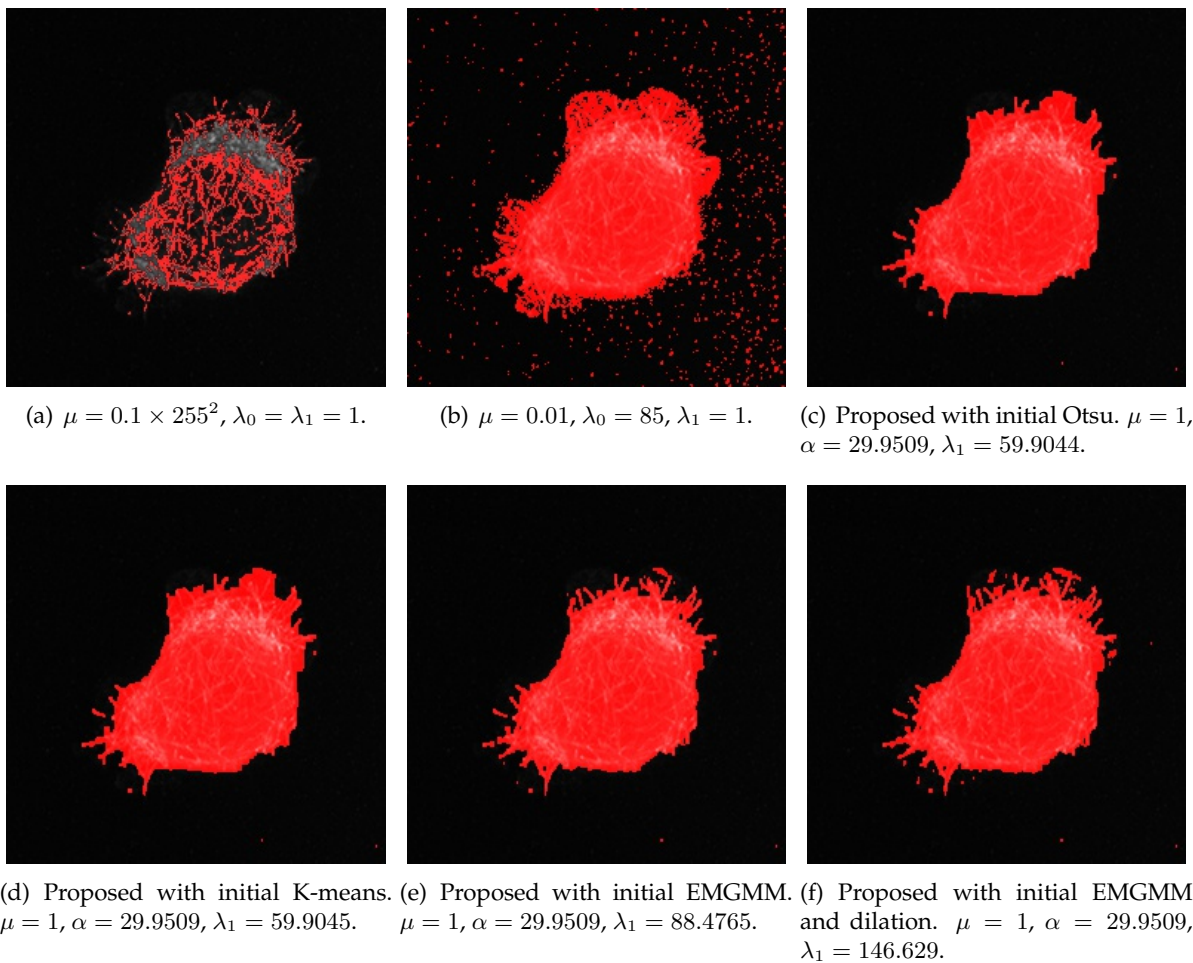


FIGURE 1.38: Image 9 from test set Appendix A segmentation results.

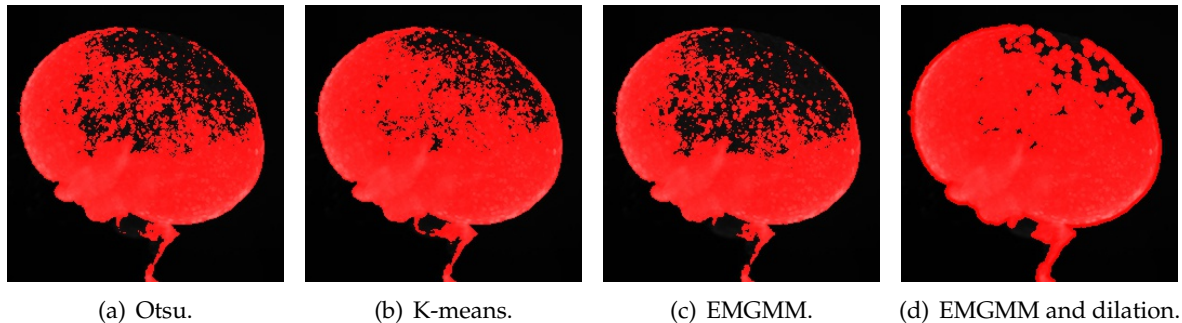


FIGURE 1.39: Image 10 from test set Appendix A initial masks.

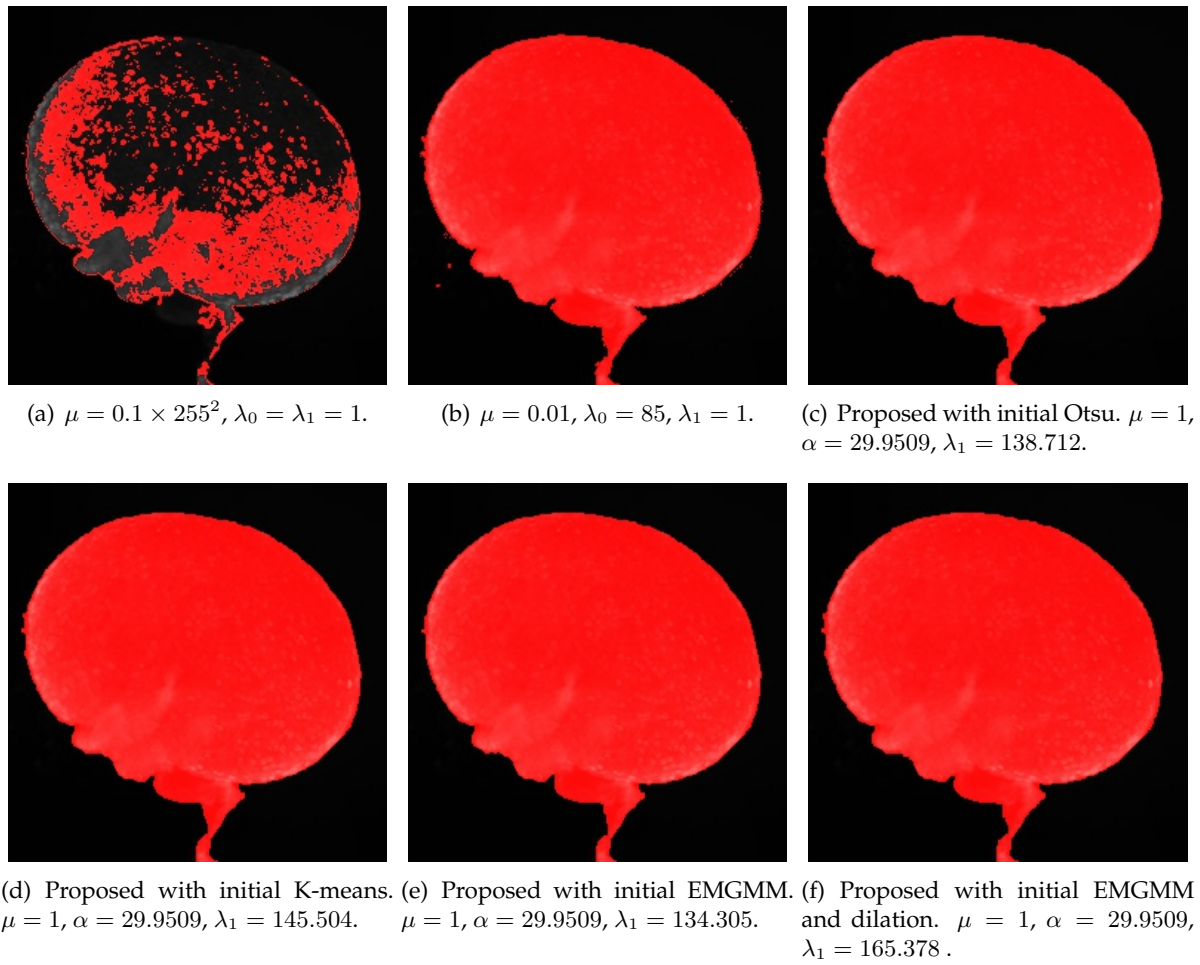


FIGURE 1.40: Image 10 from test set Appendix A segmentation results.

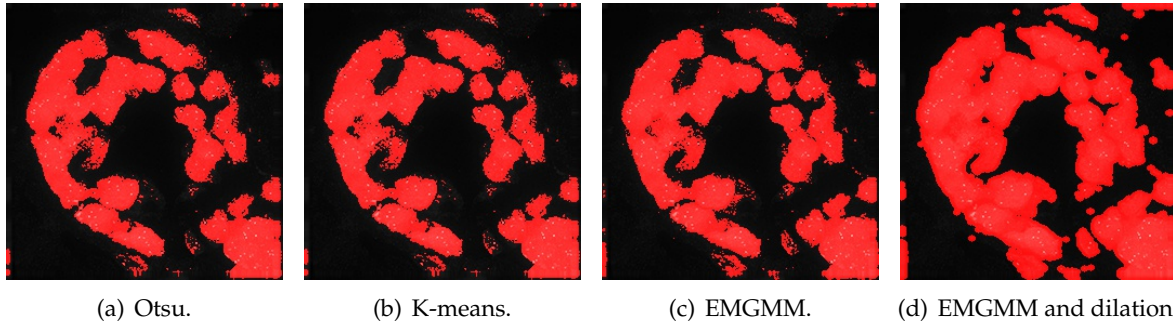


FIGURE 1.41: Image 11 from test set Appendix A initial masks.

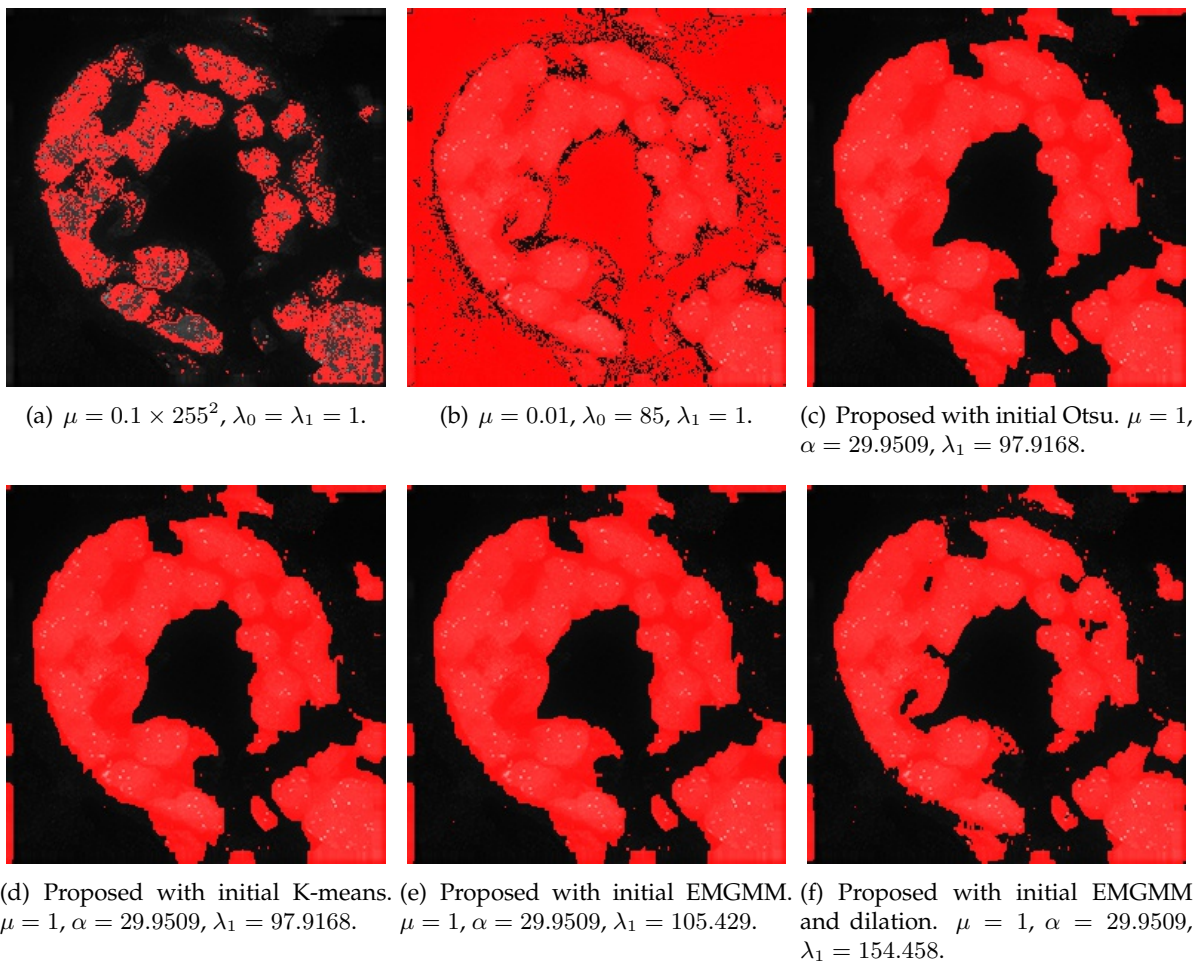


FIGURE 1.42: Image 11 from test set Appendix A segmentation results.

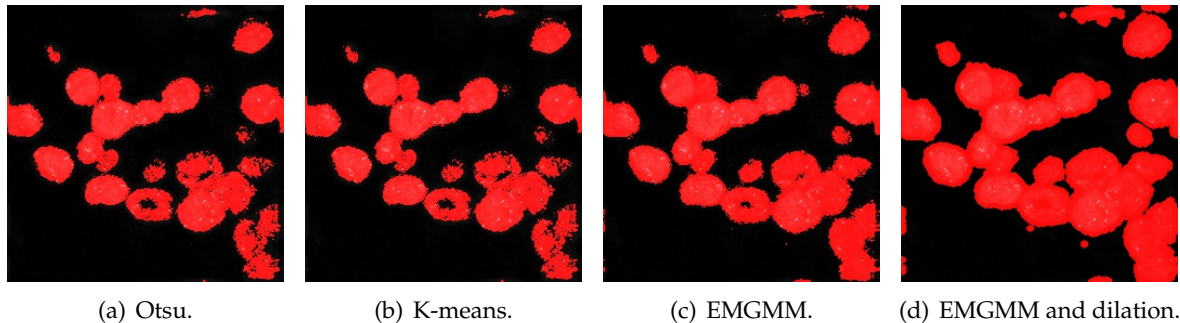


FIGURE 1.43: Image 12 from test set Appendix A initial masks.

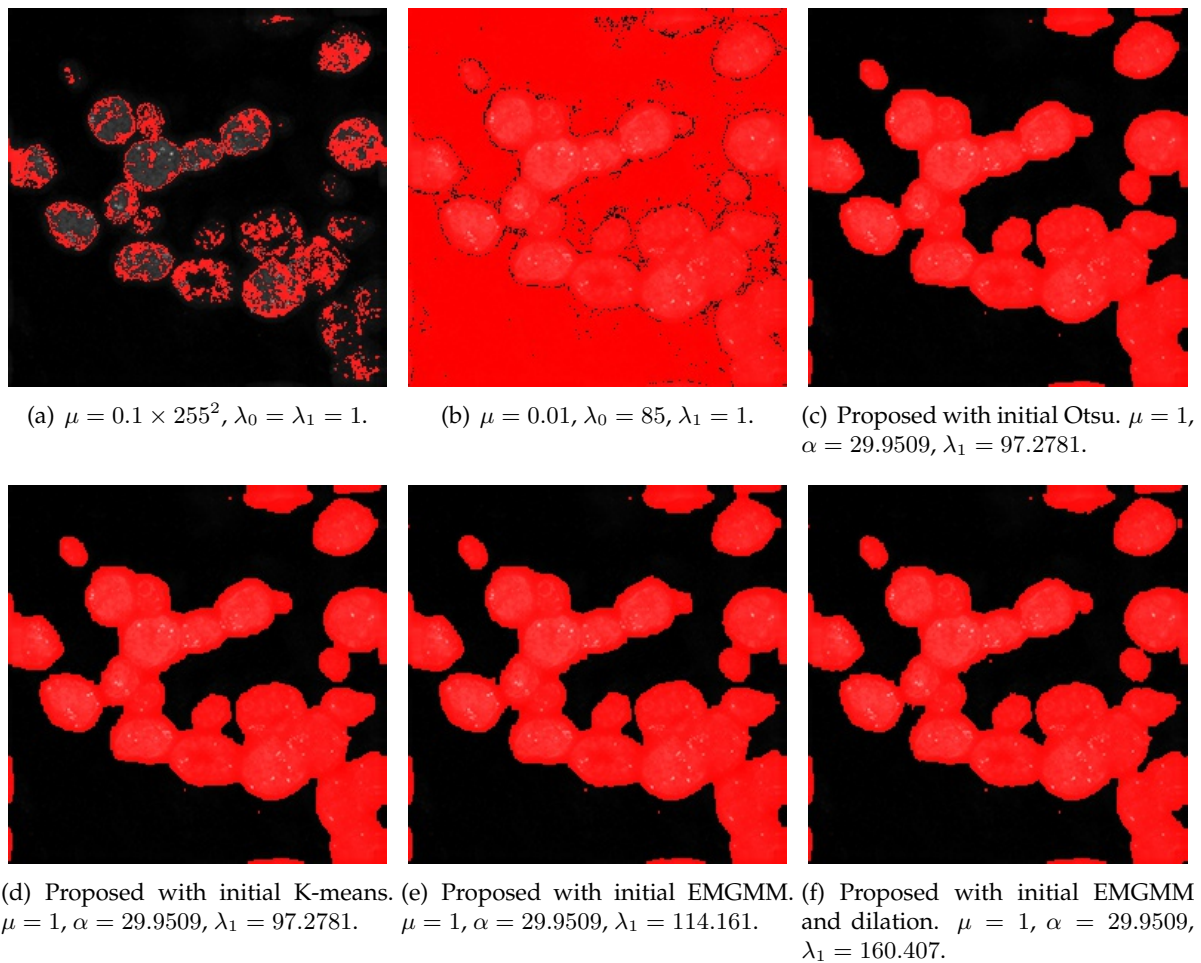


FIGURE 1.44: Image 12 from test set Appendix A segmentation results.

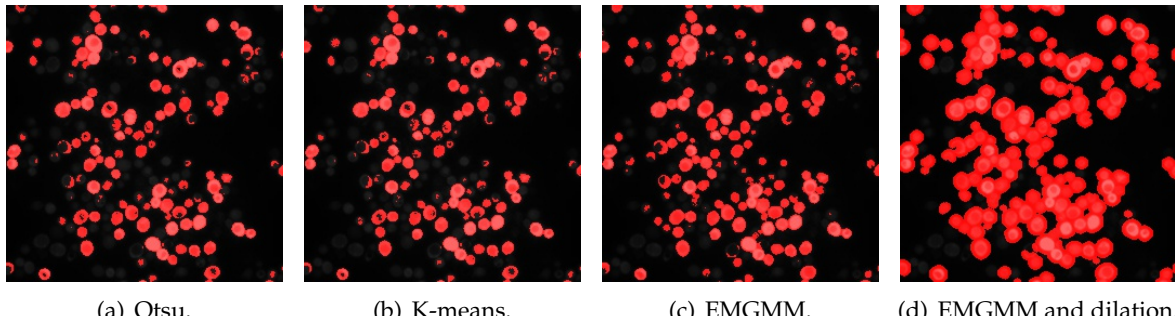


FIGURE 1.45: Image 13 from test set Appendix A initial masks.

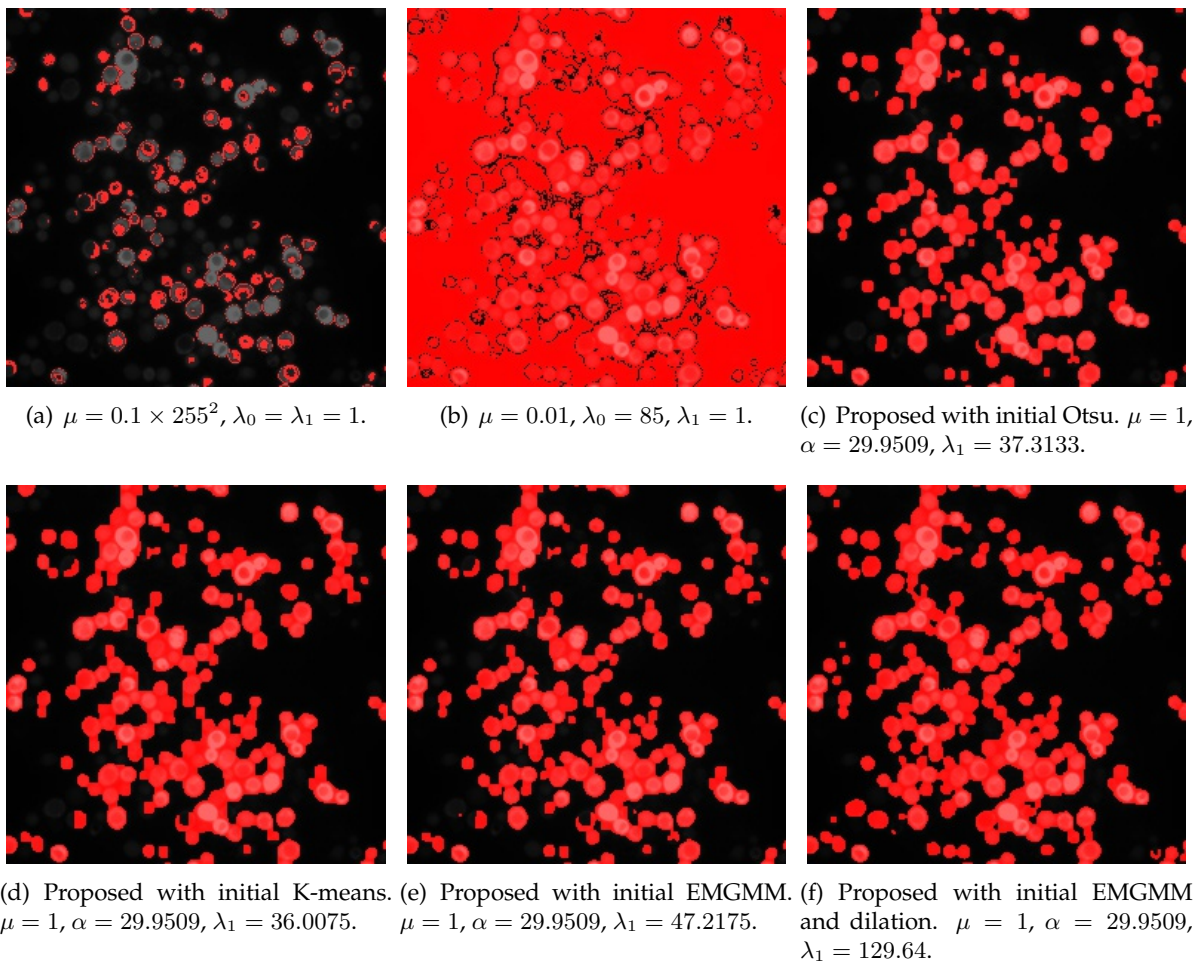


FIGURE 1.46: Image 13 from test set Appendix A segmentation results.

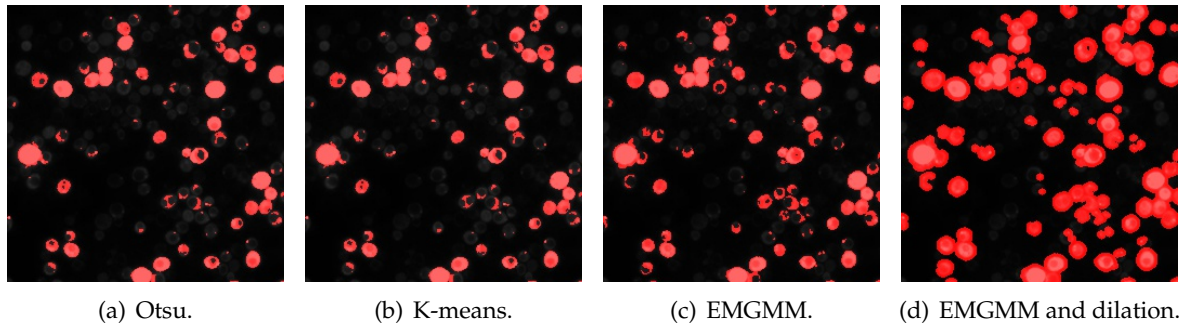


FIGURE 1.47: Image 14 from test set Appendix A initial masks.

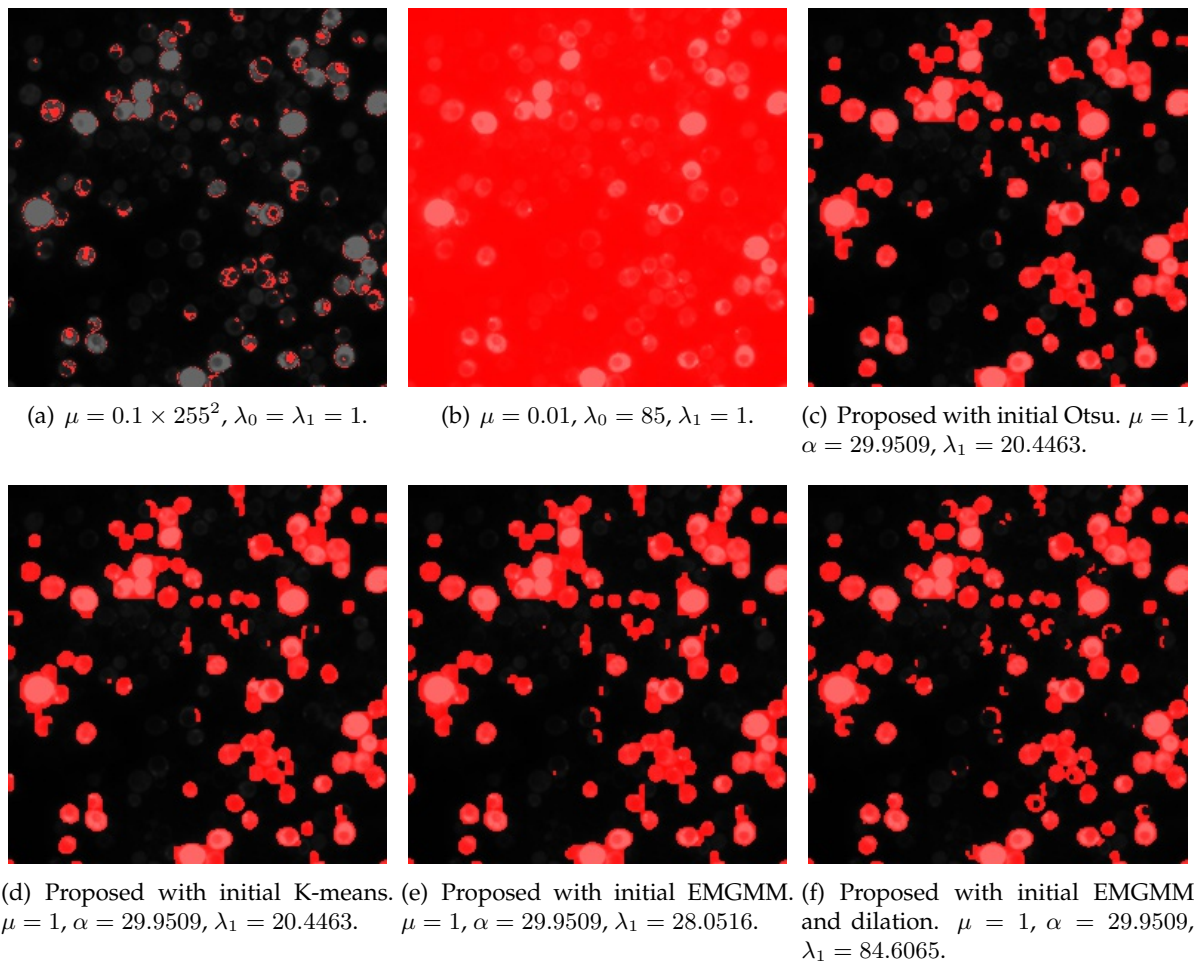


FIGURE 1.48: Image 14 from test set Appendix A segmentation results.

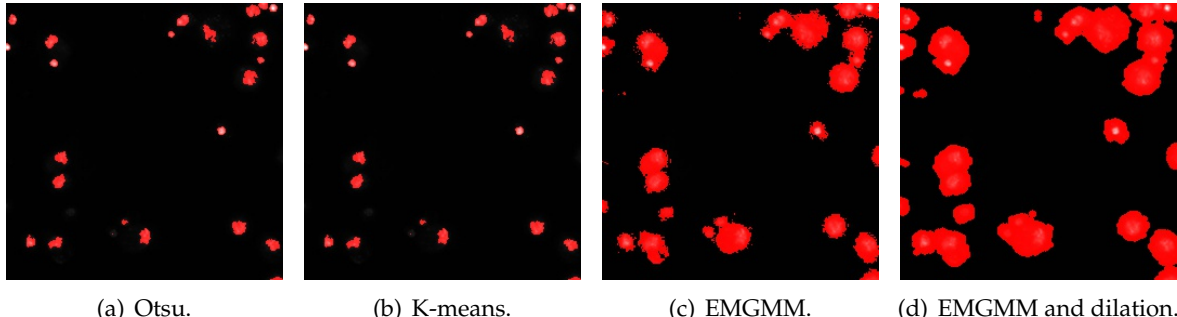


FIGURE 1.49: Image 15 from test set Appendix A initial masks.

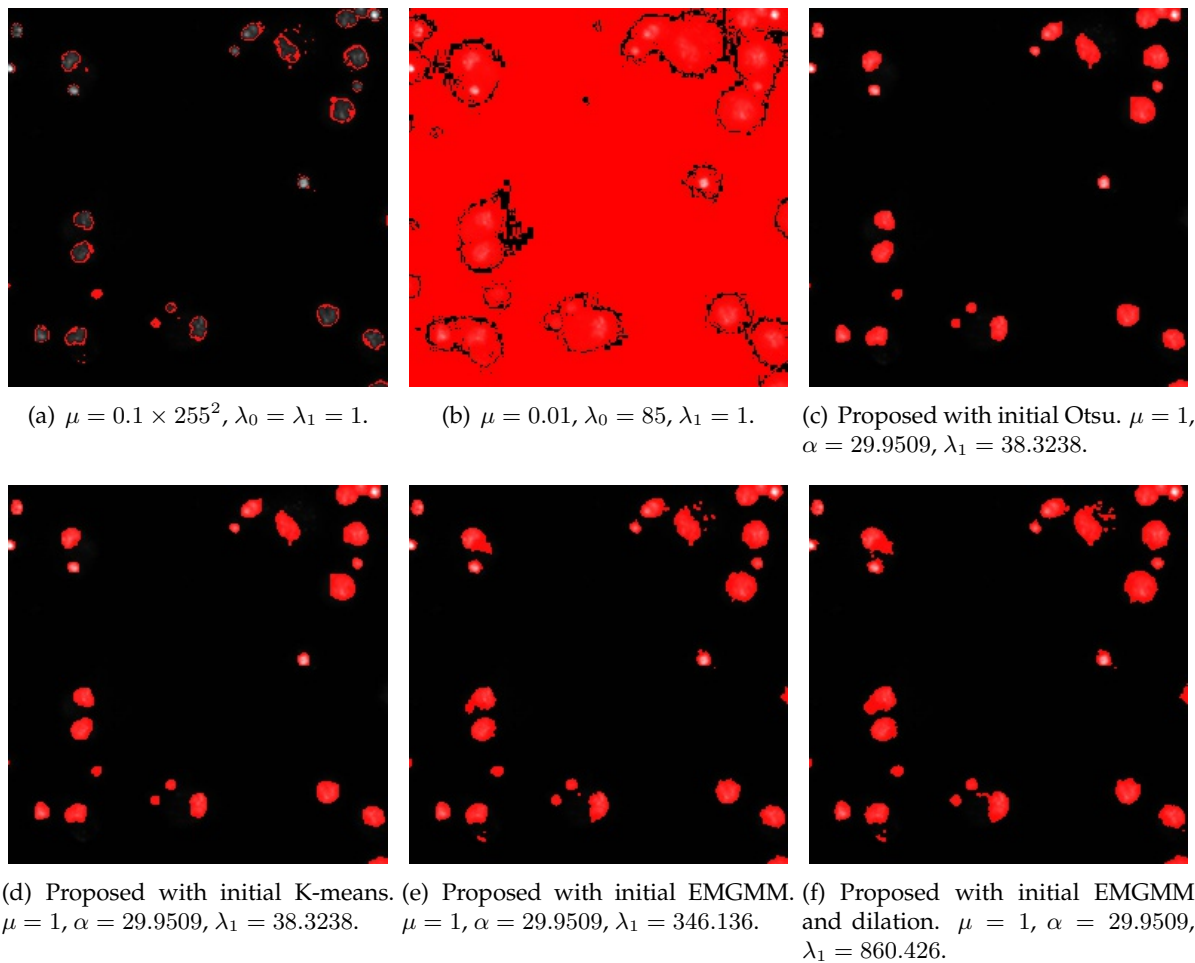


FIGURE 1.50: Image 15 from test set Appendix A segmentation results.

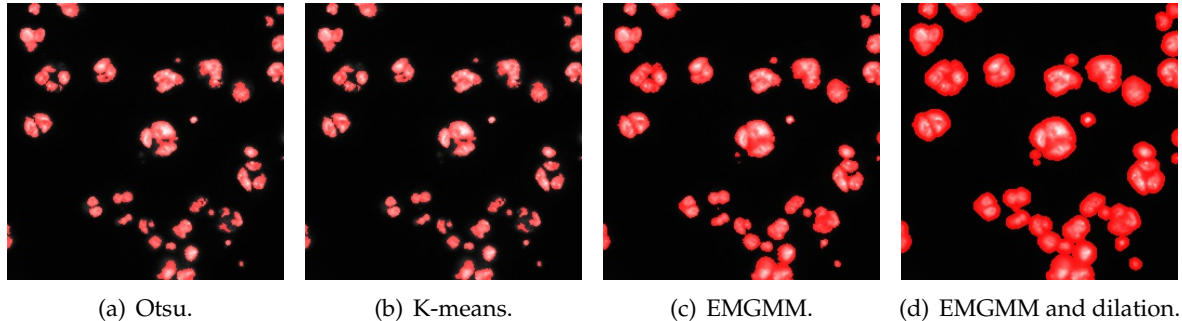


FIGURE 1.51: Image 16 from test set Appendix A initial masks.

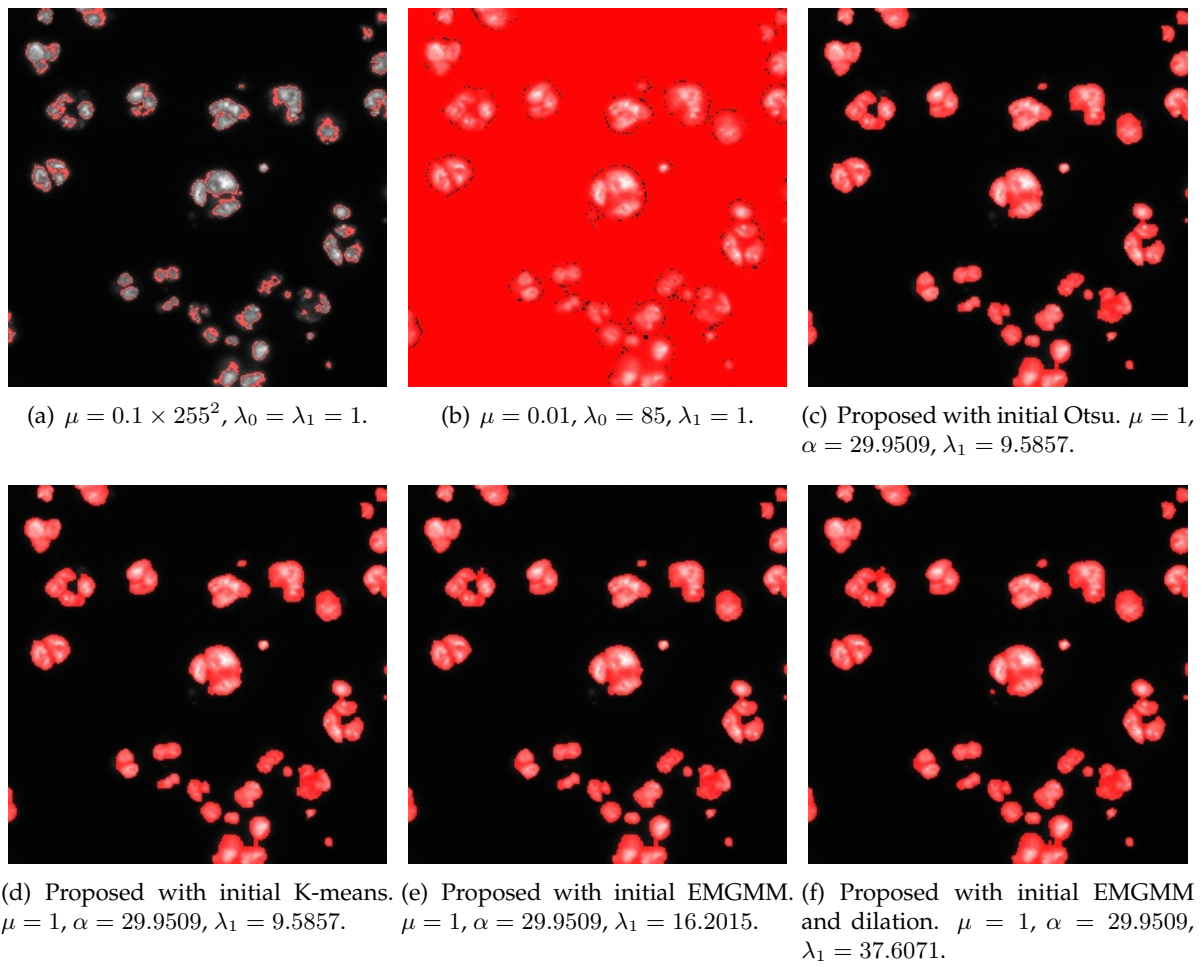


FIGURE 1.52: Image 16 from test set Appendix A segmentation results.

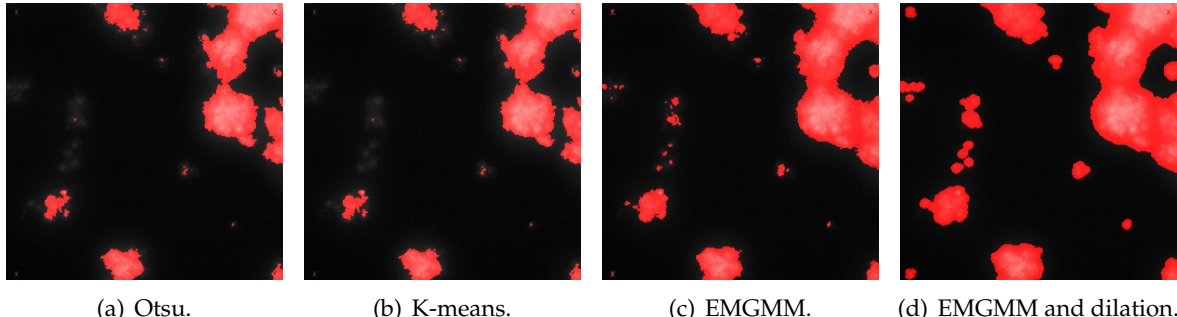


FIGURE 1.53: Image 17 from test set Appendix A initial masks.

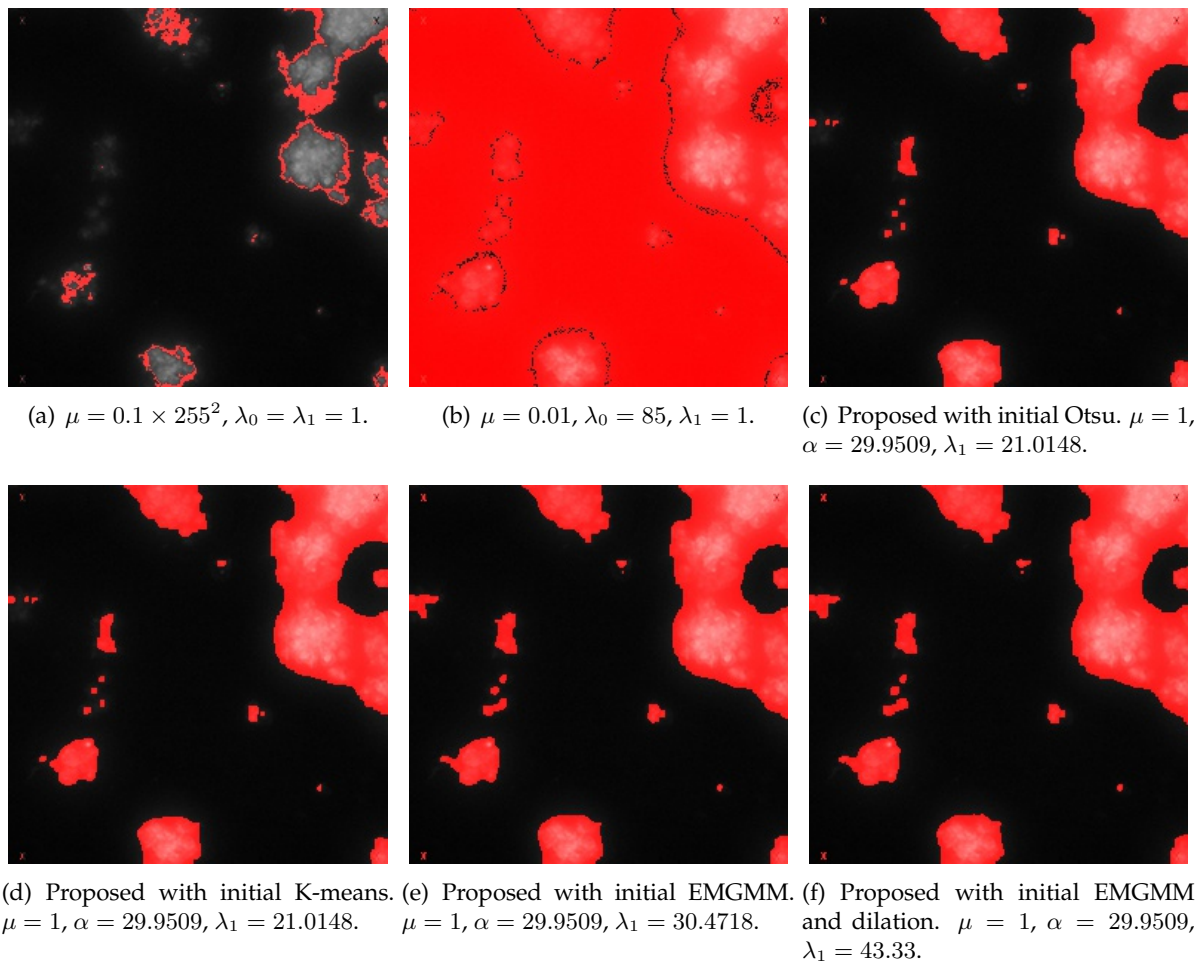


FIGURE 1.54: Image 17 from test set Appendix A segmentation results.

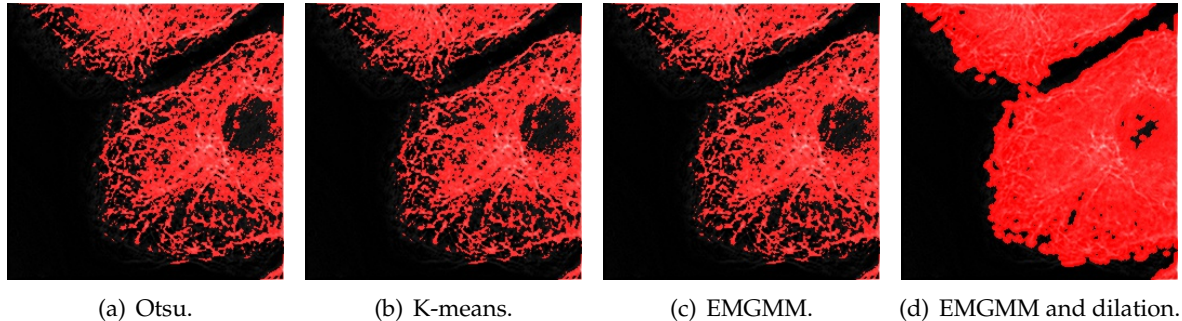


FIGURE 1.55: Image 18 from test set Appendix A initial masks.

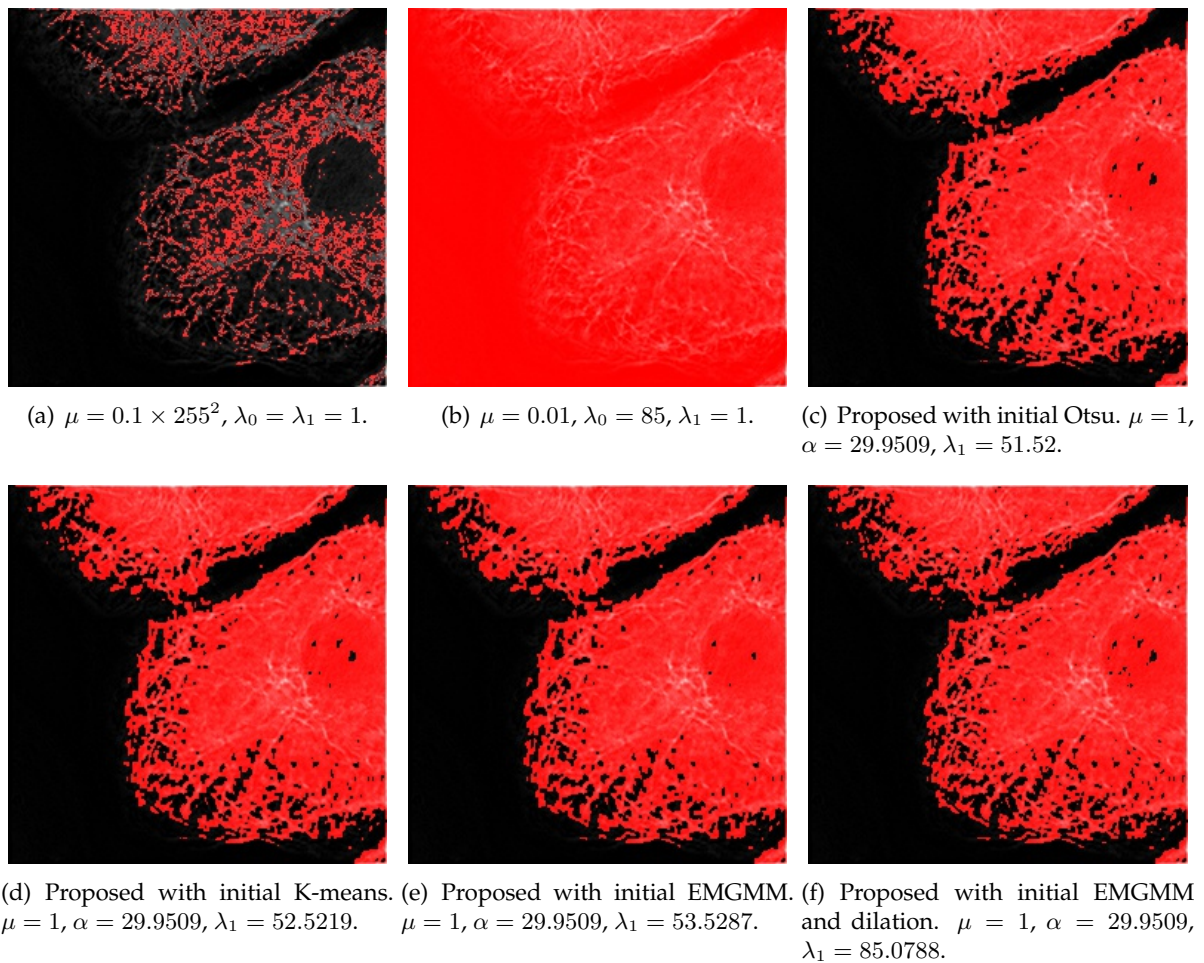


FIGURE 1.56: Image 18 from test set Appendix A segmentation results.

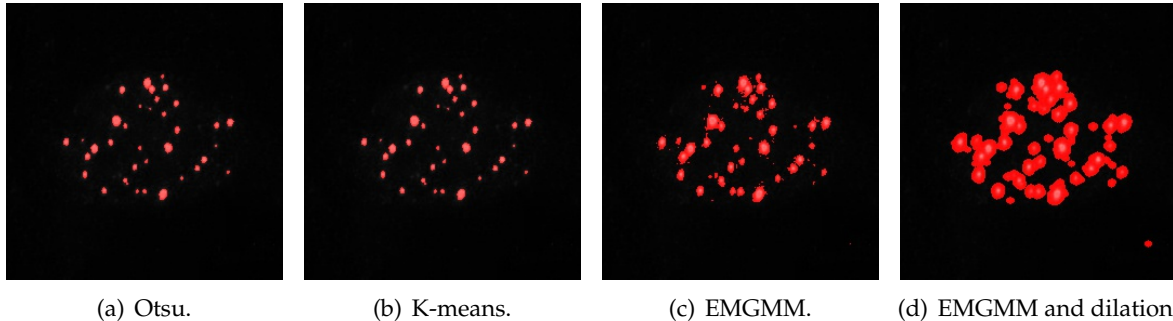


FIGURE 1.57: Image 19 from test set Appendix A initial masks.

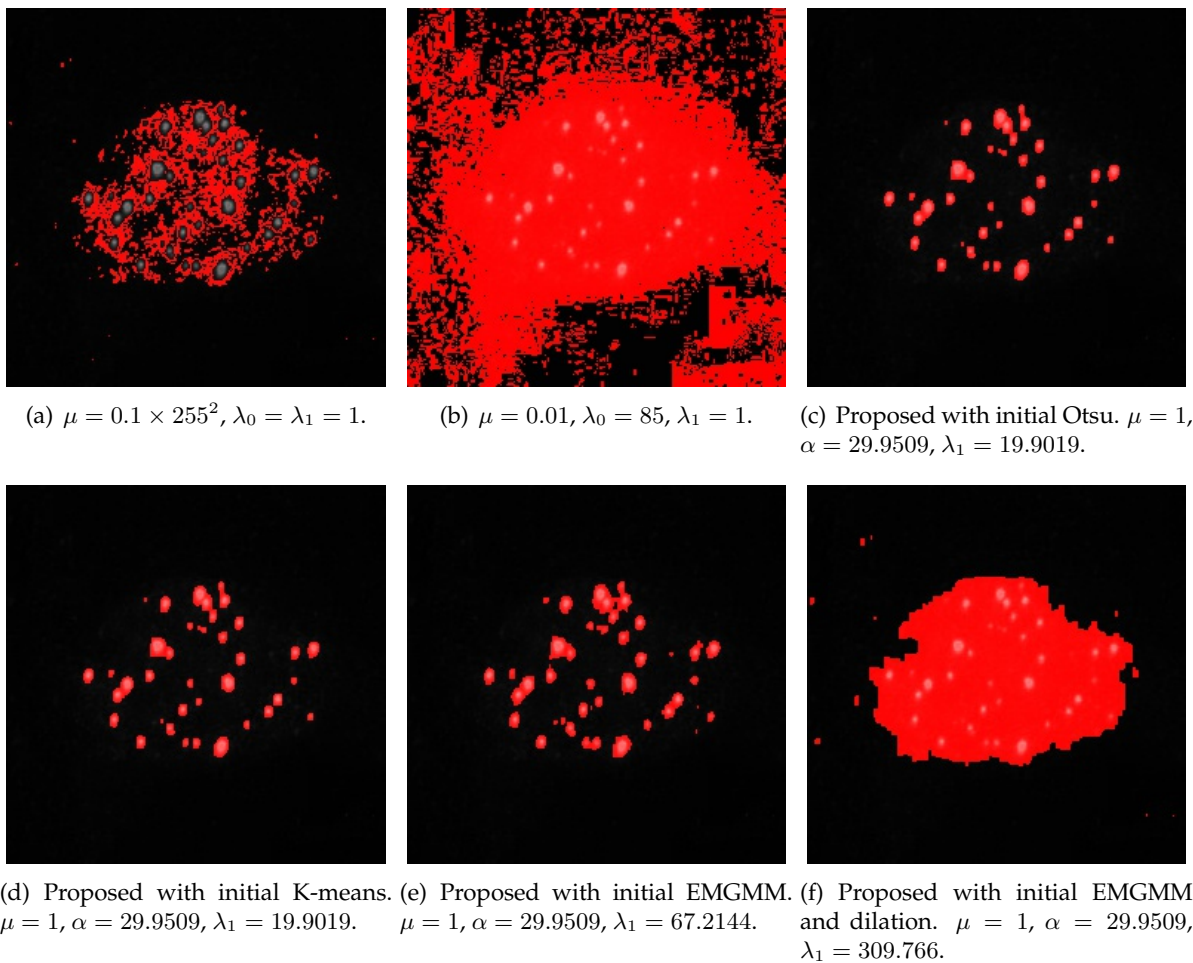


FIGURE 1.58: Image 19 from test set Appendix A segmentation results.

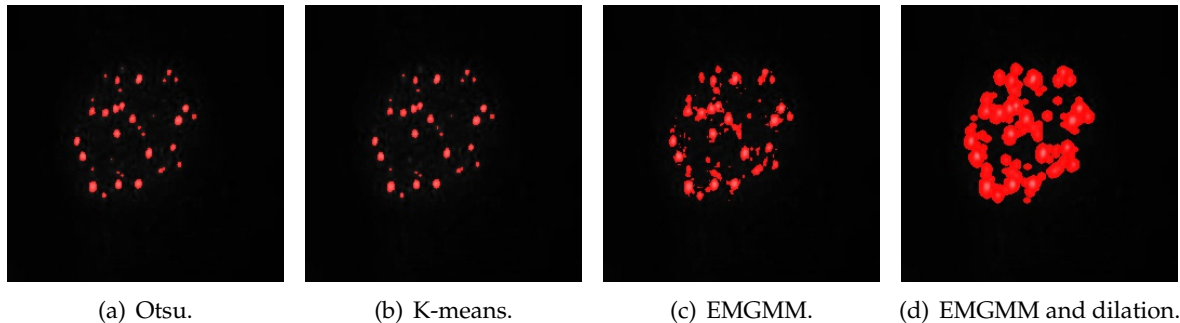


FIGURE 1.59: Image 20 from test set Appendix A initial masks.

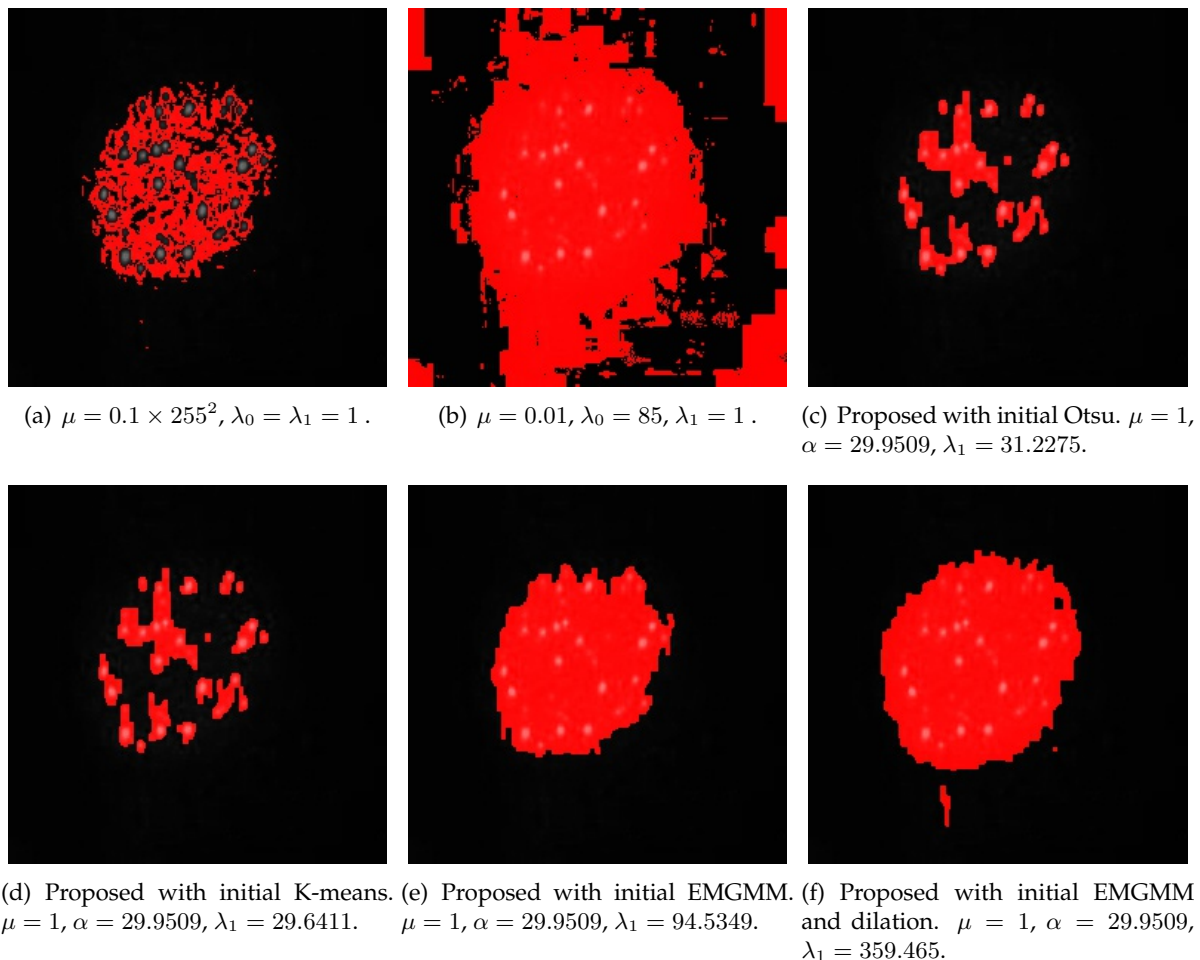


FIGURE 1.60: Image 20 from test set Appendix A segmentation results.

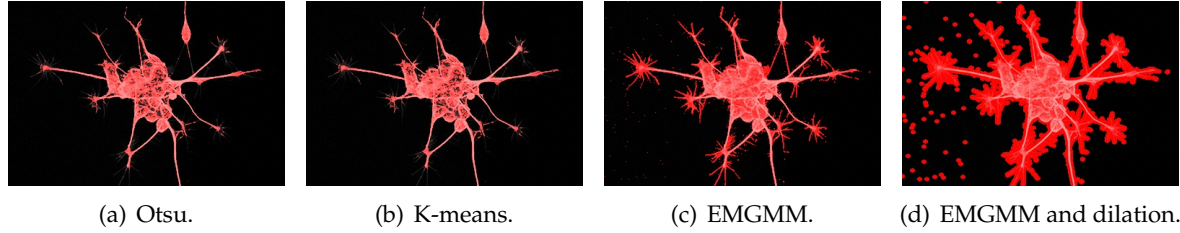


FIGURE 1.61: Image 21 from test set Appendix A initial masks.

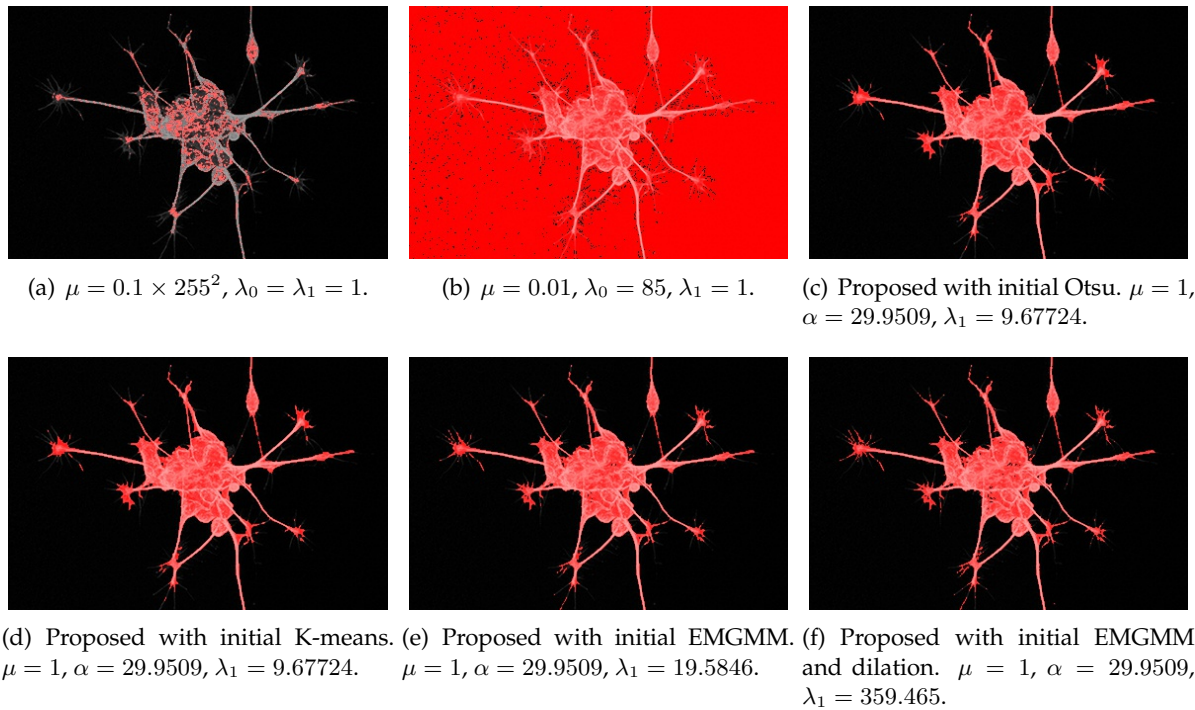


FIGURE 1.62: Image 21 from test set Appendix A segmentation results.

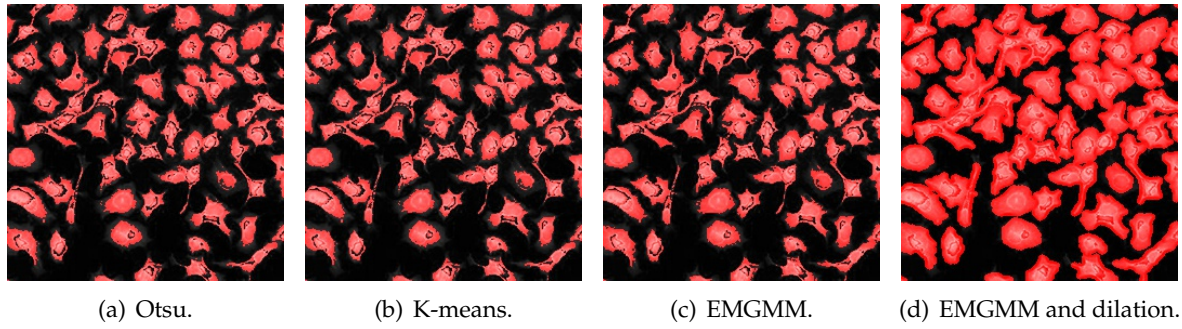


FIGURE 1.63: Image 22 from test set Appendix A initial masks.

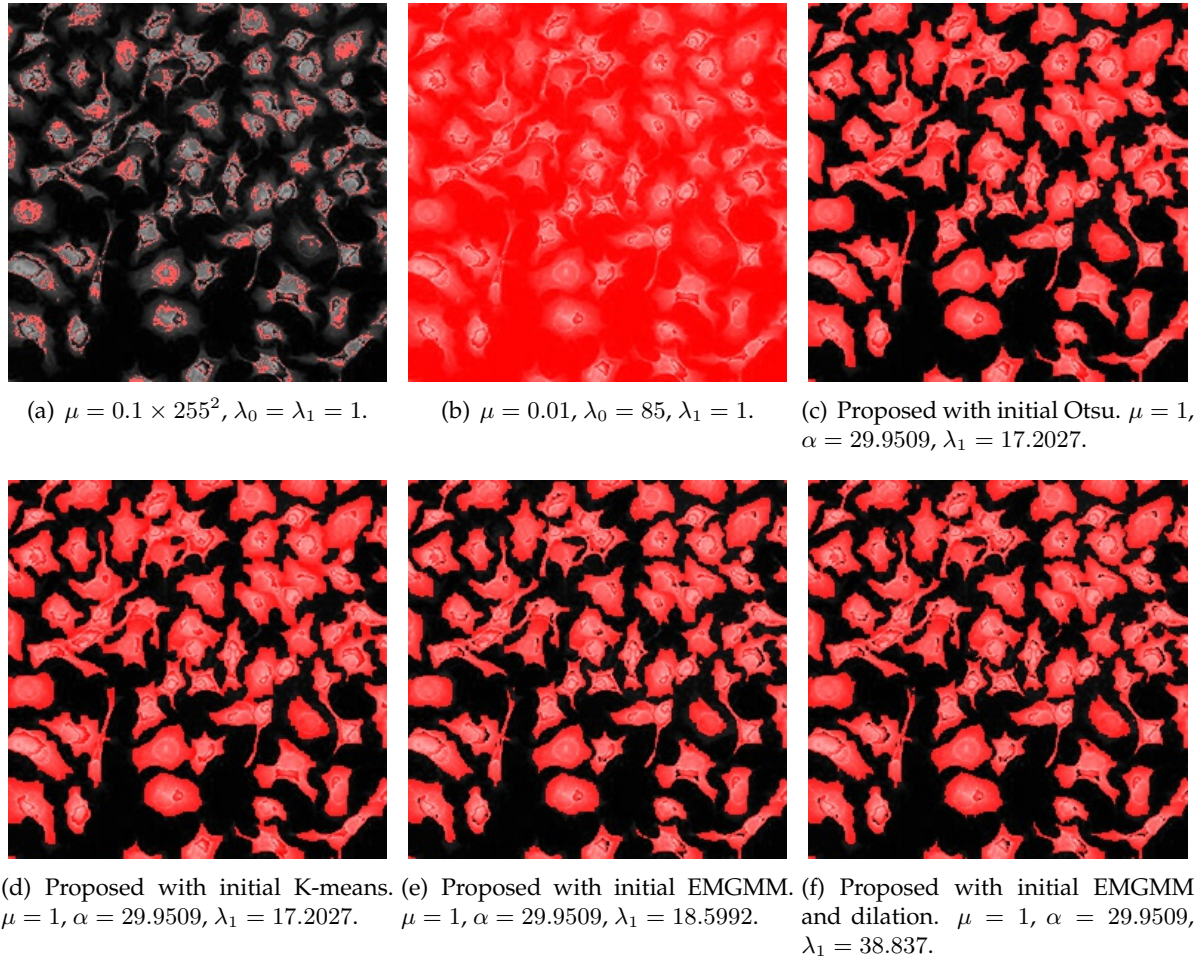


FIGURE 1.64: Image 22 from test set Appendix A segmentation results.

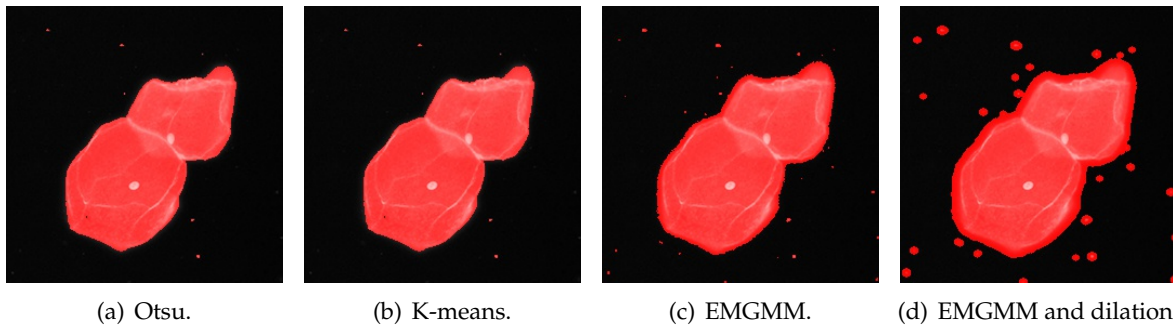


FIGURE 1.65: Image 23 from test set Appendix A initial masks.

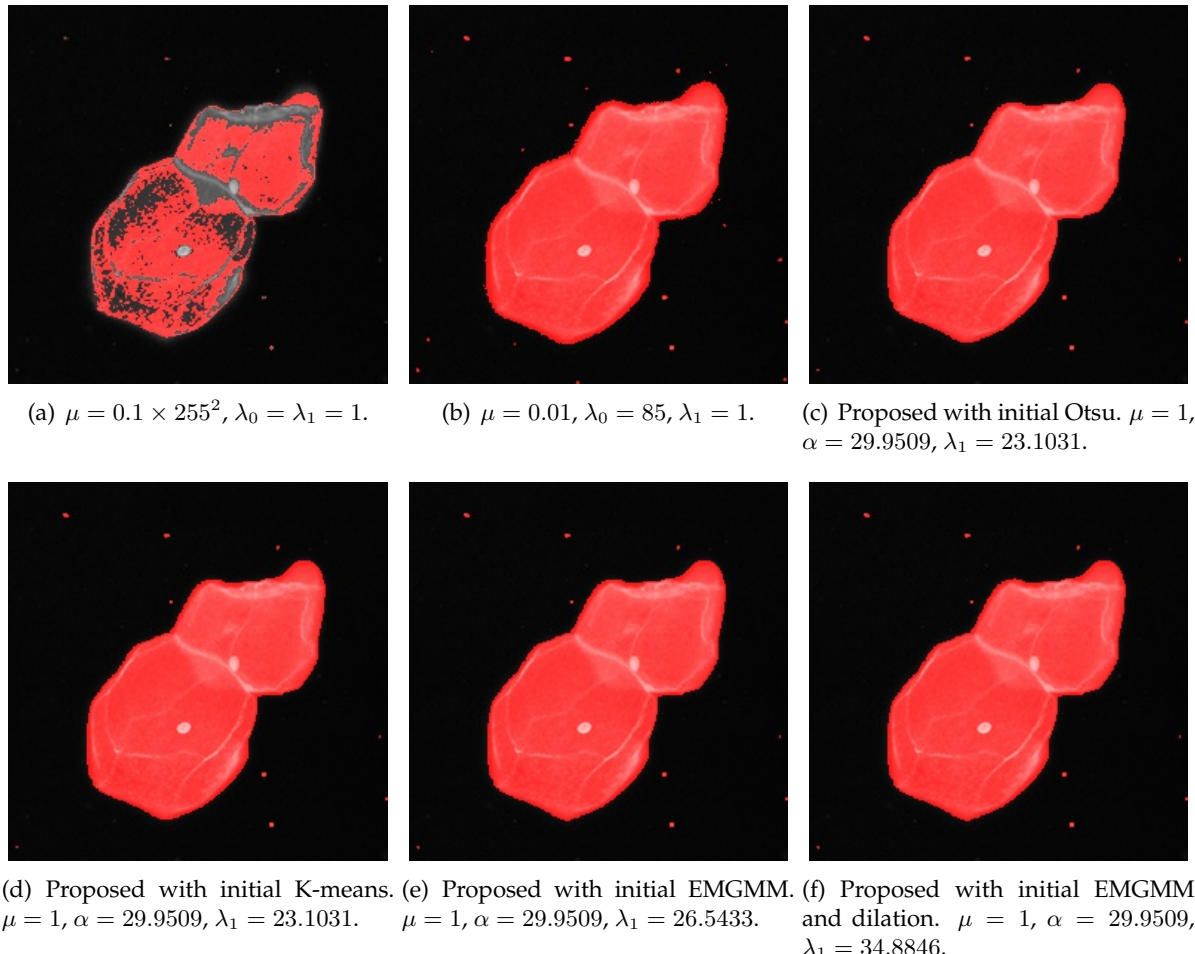


FIGURE 1.66: Image 23 from test set Appendix A segmentation results.

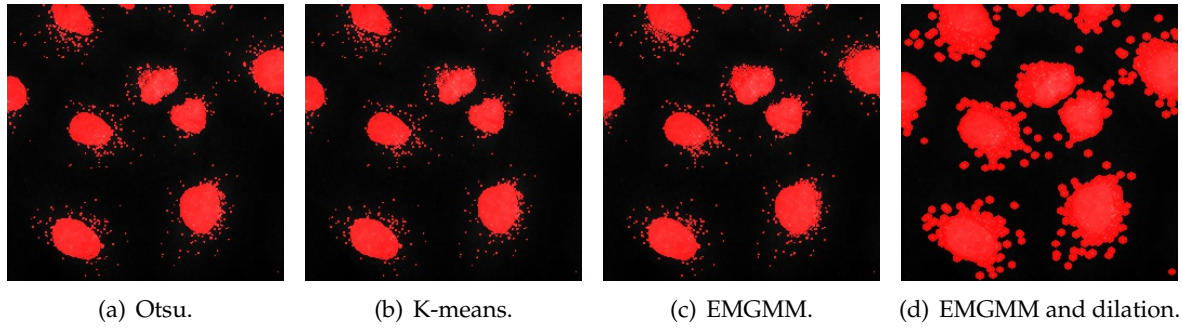


FIGURE 1.67: Image 24 from test set Appendix A initial masks.

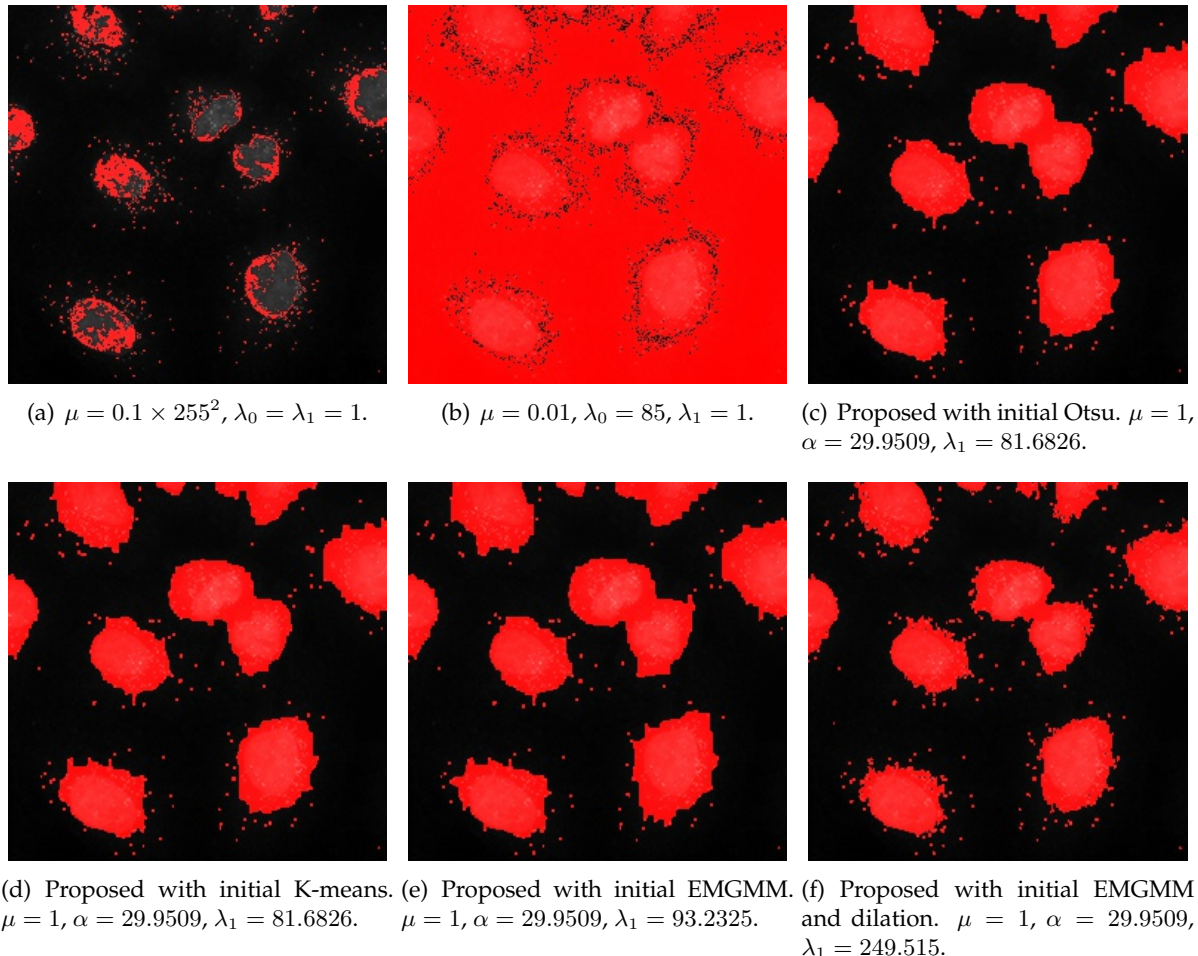


FIGURE 1.68: Image 24 from test set Appendix A segmentation results.

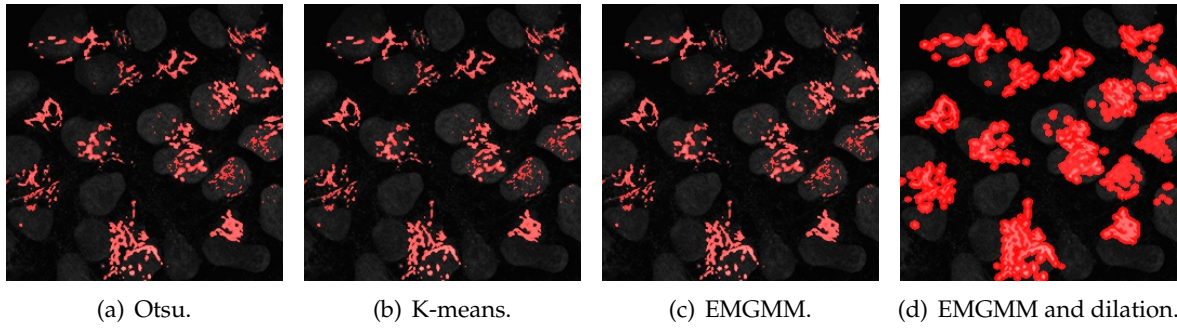


FIGURE 1.69: Image 25 from test set Appendix A initial masks.



FIGURE 1.70: Image 25 from test set Appendix A segmentation results.

TABLE 1.7: Parameter Settings and Segmentation Results.

Image	Initial		Calculated				Final		Ideal		$ \Delta c_0 + \Delta c_1 $
	c_0	c_1	p_e	h	α	λ_1	c_0	c_1	c_0	c_1	
1-n	0.00895	0.40423	-	-	-	-	0.13967	0.50221	0.00165	0.41653	0.22371
1-m	0.00895	0.40423	-	-	-	-	0.00586	0.43683			0.02452
1-o	0.02625	0.46444	0.09395	0.20711	29.9509	7.47524	0.00556	0.43593			0.02332
1-k	0.02625	0.46444	0.09395	0.20711	29.9509	7.47525	0.00556	0.43593			0.02333
1-e	0.00873	0.44298	0.07582	0.18796	29.9509	7.61164	0.00638	0.43808			0.02629
1-d	0.00256	0.42168	0.06732	0.17555	29.9509	8.17148	0.00785	0.44130			0.03098
2-n	0.05448	0.06033	-	-	-	-	0.05264	0.11120	0.03371	0.10663	0.02352
2-m	0.05448	0.06033	-	-	-	-	0.05490	0.05822			0.06960
2-o	0.04080	0.14206	0.05645	0.08259	29.9509	139.983	0.03037	0.09425			0.00905
2-k	0.04080	0.14206	0.05645	0.08259	29.9509	139.984	0.03037	0.09425			0.00905
2-e	0.04001	0.13836	0.05521	0.08061	29.9509	148.373	0.03014	0.09362			0.00945
2-d	0.02952	0.07818	0.03704	0.04961	29.9509	606.199	0.02838	0.09184			0.00945
3-n	0.42108	0.11303	-	-	-	-	0.03498	0.33562	0.01567	0.37442	0.05812
3-m	0.42108	0.11303	-	-	-	-	0.00591	0.24458			0.12009
3-o	0.01897	0.39916	0.07772	0.17589	29.9509	9.93033	0.01364	0.35543			0.01697
3-k	0.01897	0.39916	0.07772	0.17589	29.9509	9.93034	0.01364	0.35543			0.01697
3-e	0.01118	0.32665	0.05992	0.14139	29.9509	14.4226	0.01312	0.34998			0.02190
3-d	0.00485	0.21558	0.03741	0.09183	29.9509	32.3237	0.01235	0.34116			0.02995
4-n	0.07545	0.20713	-	-	-	-	0.12290	0.47460	0.06335	0.45869	0.07546
4-m	0.07545	0.20713	-	-	-	-	0.05485	0.41407			0.03612
4-o	0.06630	0.48896	0.13160	0.24075	29.9509	8.03467	0.05593	0.42575			0.02552
4-k	0.06630	0.48896	0.13170	0.24076	29.9509	8.03468	0.05593	0.42575			0.02552
4-e	0.05670	0.43339	0.11490	0.21218	29.9509	10.1158	0.05996	0.45888			0.00319
4-d	0.05442	0.40712	0.10892	0.19999	29.9509	11.5385	0.05930	0.45449			0.00015
5-n	0.13533	0.32821	-	-	-	-	0.15583	0.47288	0.12897	0.46482	0.03493
5-m	0.13533	0.32821	-	-	-	-	0.07446	0.41944			0.00914
5-o	0.09483	0.46700	0.15233	0.24844	29.9509	10.3623	0.07522	0.42195			0.01088
5-k	0.09483	0.46701	0.15234	0.24844	29.9509	10.3624	0.07522	0.42196			0.01088
5-e	0.08698	0.45324	0.14357	0.23815	29.9509	10.7002	0.08706	0.45341			0.03049
5-d	0.08161	0.43958	0.13692	0.22936	29.9509	11.2011	0.08709	0.45348			0.03054
6-n	0.02387	0.06961	-	-	-	-	0.04522	0.10423	0.00365	0.08386	0.06194
6-m	0.02387	0.06961	-	-	-	-	0.02346	0.05387			0.04979
6-o	0.03077	0.15296	0.04965	0.08121	29.9509	96.1295	0.00650	0.09013			0.00913
6-k	0.03173	0.15753	0.05117	0.08366	29.9509	90.7016	0.00733	0.09131			0.01113
6-e	0.03348	0.16650	0.05404	0.08839	29.9509	81.1216	0.00798	0.09229			0.01276
6-d	0.02350	0.11789	0.03809	0.06246	29.9509	161.108	0.00446	0.08688			0.00384
7-n	0.01226	0.04400	-	-	-	-	0.02896	0.09064	0.01346	0.08035	0.02579
7-m	0.01226	0.04400	-	-	-	-	0.01214	0.07147			0.00755
7-o	0.02098	0.16457	0.04317	0.08025	29.9509	69.6183	0.01476	0.09537			0.01632
7-k	0.02098	0.16457	0.04317	0.08025	29.9509	69.6184	0.01477	0.09538			0.01634
7-e	0.01766	0.12742	0.03462	0.06297	29.9509	119.128	0.01353	0.08515			0.00488
7-d	0.02163	0.16513	0.02354	0.04053	29.9509	331.532	0.01393	0.09152			0.01165
8-n	0.04166	0.09509	-	-	-	-	0.07004	0.14628	0.02345	0.10122	0.09166
8-m	0.04166	0.09509	-	-	-	-	0.04011	0.07601			0.04187
8-o	0.05632	0.25262	0.08666	0.13735	29.9509	37.2522	0.04505	0.16167			0.08207
8-k	0.05632	0.25262	0.08666	0.13735	29.9509	37.2523	0.04505	0.16167			0.08207
8-e	0.05497	0.23995	0.08355	0.13133	29.9509	41.9465	0.04440	0.15773			0.07747
8-d	0.04971	0.18973	0.07134	0.10750	29.9509	73.2113	0.03964	0.13450			0.04949
9-n	0.01870	0.06039	-	-	-	-	0.03729	0.14899	0.02003	0.15095	0.01921
9-m	0.01870	0.06039	-	-	-	-	0.01830	0.12179			0.02743
9-o	0.02349	0.17829	0.04741	0.08739	29.9509	59.9044	0.01959	0.14422			0.00629
9-k	0.02349	0.17829	0.04741	0.08739	29.9509	59.9045	0.01959	0.14422			0.00629
9-e	0.01962	0.14699	0.03929	0.07219	29.9509	88.4765	0.01988	0.14957			0.00124

9-d	0.01864	0.11758	0.03393	0.05948	29.9509	146.629	0.01965	0.14696			0.00361
10-n	0.01651	0.08788	-	-	-	-	0.04651	0.11558			0.04501
10-m	0.01651	0.08788	-	-	-	-	0.00991	0.10639			0.00042
10-o	0.02193	0.12366	0.03765	0.06392	29.9509	138.712	0.01007	0.10694	0.01009	0.10699	0.00003
10-k	0.01674	0.11606	0.03209	0.05774	29.9509	145.504	0.01005	0.10689			0.00006
10-e	0.02429	0.12767	0.04027	0.06696	29.9509	134.305	0.01008	0.10697			0.00001
10-d	0.01316	0.10633	0.02756	0.05162	29.9509	165.378	0.01000	0.10671			0.00019
11-n	0.06341	0.10813	-	-	-	-	0.07140	0.17037			0.03199
11-m	0.06341	0.10813	-	-	-	-	0.06248	0.09365			0.07948
11-o	0.05184	0.17292	0.07055	0.10182	29.9509	97.9168	0.04129	0.14344	0.04957	0.16022	0.00849
11-k	0.05184	0.17292	0.07055	0.10182	29.9509	97.9168	0.04129	0.14344			0.00849
11-e	0.04848	0.16516	0.06651	0.09664	29.9509	105.429	0.04061	0.14129			0.00997
11-d	0.06373	0.18362	0.05598	0.08088	29.9509	154.458	0.04301	0.14940			0.00426
12-n	0.02937	0.05704	-	-	-	-	0.03715	0.12645			0.02699
12-m	0.02937	0.05704	-	-	-	-	0.02924	0.04705			0.09006
12-o	0.01644	0.13791	0.03521	0.06658	29.9509	97.2781	0.00783	0.10746	0.01438	0.12225	0.00824
12-k	0.01644	0.13791	0.03521	0.06658	29.9509	97.2781	0.00783	0.10746			0.00824
12-e	0.01226	0.12439	0.02958	0.05854	29.9509	114.161	0.00746	0.10557			0.00975
12-d	0.02173	0.14265	0.02199	0.04642	29.9509	160.407	0.00784	0.10775			0.00796
13-n	0.03887	0.07238	-	-	-	-	0.05347	0.16217			0.03158
13-m	0.03887	0.07238	-	-	-	-	0.03714	0.06115			0.11628
13-o	0.03368	0.22981	0.06398	0.11463	29.9509	37.3133	0.02422	0.16750	0.03707	0.17735	0.00299
13-k	0.03430	0.23396	0.06515	0.11671	29.9509	36.0075	0.02267	0.15618			0.00677
13-e	0.02970	0.20405	0.05664	0.10167	29.9509	47.2175	0.02342	0.16248			0.00122
13-d	0.02115	0.12638	0.03742	0.06459	29.9509	129.640	0.02045	0.14440			0.01633
14-n	0.06029	0.06139	-	-	-	-	0.05777	0.16960			0.02761
14-m	0.06029	0.06139	-	-	-	-	0.00000	0.06097			0.07232
14-o	0.03772	0.30268	0.07866	0.14709	29.9509	20.4463	0.02669	0.19334	0.03323	0.16654	0.02027
14-k	0.03772	0.30268	0.07866	0.14709	29.9509	20.4463	0.02669	0.19334			0.02027
14-e	0.03359	0.25979	0.06854	0.12696	29.9509	28.0516	0.02523	0.18031			0.00578
14-d	0.02592	0.15617	0.04605	0.07969	29.9509	84.6065	0.02585	0.18815			0.01425
15-n	0.01840	0.00893	-	-	-	-	0.01161	0.07348			0.06484
15-m	0.01840	0.00893	-	-	-	-	0.00784	0.01275			0.12179
15-o	0.00746	0.20099	0.03736	0.08734	29.9509	38.3238	0.00627	0.14850	0.00599	0.13270	0.01609
15-k	0.00746	0.20099	0.03736	0.08734	29.9509	38.3238	0.00627	0.14850			0.01609
15-e	0.00454	0.06893	0.01449	0.03112	29.9509	346.136	0.00584	0.12732			0.00523
15-d	0.00407	0.04491	0.01038	0.02093	29.9509	860.426	0.00564	0.11797			0.01438
16-n	0.04415	0.06767	-	-	-	-	0.05110	0.31654			0.08116
16-m	0.04415	0.06767	-	-	-	-	0.04313	0.05892			0.33081
16-o	0.02332	0.41028	0.08311	0.18304	29.9509	9.58570	0.01792	0.34656	0.01943	0.36603	0.01796
16-k	0.02332	0.41028	0.08311	0.18304	29.9509	9.58570	0.01792	0.34656			0.01796
16-e	0.01595	0.31360	0.06194	0.13881	29.9509	16.2015	0.01751	0.34066			0.02346
16-d	0.01240	0.20776	0.04258	0.09304	29.9509	37.6071	0.01674	0.32819			0.03515
17-n	0.07135	0.09023	-	-	-	-	0.07254	0.22327			0.06720
17-m	0.07135	0.09023	-	-	-	-	0.07058	0.07857			0.20994
17-o	0.04768	0.30903	0.08806	0.15555	29.9509	21.0148	0.03922	0.24421	0.04673	0.26467	0.01294
17-k	0.04768	0.30903	0.08806	0.15555	29.9509	21.0148	0.03922	0.24421			0.01294
17-e	0.04090	0.25794	0.07444	0.13049	29.9509	30.4718	0.03779	0.23286			0.02287
17-d	0.03681	0.21881	0.06493	0.11193	29.9509	43.3300	0.03736	0.22938			0.02592
18-n	0.08499	0.09648	-	-	-	-	0.07755	0.18418			0.09629
18-m	0.08499	0.09648	-	-	-	-	0.00000	0.09214			0.04843
18-o	0.03657	0.20349	0.06237	0.10547	29.9509	51.5200	0.01491	0.16035	0.01243	0.15301	0.00982
18-k	0.03498	0.20029	0.06053	0.10322	29.9509	52.5219	0.01479	0.16009			0.00944
18-e	0.03336	0.19711	0.05866	0.10095	29.9509	53.5287	0.01364	0.15719			0.00539
18-d	0.01379	0.14367	0.03386	0.06740	29.9509	85.0788	0.01438	0.16005			0.00900
19-n	0.00892	0.02787	-	-	-	-	0.01849	0.04199			0.01771
19-m	0.00892	0.02787	-	-	-	-	0.00784	0.02717	0.01094	0.05214	0.02187

19-o	0.01731	0.28587	0.05881	0.12816	29.9509	19.9019	0.01611	0.18929				0.14232
19-k	0.01731	0.28587	0.05881	0.12816	29.9509	19.9019	0.01611	0.18929				0.14232
19-e	0.01568	0.16181	0.03826	0.07599	29.9509	67.2144	0.01563	0.15783				0.11039
19-d	0.01388	0.08195	0.02439	0.04198	29.9509	309.766	0.01059	0.05115				0.00064
20-n	0.00778	0.02631	-	-	-	-	0.01592	0.04527				0.01634
20-m	0.00778	0.02631	-	-	-	-	0.00784	0.02987				0.02367
20-o	0.01658	0.23098	0.04971	0.10508	29.9509	31.2275	0.01410	0.10095	0.01017	0.05587		0.04902
20-k	0.01666	0.23671	0.05066	0.10749	29.9509	29.6411	0.01420	0.10368				0.05185
20-e	0.01507	0.13829	0.03411	0.06594	29.9509	94.5349	0.01065	0.06009				0.00471
20-d	0.01287	0.07606	0.02264	0.03896	29.9509	359.465	0.00954	0.05207				0.00317
21-n	0.03017	0.07699	-	-	-	-	0.03501	0.36663				0.08947
21-m	0.03017	0.07699	-	-	-	-	0.02604	0.04685				0.27208
21-o	0.01359	0.39872	0.07309	0.17256	29.9509	9.67724	0.01025	0.35268	0.00965	0.30254		0.05076
21-k	0.01359	0.39872	0.07309	0.17256	29.9509	9.67724	0.01025	0.35268				0.05076
21-e	0.00772	0.27844	0.04955	0.11946	29.9509	19.5846	0.01018	0.35304				0.05104
21-d	0.00717	0.13728	0.02264	0.03896	29.9509	359.465	0.00954	0.05207				0.25036
22-n	0.14636	0.15438	-	-	-	-	0.13589	0.34221				0.15033
22-m	0.14636	0.15438	-	-	-	-	0.00000	0.15135				0.09591
22-o	0.06587	0.35472	0.11050	0.18509	29.9509	17.2027	0.03676	0.27528	0.04026	0.28753		0.00874
22-k	0.06587	0.35472	0.11050	0.18509	29.9509	17.2027	0.03676	0.27528				0.00874
22-e	0.05808	0.33588	0.10100	0.17274	29.9509	18.5992	0.04178	0.29272				0.00673
22-d	0.03248	0.22473	0.06219	0.11184	29.9509	38.8370	0.03865	0.28447				0.00145
23-n	0.02449	0.12763	-	-	-	-	0.05654	0.26228				0.04183
23-m	0.02449	0.12763	-	-	-	-	0.02594	0.26215				0.01136
23-o	0.02805	0.27730	0.06656	0.13093	29.9509	23.1031	0.02650	0.26851	0.02827	0.27584		0.00556
23-k	0.02805	0.27730	0.06656	0.13093	29.9509	23.1031	0.02650	0.26851				0.00556
23-e	0.02569	0.25823	0.06162	0.12167	29.9509	26.5433	0.02649	0.26838				0.00568
23-d	0.02501	0.22786	0.05635	0.10874	29.9509	34.8846	0.02649	0.26839				0.00567
24-n	0.04744	0.05351	-	-	-	-	0.04570	0.14237				0.03186
24-m	0.04744	0.05351	-	-	-	-	0.04705	0.05137				0.12421
24-o	0.03258	0.16514	0.05307	0.08729	29.9509	81.6826	0.02706	0.11987	0.03581	0.16433		0.03571
24-k	0.03258	0.16514	0.05307	0.08729	29.9509	81.6826	0.02706	0.11987				0.03571
24-e	0.03115	0.15523	0.05033	0.08237	29.9509	93.2325	0.02639	0.11461				0.04031
24-d	0.02616	0.10201	0.03788	0.05747	29.9509	249.515	0.02781	0.12694				0.02940
25-n	0.07693	0.09011	-	-	-	-	0.07952	0.15395				0.06571
25-m	0.07693	0.09011	-	-	-	-	0.00000	0.08513				0.02585
25-o	0.06532	0.33175	0.10648	0.17529	29.9509	20.2207	0.03901	0.16680	0.02839	0.13938		0.03806
25-k	0.06567	0.33628	0.10749	0.17737	29.9509	19.6022	0.03990	0.16887				0.04101
25-e	0.06532	0.33175	0.10640	0.17529	29.9509	20.2207	0.03901	0.16680				0.03806
25-d	0.08493	0.40334	0.07377	0.10217	29.9509	118.726	0.02844	0.14221				0.00289

As can be seen, the parameter settings presented previously in literature are not robust over a large range of image types that commonly occur in fluorescence microscopy whereas the proposed method produces more subjectively consistent and visually accurate segmentations. From the table we can also see that the final means from the proposed method are closer to the ideal means obtained from the groundtruth.

Measuring Segmentation Efficiency **Talk about the efficiency measures, etc.** We now objectively compare the the methods under critique. We use a confusion matrix to quantify the number of correct and incorrect classifications. We relate the classification of each pixel as:

TP (True Positives) An object pixel that is correctly classified as an object.

TN (True Negatives) A background pixel that is correctly classified as a background.

FP (False Positives) A background pixel that is incorrectly classified as an object.

FN (False Negatives) An object pixel that is incorrectly classified as a background.

From these counts we calculate the following binary classification measures:

$$precision = \frac{TP}{TP + FP}$$

$$recall = \frac{TP}{TP + FN}$$

$$accuracy = \frac{TP + TN}{TP + TN + FP + FN}$$

$$MCC = \frac{TP \times TN - FP \times FN}{\sqrt{(TP + FP)(TP + FN)(TN + FP)(TN + FN)}}$$

Accuracy is the fraction of the pixels that are correctly classified from among all pixels. MCC is the *Matthews Correlation Coefficient* and is more accurate measure of accuracy when comparing classes whose sizes differ greatly. Its results is a value between -1 and $+1$, where -1 is refers to a complete opposite classification, i.e. all background pixels are classified as object and all object are classified as background, and $+1$ means a perfect classification, 0 is equivalent to a random classification. The results for each image in the test set is tabulated in Table 1.8. The overall efficiency for each method is tabulated in Table 1.9. For each table, rows that are highlighted in blue show the method that performed the best for each image in Table 1.8 and over the test set in Table 1.9.

TABLE 1.8: Segmentation Efficiency.

Image	TP	TN	FP	FN	Precision	Recall	Accuracy	MCC
1-n	24954	25516	0	15066	1.000000	0.623538	0.770111	0.626140
1-m	37875	25506	10	2145	0.999736	0.946402	0.967117	0.934010
1-o	37973	25506	10	2047	0.999737	0.948851	0.968613	0.936880
1-k	37973	25506	10	2047	0.999737	0.948851	0.968613	0.936880
1-e	37736	25510	6	2284	0.999841	0.942929	0.965057	0.930095
1-d	37364	25513	3	2656	0.999920	0.933633	0.959427	0.919468
2-n	5561	43411	179	16385	0.968815	0.253395	0.747253	0.416180
2-m	21864	120	43470	82	0.334650	0.996264	0.335449	-0.008374
2-o	21856	37015	6575	90	0.768738	0.995899	0.898300	0.804725
2-k	21856	37015	6575	90	0.768738	0.995899	0.898300	0.804725
2-e	21878	36617	6973	68	0.758310	0.996901	0.892563	0.795678
2-d	21867	34669	8921	79	0.710244	0.996400	0.862671	0.748686
3-n	9113	55407	24	992	0.997373	0.901831	0.984497	0.939774
3-m	10105	47657	7774	0	0.565188	1.000000	0.881378	0.697081
3-o	10104	54541	890	1	0.919047	0.999901	0.986404	0.950885
3-k	10104	54541	890	1	0.919047	0.999901	0.986404	0.950885
3-e	10105	54277	1154	0	0.897504	1.000000	0.982391	0.937454
3-d	10105	53847	1584	0	0.864488	1.000000	0.975830	0.916397
4-n	10654	49844	99	4939	0.990793	0.683255	0.923126	0.783314
4-m	15593	46825	3118	0	0.833360	1.000000	0.952423	0.883930

4-o	15593	47552	2391	0	0.867048	1.000000	0.963516	0.90859
4-k	15593	47552	2391	0	0.867048	1.000000	0.963516	0.90859
4-e	14839	48771	1172	754	0.926800	0.951645	0.970612	0.919839
4-d	14920	48593	1350	673	0.917025	0.956840	0.969131	0.916491
5-n	21195	38591	2276	3474	0.903029	0.859175	0.912262	0.811918
5-m	24669	31160	9707	0	0.717623	1.000000	0.851883	0.739708
5-o	24669	31482	9385	0	0.724408	1.000000	0.856796	0.747027
5-k	24669	31482	9385	0	0.724408	1.000000	0.856796	0.747027
5-e	24669	35418	5449	0	0.819078	1.000000	0.916855	0.842536
5-d	24669	35427	5440	0	0.819323	1.000000	0.916992	0.842769
6-n	8041	25755	0	31740	1.000000	0.202132	0.515686	0.300907
6-m	38173	1358	24397	1608	0.610085	0.959579	0.603195	0.028915
6-o	35876	25713	42	3905	0.998831	0.901838	0.939774	0.883440
6-k	35096	25729	26	4685	0.999260	0.882230	0.928116	0.863032
6-e	34459	25734	21	5322	0.999391	0.866218	0.918472	0.846506
6-d	37815	25503	252	1966	0.993380	0.950579	0.966156	0.931253
7-n	3213	47332	19	14972	0.994121	0.176684	0.771255	0.364534
7-m	17876	43120	4231	309	0.808613	0.983008	0.930725	0.846322
7-o	13903	47235	116	4282	0.991726	0.764531	0.932892	0.832125
7-k	13903	47235	116	4282	0.991726	0.764531	0.932892	0.832125
7-e	16478	46937	414	1707	0.975491	0.906131	0.967636	0.918642
7-d	14740	46846	505	3445	0.966874	0.810558	0.939728	0.847704
8-n	4494	22158	0	38884	1.000000	0.103601	0.406677	0.193924
8-m	42118	133	22025	1260	0.656627	0.970953	0.644699	-0.075582
8-o	16780	22158	0	26598	1.000000	0.386832	0.594147	0.419288
8-k	16780	22158	0	26598	1.000000	0.386832	0.594147	0.419288
8-e	17641	22158	0	25737	1.000000	0.406681	0.607285	0.433758
8-d	24348	22141	17	19030	0.999302	0.561298	0.709366	0.548682
9-n	4890	53207	3	7436	0.999387	0.396722	0.886490	0.589732
9-m	12325	49186	4024	1	0.753869	0.999919	0.938583	0.834732
9-o	12301	52336	874	25	0.933662	0.997972	0.986282	0.957060
9-k	12301	52336	874	25	0.933662	0.997972	0.986282	0.957060
9-e	12258	52948	262	68	0.979073	0.994483	0.994965	0.983657
9-d	12298	52633	577	28	0.955184	0.997728	0.990768	0.970635
10-n	14187	31146	2	20201	0.999859	0.412557	0.691727	0.500151
10-m	34387	30887	261	1	0.992467	0.999971	0.996002	0.992013
10-o	34373	31109	39	15	0.998867	0.999564	0.999176	0.998348
10-k	34381	31095	53	7	0.998461	0.999796	0.999084	0.998165
10-e	34363	31115	33	25	0.999041	0.999273	0.999115	0.998226
10-d	34384	31013	135	4	0.996089	0.999884	0.997879	0.995755
11-n	14671	40720	132	10013	0.991083	0.594353	0.845200	0.684969
11-m	24500	3572	37280	184	0.396568	0.992546	0.428345	0.166735
11-o	24284	33091	7761	400	0.757809	0.983795	0.875473	0.769468
11-k	24284	33091	7761	400	0.757809	0.983795	0.875473	0.769468
11-e	24347	32248	8604	337	0.738885	0.986347	0.863571	0.751768
11-d	24030	35179	5673	654	0.809009	0.973505	0.903458	0.812402

12-n	7204	45666	295	12371	0.960661	0.368020	0.806732	0.519903
12-m	19530	776	45185	45	0.301785	0.997701	0.309845	0.060018
12-o	19415	39881	6080	160	0.761522	0.991826	0.904785	0.806923
12-k	19415	39881	6080	160	0.761522	0.991826	0.904785	0.806923
12-e	19465	39285	6676	110	0.744616	0.994381	0.896454	0.793664
12-d	19408	39947	6014	167	0.763433	0.991469	0.905685	0.808358
13-n	2608	53651	1298	7979	0.667691	0.246340	0.858444	0.346226
13-m	10541	2533	52416	46	0.167432	0.995655	0.199493	0.079031
13-o	9284	47991	6958	1303	0.571604	0.876925	0.873947	0.639563
13-k	9606	46365	8584	981	0.528092	0.907339	0.854050	0.617332
13-e	9525	47363	7586	1062	0.556659	0.899688	0.868042	0.638175
13-d	10320	44499	10450	267	0.496870	0.974780	0.836472	0.620618
14-n	1461	51387	508	12180	0.742001	0.107104	0.806396	0.231433
14-m	13641	0	51895	0	0.208145	1.000000	0.208145	NaN
14-o	9703	48117	3778	3938	0.719754	0.711311	0.882263	0.641301
14-k	9703	48117	3778	3938	0.719754	0.711311	0.882263	0.641301
14-e	10329	47119	4776	3312	0.683813	0.757203	0.876587	0.641224
14-d	10154	47865	4030	3487	0.715877	0.744374	0.885300	0.657278
15-n	936	62133	33	2434	0.965944	0.277745	0.962357	0.507270
15-m	3370	3061	59105	0	0.053942	1.000000	0.098129	0.051537
15-o	2847	62143	23	523	0.991986	0.844807	0.991669	0.911385
15-k	2847	62143	23	523	0.991986	0.844807	0.991669	0.911385
15-e	3345	61918	248	25	0.930977	0.992582	0.995834	0.959144
15-d	3363	61528	638	7	0.840540	0.997923	0.990158	0.911074
16-n	4543	58089	4	2900	0.999120	0.610372	0.955688	0.762067
16-m	7443	99	57994	0	0.113743	1.000000	0.115082	0.013923
16-o	7434	57377	716	9	0.912147	0.998791	0.988937	0.948497
16-k	7434	57377	716	9	0.912147	0.998791	0.988937	0.948497
16-e	7434	57155	938	9	0.887960	0.998791	0.985550	0.934020
16-d	7437	56680	1413	6	0.840339	0.999194	0.978348	0.905052
17-n	2858	55353	634	6691	0.818442	0.299298	0.888229	0.452365
17-m	9536	298	55689	13	0.146202	0.998639	0.150055	0.020336
17-o	8509	51944	4043	1040	0.677900	0.891088	0.922440	0.734195
17-k	8509	51944	4043	1040	0.677900	0.891088	0.922440	0.734195
17-e	8915	51233	4754	634	0.652206	0.933606	0.917786	0.736986
17-d	9006	50960	5027	543	0.641773	0.943135	0.915009	0.733933
18-n	10662	28372	3	26499	0.999719	0.286914	0.595612	0.384991
18-m	37161	0	28375	0	0.567032	1.000000	0.567032	NaN
18-o	34582	28099	276	2579	0.992082	0.930599	0.956436	0.914421
18-k	34653	28086	289	2508	0.991729	0.932510	0.957321	0.916017
18-e	35373	27881	494	1788	0.986227	0.951885	0.965179	0.930209
18-d	34845	28118	257	2316	0.992678	0.937677	0.960739	0.922580
19-n	6080	49795	190	9471	0.969697	0.390972	0.852585	0.559970
19-m	15551	21811	28174	0	0.355655	1.000000	0.570099	0.393942
19-o	1743	49985	0	13808	1.000000	0.112083	0.789307	0.296349
19-k	1743	49985	0	13808	1.000000	0.112083	0.789307	0.296349

19-e	2340	49985	0	13211	1.000000	0.150473	0.798416	0.344988
19-d	15144	48771	1214	407	0.925786	0.973828	0.975266	0.933388
20-n	7631	52325	94	5486	0.987832	0.581764	0.914856	0.719637
20-m	13112	31433	20986	5	0.384539	0.999619	0.679703	0.479944
20-o	3934	52419	0	9183	1.000000	0.299916	0.859879	0.505181
20-k	3742	52419	0	9375	1.000000	0.285279	0.856949	0.491933
20-e	11467	52403	16	1650	0.998607	0.874209	0.974579	0.919788
20-d	12993	50360	2059	124	0.863208	0.990547	0.966690	0.904878
21-n	5859	54029	0	5648	1.000000	0.509168	0.913818	0.678954
21-m	11504	410	53619	3	0.176650	0.999739	0.181793	0.035231
21-o	9354	54019	10	2153	0.998932	0.812896	0.966995	0.883569
21-k	9354	54019	10	2153	0.998932	0.812896	0.966995	0.883569
21-e	9367	54019	10	2140	0.998934	0.814026	0.967194	0.884286
21-d	9386	54016	13	2121	0.998617	0.815677	0.967438	0.885155
22-n	9992	36090	0	19454	1.000000	0.339333	0.703156	0.469557
22-m	29446	0	36090	0	0.449310	1.000000	0.449310	NaN
22-o	29301	33903	2187	145	0.930545	0.995076	0.964417	0.930373
22-k	29301	33903	2187	145	0.930545	0.995076	0.964417	0.930373
22-e	28465	35927	163	981	0.994306	0.966685	0.982544	0.964943
22-d	29163	35176	914	283	0.969611	0.990389	0.981735	0.963345
23-n	11850	49497	42	4147	0.996468	0.740764	0.936081	0.824684
23-m	15994	48127	1412	3	0.918879	0.999812	0.978409	0.944698
23-o	15978	48676	863	19	0.948756	0.998812	0.986542	0.964737
23-k	15978	48676	863	19	0.948756	0.998812	0.986542	0.964737
23-e	15978	48664	875	19	0.948080	0.998812	0.986359	0.964275
23-d	15978	48665	874	19	0.948137	0.998812	0.986374	0.964313
24-n	3284	57098	577	4577	0.850557	0.417759	0.921356	0.562635
24-m	7861	1055	56620	0	0.121912	1.000000	0.136047	0.047223
24-o	7853	48469	9206	8	0.460344	0.998982	0.859406	0.621496
24-k	7853	48469	9206	8	0.460344	0.998982	0.859406	0.621496
24-e	7858	47094	10581	3	0.426162	0.999618	0.838501	0.589715
24-d	7844	50004	7671	17	0.505575	0.997837	0.882690	0.661018
25-n	5597	32002	27	27910	0.995199	0.167040	0.573715	0.296608
25-m	33507	0	32029	0	0.511276	1.000000	0.511276	NaN
25-o	23435	31813	216	10072	0.990867	0.699406	0.843018	0.720953
25-k	22771	31815	214	10736	0.990690	0.679589	0.832916	0.704884
25-e	23435	31813	216	10072	0.990867	0.699406	0.843018	0.720953
25-d	31767	31142	887	1740	0.972836	0.948071	0.959915	0.920148

From the marked-up rows, we can clearly see that the proposed method supercedes the competitor methods. This is better shown in Table 1.9. From the data in Table 1.8 we plot Precision vs Recall in Figure 1.71. From Figure 1.71 we can see that the parameter settings proposed by Masaka *et al.* tend to have low precision bu a very high recall. We can also see that the parameter settings proposed by El Zehiry *et al.* tend to have very low recall but a high precision. The proposed method, for all initialisation methods, have a relatively high precision and recall. We plot the accuracy over the test set which is shown in Figure 1.72. We can clearly

see the the performance of the competitor parameter settings are very erratic. The proposed method is much more stable which is verified by the standard deviation of the accuracy shown in Table 1.9.

TABLE 1.9: Overall Segmentation Efficiency.

Method	Precision		Recall		Accuracy	
	Mean	Std. Dev.	Mean	Std. Dev.	Mean	Std. Dev.
El-Zehiry <i>et al.</i>	0.951912	0.088710	0.421993	0.226299	0.805732	0.151199
Maska <i>et al.</i>	0.485812	0.292765	0.993592	0.014007	0.547369	0.321099
Prop. - Otsu	0.876652	0.153530	0.845668	0.240808	0.911657	0.087720
Prop. - K-means	0.874892	0.157316	0.844808	0.242856	0.909905	0.088468
Prop. - EMGMM	0.875713	0.161034	0.883279	0.202419	0.918983	0.087190
Prop. - EMGMM+Dilate	0.860245	0.149355	0.939366	0.103397	0.935329	0.064493

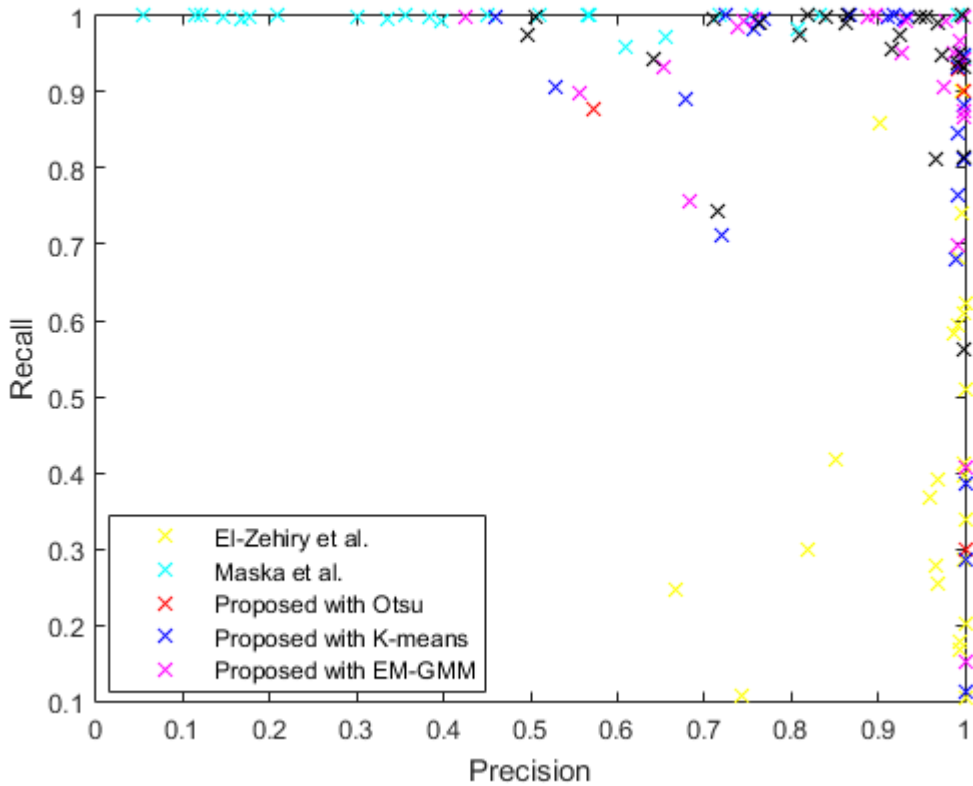


FIGURE 1.71: Precision vs Recall over test set.

1.4 Discussion

Discuss the proposed method against the competing methods here.

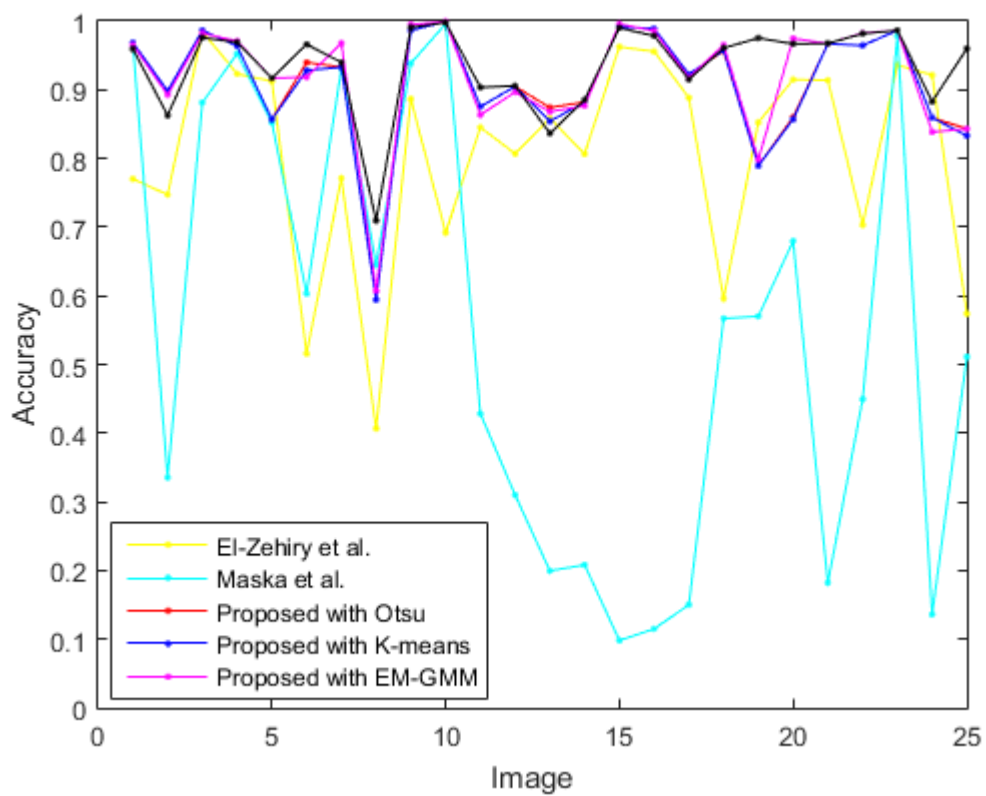


FIGURE 1.72: Accuracy over test set.

Appendix A

Cell Images Dataset

The dataset is composed of two subsets. One as the sample set and one as the test set. The sample set is used for tuning parameters and testing theories or predictions. This dataset is composed of images that are relatively simple but still try to maintain some of the variation of images obtained in fluorescence microscopy. The other dataset is the test set. This dataset is contains more complex images and is used to test the robustness of the segmentation schemes or techniques. We aim for a larger coverage of the types of images that are frequently obtained in fluorescence microscopy.

A.1 Sample Set

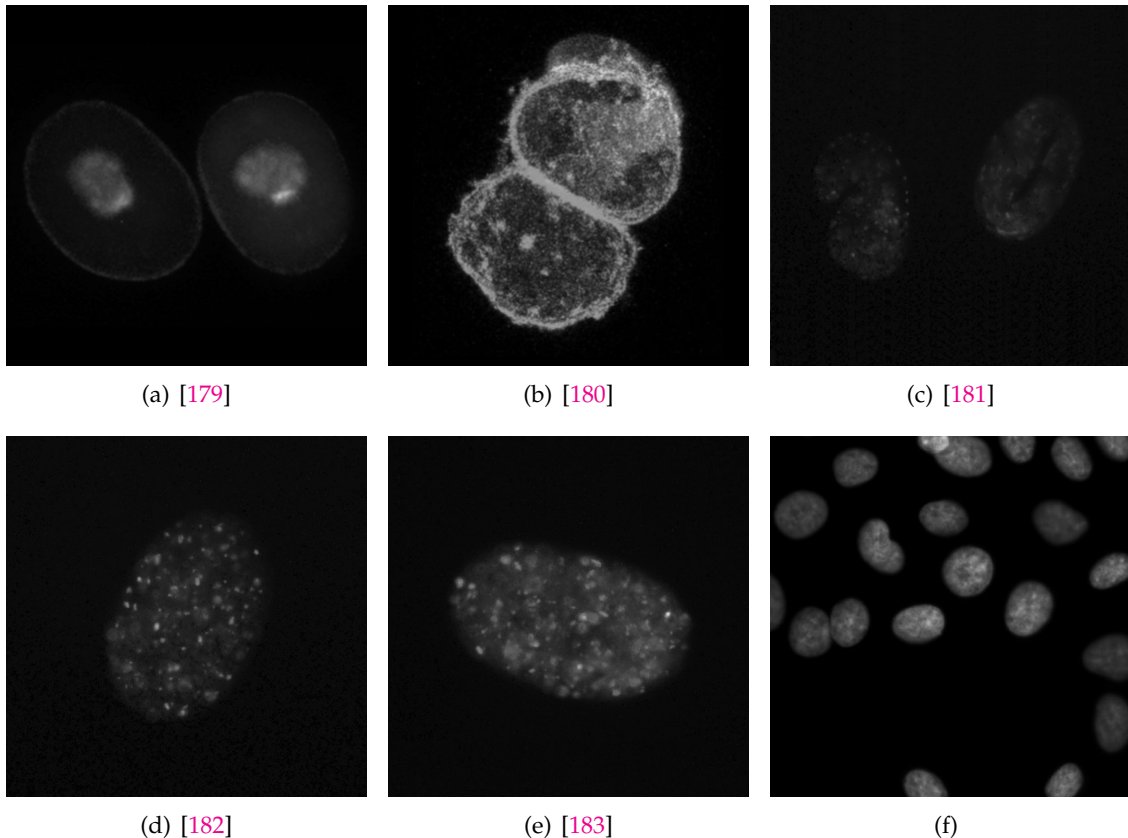
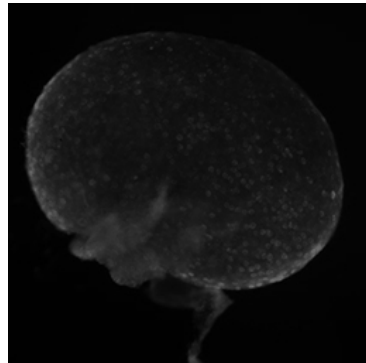


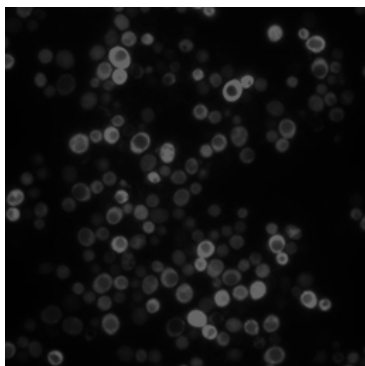
FIGURE A.1: Sample set.

A.2 Test Set

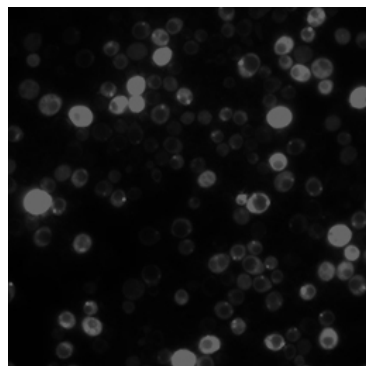


(a) [184]

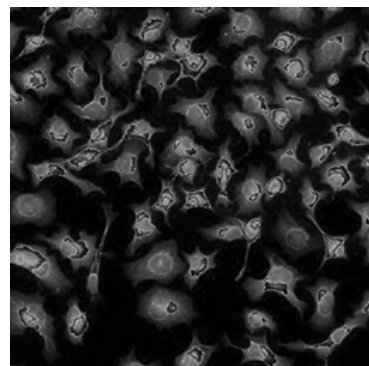
FIGURE A.2: Uneven Illumination



(a) [185]



(b) [186]



(c) [187]

FIGURE A.3: High cell density

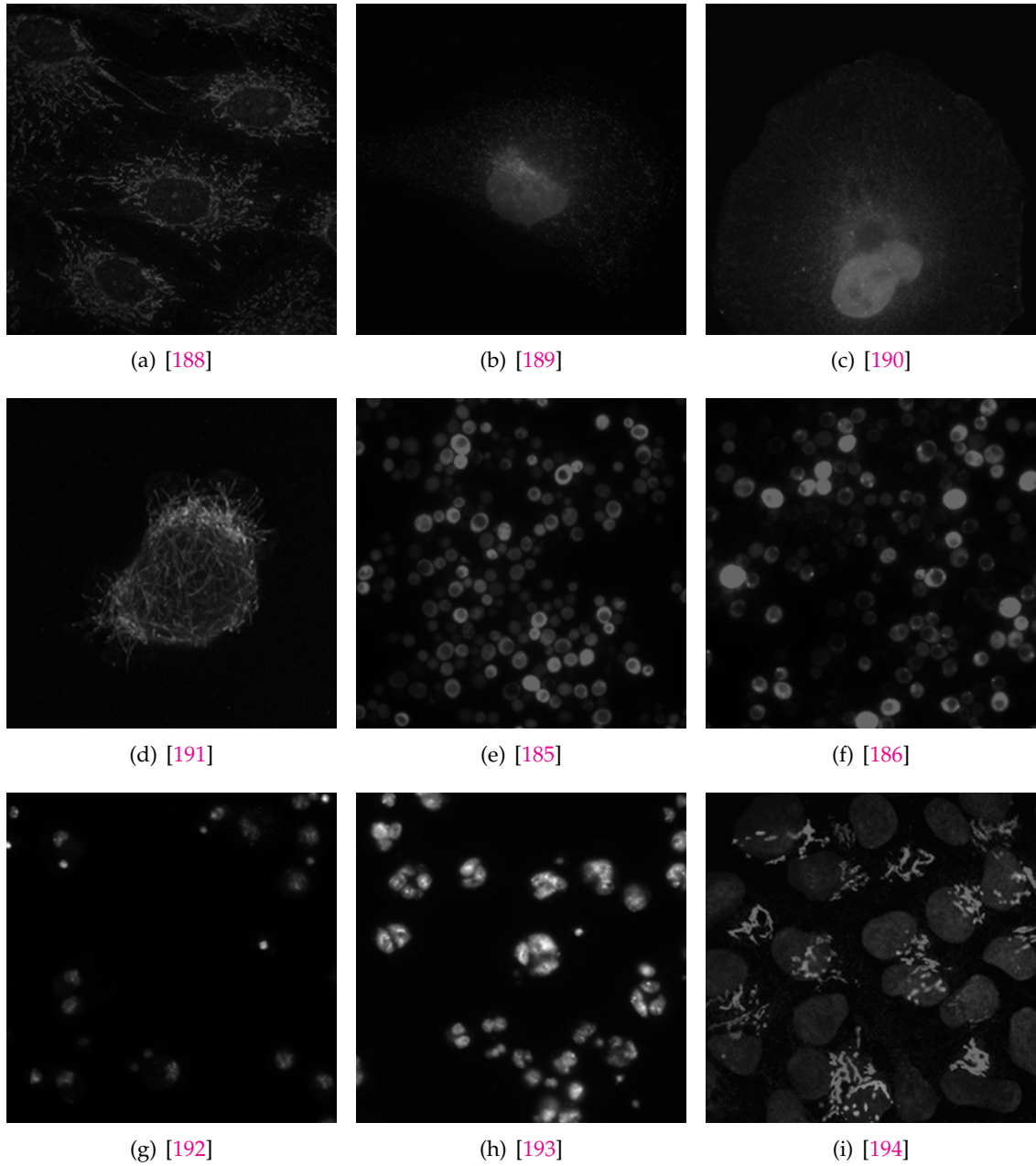


FIGURE A.4: Multi-modal (non-bi-modal)

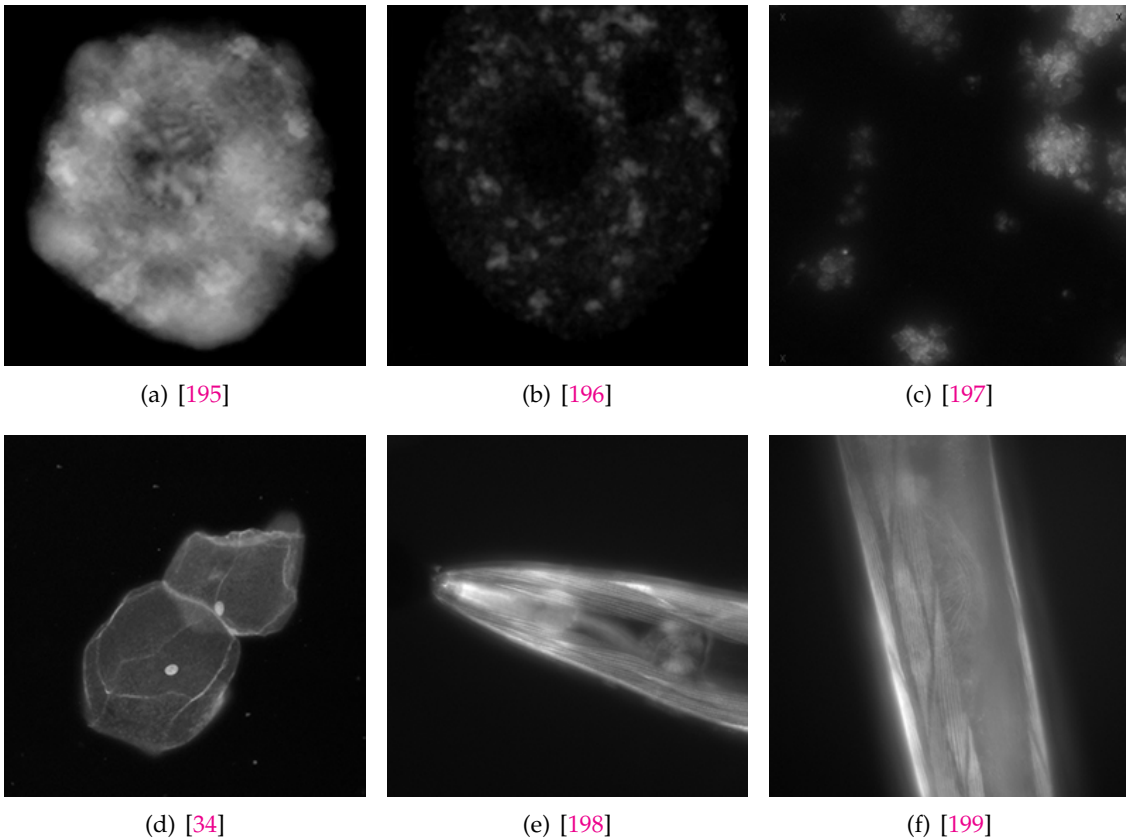


FIGURE A.5: Hazy/Glowing Edges

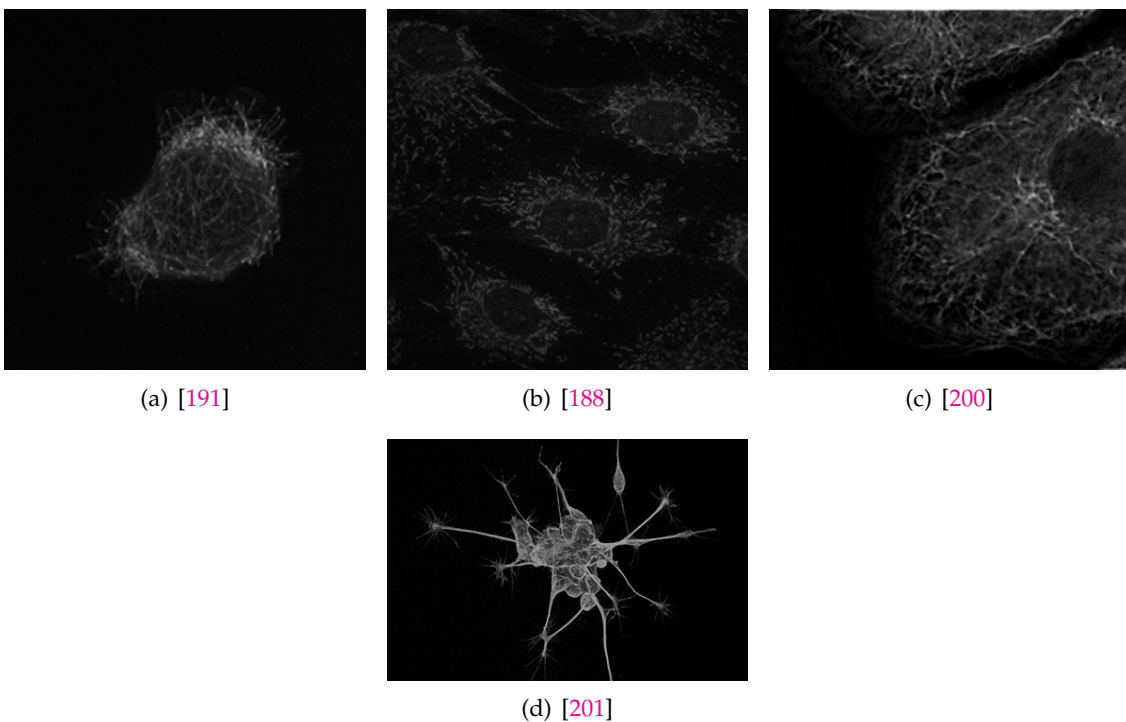


FIGURE A.6: Thin Tentacles

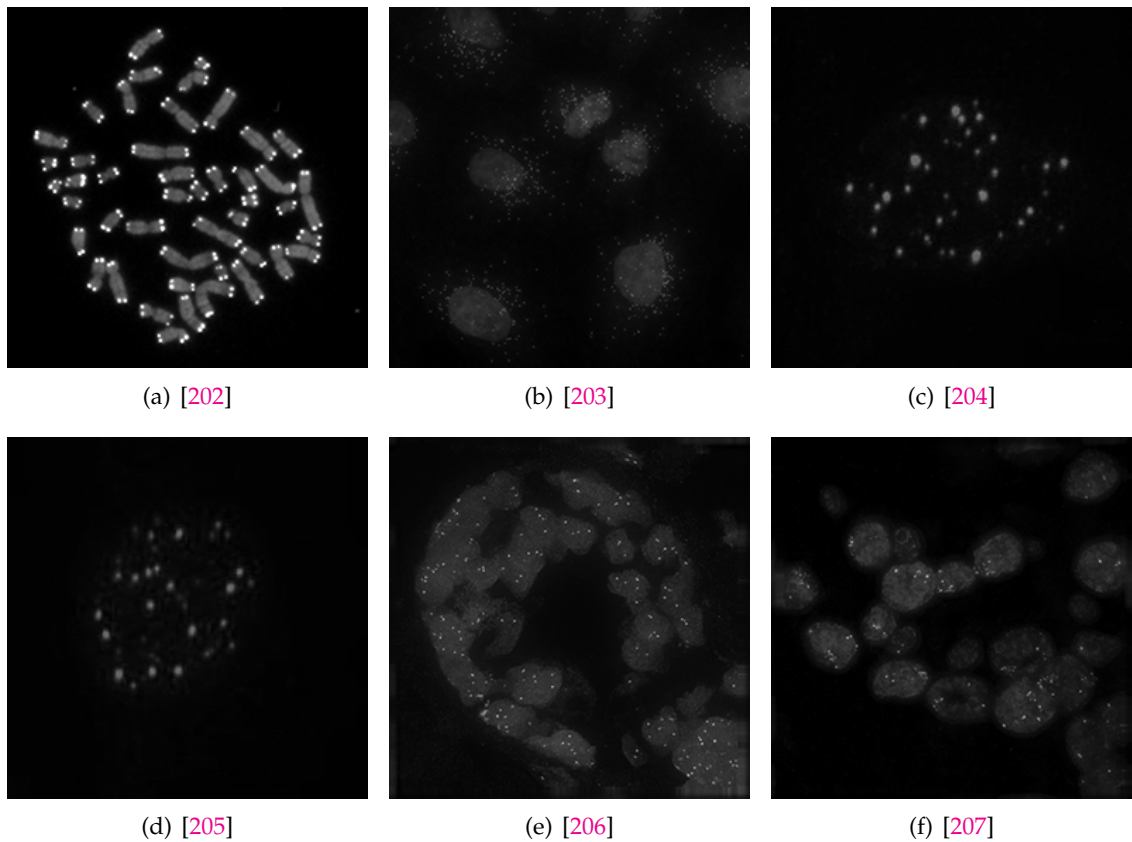


FIGURE A.7: Bright Spots and Speckles

Bibliography

- [1] Kenneth R. Spring. *Encyclopedia of Optical Engineering - Fluorescence Microscopy*. 270 Madison Avenue, New York, New York 10016: Marcel Dekker, Inc., 2003, pp. 548–555. DOI: [10.1081/E-EOE](https://doi.org/10.1081/E-EOE).
- [2] Ondřej Daněk. "Graph Cut Based Image Segmentation in Fluorescence Microscopy [online]". Doctoral theses, Dissertations. Masaryk University, Faculty of Informatics, Brno, 2012 [cit. 2016-09-08]. URL: http://is.muni.cz/th/60931/fi_d/thesis-final.pdf.
- [3] Jan Hubený. "Applications of PDE - Based Image Processing in Fluorescence Microscopy [online]". Doctoral theses, Dissertations. Masaryk University, Faculty of Informatics, Brno, 2008 [cit. 2016-09-07]. URL: http://is.muni.cz/th/4012/fi_d/.
- [4] Fatima A. Merchant and Ammasi Periasamy. "Fluorescence Imaging". In: *Microscope Image Processing*. USA: Elsevier Inc, 2008, pp. 247–271. ISBN: 978-0-12-372578-3.
- [5] Pavel Matula. "Image Processing in Fluorescence Microscopy and its Utilization in Cell Biology Experiments [online]". Doctoral theses, Dissertations. Masaryk University, Faculty of Informatics, Brno, 2012 [cit. 2016-09-09].
- [6] Karl-Friedrich Koch. *Fluorescence Microscopy - Instruments, Methods, Applications*. Lietz Wetzlar, 1972.
- [7] Andrew Vaughan. *Principles of Fluorescence Microscopy*. Document. (accessed September 6, 2016).
- [8] Pinaki Sarder and Arye Nehorai. "Deconvolution Methods for 3-D Fluorescence Microscopy Images". In: *IEEE Signal Processing Magazine* 23.3 (2006), 32—45. DOI: [10.1049/j.1365-2818.2000.00754.x](https://doi.org/10.1049/j.1365-2818.2000.00754.x).
- [9] Mortimer Abramowitz and Michael W. Davidson. *Introduction to Fluorescence*. Website. (accessed September 6, 2016). URL: <http://www.olympusmicro.com/primer/lightandcolor/fluorointroduction.html>.
- [10] Kenneth R. Spring and Michael W. Davidson. *Introduction to Fluorescence Microscopy*. Website. (accessed September 6, 2016). URL: <http://www.microscopyu.com/techniques/fluorescence/introduction-to-fluorescence-microscopy>.
- [11] Jurek W. Dobrucki. "Fluorescence Microscopy". In: *Fluorescence Microscopy: From Principles to Biological Applications*. 1st Edition. Wiley-VCH Verlag GmbH & Co., 2013, pp. 97–142.
- [12] Nobel Media AB. *The Fluorescence Microscopy*. Website. (accessed September 6, 2016). URL: <http://www.nobelprize.org/educational/physics/microscopes/fluorescence/>.
- [13] *Fluorescence SpectraViewer*. Website. (accessed September 18, 2016). URL: <https://www.thermofisher.com/us/en/home/life-science/cell-analysis/labeling-chemistry/fluorescence-spectraviewer.html>.

- [14] Roger Y. Tsien. "The Green Fluorescent Protein". In: *Annual Review of Biochemistry* 67 (1998), pp. 509–544.
- [15] Michal Kozubek. "FISH imaging". In: *Confocal and Two-Photon Microscopy: Foundations, Applications and Advances* (2001), 389—429.
- [16] Z. Theodosiou et al. "Automated Analysis of FISH and immunohistochemistry images: A Review". In: *Cytometry Part A* 71.7 (2007), pp. 439–450.
- [17] Rudolf Amann and Bernhard M. Fuchs. "Single-cell identification in microbial communities by improved fluorescence in situ hybridization techniques". In: *Nature Reviews Microbiology* 6.5 (2008), 339—348. DOI: [10.1038/nrmicro1888](https://doi.org/10.1038/nrmicro1888).
- [18] Kelly Cude and Kelly Burke. "Introduction to Fluorescence Microscopy". In: (14 July 2012).
- [19] Kishore Reddy Katikireddy and Finbarr O'Sullivan. "Immunohistochemical and Immunofluorescence Procedures for Protein Analysis". In: *Gene Expression Profiling: Methods and Protocols*. Ed. by Lorraine O'Driscoll. Totowa, NJ: Humana Press, 2011, pp. 155–167. ISBN: 978-1-61779-289-2. DOI: [10.1007/978-1-61779-289-2_11](https://doi.org/10.1007/978-1-61779-289-2_11). URL: http://dx.doi.org/10.1007/978-1-61779-289-2_11.
- [20] Jeff W. Lichtman and José-Angel Conchello. *Nature Methods - Fluorescence microscopy*. Vol. 2. 12. Nature Publishing Group, Decmeber 2005, pp. 910–919. DOI: [10.1038/NMETH817](https://doi.org/10.1038/NMETH817). URL: <http://www.nature.com/naturemethods>.
- [21] Paul D. Andrews, Ian S. Harper, and Jason R. Swedlow. "To 5D and Beyond: Quantitative Fluorescence Microscopy in the Postgenomic Era". In: *Traffic*. Vol. 3. Munksgaard International Publishers, 2002, pp. 29–36.
- [22] George Rice. *Fluorescent Microscopy*. Website. (accessed September 6, 2016). URL: http://serc.carleton.edu/microbelife/research_methods/microscopy/fluromic.html.
- [23] Kavita Aswani, Tushare Jinadasa, and Claire M. Brown. "Fluorescence Microscopy Light Sources". In: *Microscopy Today*. 2012, pp. 22–28. DOI: [10.1017/S1551929512000399](https://doi.org/10.1017/S1551929512000399). URL: www.microscopy-today.com.
- [24] Thermo Fisher Scientific. *Fundamentals of Fluorescence Microscopy*. Website. (accessed September 6, 2016). URL: <https://www.thermofisher.com/us/en/home/life-science/cell-analysis/cell-analysis-learning-center/molecular-probes-school-of-fluorescence/fundamentals-of-fluorescence-microscopy.html>.
- [25] Douglas B. Murphy. *Fundamentals of Light Microscopy and Electronic Imaging*. 2nd Edition. USA: John Wiley & Sons, Inc., 2001. ISBN: 0-471-25391-X.
- [26] Ian T. Young. "Shading Correction: Compensation for Illumination and Sensor Inhomogeneities". In: *Current Protocols in Cytometry*. John Wiley & Sons, Inc., 2001. ISBN: 9780471142959. DOI: [10.1002/0471142956.cy0211s14](https://doi.org/10.1002/0471142956.cy0211s14). URL: <http://dx.doi.org/10.1002/0471142956.cy0211s14>.
- [27] Ghauharali, Hofstraat, and Brakenhoff. "Fluorescence photobleaching-based shading correction for fluorescence microscopy". In: *Journal of Microscopy* 192.2 (1998), pp. 99–113. ISSN: 1365-2818. DOI: [10.1046/j.1365-2818.1998.00412.x](https://doi.org/10.1046/j.1365-2818.1998.00412.x). URL: <http://dx.doi.org/10.1046/j.1365-2818.1998.00412.x>.

- [28] Michael Model. "Intensity Calibration and Flat-Field Correction for Fluorescence Microscopes". In: *Current Protocols in Cytometry*. John Wiley & Sons, Inc., 2001. ISBN: 9780471142959. DOI: [10.1002/0471142956.cy1014s68](https://doi.org/10.1002/0471142956.cy1014s68). URL: <http://dx.doi.org/10.1002/0471142956.cy1014s68>.
- [29] Michael A. Model and Janis K. Burkhardt. "A standard for calibration and shading correction of a fluorescence microscope". In: *Cytometry* 44.4 (2001), pp. 309–316. ISSN: 1097-0320. DOI: [10.1002/1097-0320\(20010801\)44:4<309::AID-CYTO1122>3.0.CO;2-3](https://doi.org/10.1002/1097-0320(20010801)44:4<309::AID-CYTO1122>3.0.CO;2-3). URL: [http://dx.doi.org/10.1002/1097-0320\(20010801\)44:4<309::AID-CYTO1122>3.0.CO;2-3](http://dx.doi.org/10.1002/1097-0320(20010801)44:4<309::AID-CYTO1122>3.0.CO;2-3).
- [30] Anne Carpenter. *CIL 21739*. Picture. (accessed September 9, 2016). URL: <http://www.cellimagelibrary.org/images/21739>.
- [31] Stephen A. Boppart et al. "Optical probes and techniques for molecular contrast enhancement in coherence imaging". In: *Journal of Biomedical Optics* 10.4 (2005), pp. 041208–041208–14. DOI: [10.1117/1.2008974](https://doi.org/10.1117/1.2008974). URL: <http://dx.doi.org/10.1117/1.2008974>.
- [32] Molecular Expressions. *Photobleaching*. Picture. (accessed September 9, 2016). URL: <http://micro.magnet.fsu.edu/primer/java/fluorescence/photobleaching/>.
- [33] Margret Keuper. "Segmentation of Cells and Sub-cellular Structures from Microscopic Recordings [online]". Doctoral theses, Dissertations. Albert-Ludwigs-Universität, 2012 [cit. 2016-09-12]. URL: http://lmb.informatik.uni-freiburg.de/Publications/2012/Keu12/Dissertation_Keuper.pdf.
- [34] Arjan Tibbe. *CIL 40968*. Picture. (accessed September 9, 2016). URL: <http://www.cellimagelibrary.org/images/40968>.
- [35] Eran A. Mukamel, Hazen Babcock, and Xiaowei Zhuang. "Statistical Deconvolution for Superresolution Fluorescence Microscopy". In: *Biophysical Journal* 102.10 (2012), pp. 2391–2400. DOI: [10.1038/srep09894](https://doi.org/10.1038/srep09894). URL: <http://dx.doi.org/10.1016/j.bpj.2012.03.070>.
- [36] Peter J Verveer et al. "High-resolution three-dimensional imaging of large specimens with light sheet-based microscopy". In: *Nature Methods* 4 (2007), pp. 311–313. DOI: [10.1038/nmeth1017](https://doi.org/10.1038/nmeth1017). URL: <http://www.nature.com/nmeth/journal/v4/n4/abs/nmeth1017.html>.
- [37] Ammassi Periasamy, Paul Skoglund and Colten Noakes, and Raymond Keller. "An Evaluation of Two-Photon Excitation Versus Confocal and Digital Deconvolution Fluorescence Microscopy Imaging in Xenopus Morphogenesis". In: *Microscopy Research and Technique* 4 (2007), pp. 311–313. DOI: [10.1038/nmeth1017](https://doi.org/10.1038/nmeth1017). URL: <http://www.nature.com/nmeth/journal/v4/n4/abs/nmeth1017.html>.
- [38] Jason R. Swedlow. "Quantitative Fluorescence Microscopy and Image Deconvolution". In: *Digital Microscopy, 3rd Edition*. Vol. 81. Methods in Cell Biology. Academic Press, 2007, pp. 447–465. DOI: [http://dx.doi.org/10.1016/S0091-679X\(06\)81021-6](https://doi.org/10.1016/S0091-679X(06)81021-6). URL: <http://www.sciencedirect.com/science/article/pii/S0091679X06810216>.

- [39] Johan J. de Rooi, Cyril Ruckebusch, and Paul H. C. Eilers. "Sparse Deconvolution in One and Two Dimensions: Applications in Endocrinology and Single-Molecule Fluorescence Imaging". In: *Analytical Chemistry* 86.13 (2014). PMID: 24893114, pp. 6291–6298. DOI: [10.1021/ac500260h](https://doi.org/10.1021/ac500260h). eprint: <http://dx.doi.org/10.1021/ac500260h>. URL: <http://dx.doi.org/10.1021/ac500260h>.
- [40] Alexander Wong, Xiao Yu Wang, and Maud Gorbet. "Bayesian-based deconvolution fluorescence microscopy using dynamically updated nonstationary expectation estimates". In: *Scientific Reports* 5.10849 (2015), pp. 1–9. DOI: [10.1038/srep10849](https://doi.org/10.1038/srep10849). URL: <http://dx.doi.org/10.1038/srep10849>.
- [41] Boyoung Kim and Takeshi Naemura. "Blind Depth-variant Deconvolution of 3D Data in Wide-field Fluorescence Microscopy". In: *Scientific Reports* 5.9894 (2015), pp. 1–9. DOI: [10.1038/srep09894](https://doi.org/10.1038/srep09894). URL: <http://dx.doi.org/10.1038/srep09894>.
- [42] Jing Qin et al. "Detail-preserving Fluorescence Microscopy Image Deconvolution". In: *Conference on Lasers and Electro-Optics*. Optical Society of America, 2016, STh4G.7. DOI: [10.1364/CLEO_SI.2016.STh4G.7](https://doi.org/10.1364/CLEO_SI.2016.STh4G.7). URL: http://www.osapublishing.org/abstract.cfm?URI=CLEO_SI-2016-STh4G.7.
- [43] Ryan Naidoo and Jules-Raymond Tapamo. "A Preprocessing Scheme for Fluorescence Microscopy Image Segmentation". In: *International Journal of Imaging and Robotics* 16.4 (2016), pp. 1–23. ISSN: ISSN 2231–525X.
- [44] Gijsbert Michiel Peter Van Kempen. "Image Restoration in Fluorescence Microscopy [online]". Doctoral theses, Dissertations. Technische Universiteit Delft, 1999 [cit. 2016-09-08]. URL: http://www.tnw.tudelft.nl/fileadmin/Faculteit/TNW/Over_de_faculteit/Afdelingen/Imaging_Science_and_Technology/Research/Research_Groups/Quantitative_Imaging/Publications>List_Publications/doc/thesis_kempen.pdf.
- [45] Erik Meijering. "Cell Segmentation: 50 Years Down the Road [Life Sciences]". In: *IEEE Signal Processing Magazine* 29.5 (2012), pp. 140–145. ISSN: 1053-5888. DOI: [10.1109/MSP.2012.2204190](https://doi.org/10.1109/MSP.2012.2204190).
- [46] Bruce Alberts et al. *Molecular Biology of the Cell*. 5th Edition. New York, NY, USA: Garland Science, 2007. ISBN: 9780815341055.
- [47] Cédrik Vonesch et al. "The Colored Revolution of Bioimaging [An introduction to fluorescence microscopy]". In: *IEEE Signal Processing Magazine* 29.5 (2006), pp. 20–31.
- [48] Ewert Bengtsson, Carolina Wählby, and Joakim Lindblad. "Robust cell image segmentation methods". In: *Pattern Recognition and Image Analysis: Advances in Mathematical Theory and Applications* 14.52 (2004), pp. 157–167. ISSN: 1054-6618.
- [49] W.E. Tolles. "Section of Biology: The Cytoanalyzer—An Example of Physics in Medical Research*". In: *Transactions of the New York Academy of Sciences* 17.3 Series II (1955), pp. 250–256. ISSN: 2164-0947. DOI: [10.1111/j.2164-0947.1955.tb01204.x](https://doi.org/10.1111/j.2164-0947.1955.tb01204.x). URL: <http://dx.doi.org/10.1111/j.2164-0947.1955.tb01204.x>.
- [50] Judith M. S. Prewitt and Mortimer L. Mendelsohn. "The Analysis of Cell Images*". In: *Annals of the New York Academy of Sciences* 128.3 (1966), pp. 1035–1053. ISSN: 1749-6632. DOI: [10.1111/j.1749-6632.1965.tb11715.x](https://doi.org/10.1111/j.1749-6632.1965.tb11715.x). URL: <http://dx.doi.org/10.1111/j.1749-6632.1965.tb11715.x>.
- [51] Metin N. Gurcan et al. "Histopathological image analysis: A review". In: *IEEE Reviews in Biomedical Engineering* (2009), pp. 147–171.

- [52] Alden A. Dima et al. "Comparison of segmentation algorithms for fluorescence microscopy images of cells". In: *Cytometry Part A* 79A.7 (2011), pp. 545–559. ISSN: 1552-4930. DOI: [10.1002/cyto.a.21079](https://doi.org/10.1002/cyto.a.21079). URL: <http://dx.doi.org/10.1002/cyto.a.21079>.
- [53] Z. Pincus and J.A. Theriot. "Comparison of quantitative methods for cell-shape analysis". In: *Journal of Microscopy* 227.2 (2007), pp. 140–156. ISSN: 1365-2818. DOI: [10.1111/j.1365-2818.2007.01799.x](https://doi.org/10.1111/j.1365-2818.2007.01799.x). URL: <http://dx.doi.org/10.1111/j.1365-2818.2007.01799.x>.
- [54] Luís Pedro Coelho, Aabid Shariff, and Robert F. Murphy. "Nuclear Segmentation in Microscope Cell Images: A Hand-Segmented Dataset and Comparison of Algorithms". In: *Proc IEEE Int Symp Biomed Imaging* 5.193098E6.2 (2009), pp. 518–521. ISSN: 1365-2818. DOI: [10.1111/j.1365-2818.2007.01799.x](https://doi.org/10.1111/j.1365-2818.2007.01799.x). URL: <http://www.ncbi.nlm.nih.gov/pmc/articles/PMC2901896/>.
- [55] Qiang Wu, Fatima A. Merchant, and Kenneth R. Castleman. *Encyclopedia of Optical Engineering - Fluorescence Microscopy*. 1st Edition. Elsevier Inc., 2008. ISBN: 978-0-12-372578-3.
- [56] E. Meijering et al. "Design and validation of a tool for neurite tracing and analysis in fluorescence microscopy images". In: *Cytometry Part A* 58A.2 (2004), pp. 167–176. ISSN: 1552-4930. DOI: [10.1002/cyto.a.20022](https://doi.org/10.1002/cyto.a.20022). URL: <http://dx.doi.org/10.1002/cyto.a.20022>.
- [57] Quanli Wang et al. "Image segmentation and dynamic lineage analysis in single-cell fluorescence microscopy". In: *Cytometry Part A* 77A.1 (2010), pp. 101–110. ISSN: 1552-4930. DOI: [10.1002/cyto.a.20812](https://doi.org/10.1002/cyto.a.20812). URL: <http://dx.doi.org/10.1002/cyto.a.20812>.
- [58] Rafael C. Gonzalez and Richard E. Woods. *Digital Image Processing*. 3rd Edition. New Jersey, USA: Prentice Hall, Inc., 2002.
- [59] L.B. Dorini, R. Minetto, and N. J. Leite. "White blood cell segmentation using morphological operators and scale-space analysis". In: *Computer Graphics and Image Processing, 2007. SIBGRAPI 2007. XX Brazilian Symposium on*. 2007, pp. 294–304. DOI: [10.1109/SIBGRAPI.2007.33](https://doi.org/10.1109/SIBGRAPI.2007.33).
- [60] D. Anoraganingrum. "Cell segmentation with median filter and mathematical morphology operation". In: *Image Analysis and Processing, 1999. Proceedings. International Conference on*. 1999, pp. 1043–1046. DOI: [10.1109/ICIAP.1999.797734](https://doi.org/10.1109/ICIAP.1999.797734).
- [61] B.R. Kumar, D.K. Joseph, and T.V. Sreenivas. "Teager energy based blood cell segmentation". In: *Digital Signal Processing, 2002. DSP 2002. 2002 14th International Conference on*. Vol. 2. 2002, pp. 619–622. DOI: [10.1109/ICDSP.2002.1028167](https://doi.org/10.1109/ICDSP.2002.1028167).
- [62] Kan Jiang, Qing-Min Liao, and Sheng-Yang Dai. "A novel white blood cell segmentation scheme using scale-space filtering and watershed clustering". In: *Machine Learning and Cybernetics, 2003 International Conference on*. Vol. 5. 2003, pp. 2820–2825. DOI: [10.1109/ICMLC.2003.1260033](https://doi.org/10.1109/ICMLC.2003.1260033).
- [63] Gang Lin et al. "A hybrid 3D watershed algorithm incorporating gradient cues and object models for automatic segmentation of nuclei in confocal image stacks". In: *Cytometry Part A* 56A.1 (2003), pp. 23–36. ISSN: 1552-4930. DOI: [10.1002/cyto.a.10079](https://doi.org/10.1002/cyto.a.10079). URL: <http://dx.doi.org/10.1002/cyto.a.10079>.

- [64] Michael Kass, Andrew Witkin, and Demetri Terzopoulos. "Snakes: Active contour models". In: *International Journal of Computer Vision* 1.4 (1988), pp. 321–331.
- [65] Vicent Caselles, Ron Kimmel, and Guillermo Sapiro. "Geodesic Active Contours". In: *International Journal of Computer Vision* 22.1 (1997), pp. 61–79. ISSN: 0920-5691. DOI: [10.1023/A:1007979827043](https://doi.org/10.1023/A:1007979827043). URL: <http://dx.doi.org/10.1023/A:1007979827043>.
- [66] Hongsheng Li et al. "Automated actin filament segmentation, tracking and tip elongation measurements based on open active contour models". In: *2009 IEEE International Symposium on Biomedical Imaging: From Nano to Macro*. 2009, pp. 1302–1305. DOI: [10.1109/ISBI.2009.5193303](https://doi.org/10.1109/ISBI.2009.5193303).
- [67] J. Cheng and J. C. Rajapakse^{ast}. "Segmentation of Clustered Nuclei With Shape Markers and Marking Function". In: *IEEE Transactions on Biomedical Engineering* 56.3 (2009), pp. 741–748. ISSN: 0018-9294. DOI: [10.1109/TBME.2008.2008635](https://doi.org/10.1109/TBME.2008.2008635).
- [68] Stanley Osher and Ronald P. Fedkiw. *Level set methods and dynamic implicit surfaces*. Applied mathematical science. New York, N.Y.: Springer, 2003. ISBN: 0-387-95482-1. URL: <http://opac.inria.fr/record=b1099358>.
- [69] O. Dzyubachyk, W. Niessen, and E. Meijering. "Advanced level-set based multiple-cell segmentation and tracking in time-lapse fluorescence microscopy images". In: *2008 5th IEEE International Symposium on Biomedical Imaging: From Nano to Macro*. 2008, pp. 185–188. DOI: [10.1109/ISBI.2008.4540963](https://doi.org/10.1109/ISBI.2008.4540963).
- [70] C. Ortiz de Solórzano et al. "Segmentation of nuclei and cells using membrane related protein markers". In: *Journal of Microscopy* 201 (2001), pp. 404–415.
- [71] Alexandre Dufour et al. "Segmenting and tracking fluorescent cells in dynamic 3-D microscopy with coupled active surfaces." In: *IEEE Transactions on Image Processing* 14.9 (2005), pp. 1396–410. URL: <https://hal.archives-ouvertes.fr/hal-00014483>.
- [72] Oleh Dzyubachyk et al. "Advanced Level-Set-Based Cell Tracking in Time-Lapse Fluorescence Microscopy." In: *IEEE Trans. Med. Imaging* 29.3 (2010), pp. 852–867. URL: <http://dblp.uni-trier.de/db/journals/tmi/tmi29.html#DzyubachykCENM10>.
- [73] Fatima Boukari and Sokratis Makrogiannis. "Spatio-temporal Level-Set Based Cell Segmentation in Time-Lapse Image Sequences". In: *Advances in Visual Computing: 10th International Symposium, ISVC 2014, Las Vegas, NV, USA, December 8–10, 2014, Proceedings, Part II*. Ed. by George Bebis et al. Cham: Springer International Publishing, 2014, pp. 41–50. ISBN: 978-3-319-14364-4. DOI: [10.1007/978-3-319-14364-4_5](https://doi.org/10.1007/978-3-319-14364-4_5). URL: http://dx.doi.org/10.1007/978-3-319-14364-4_5.
- [74] Martin Maška et al. "A Comparison of Fast Level Set-Like Algorithms for Image Segmentation in Fluorescence Microscopy". In: *Advances in Visual Computing: Third International Symposium, ISVC 2007, Lake Tahoe, NV, USA, November 26–28, 2007, Proceedings, Part II*. Ed. by George Bebis et al. Berlin, Heidelberg: Springer Berlin Heidelberg, 2007, pp. 571–581. ISBN: 978-3-540-76856-2. DOI: [10.1007/978-3-540-76856-2_56](https://doi.org/10.1007/978-3-540-76856-2_56). URL: http://dx.doi.org/10.1007/978-3-540-76856-2_56.

- [75] Ondřej Daněk et al. "Segmentation of Touching Cell Nuclei Using a Two-Stage Graph Cut Model". In: *Image Analysis: 16th Scandinavian Conference, SCIA 2009, Oslo, Norway, June 15-18, 2009. Proceedings*. Ed. by Arnt-Børre Salberg, Jon Yngve Hardeberg, and Robert Jenssen. Berlin, Heidelberg: Springer Berlin Heidelberg, 2009, pp. 410–419. ISBN: 978-3-642-02230-2. DOI: [10.1007/978-3-642-02230-2_42](https://doi.org/10.1007/978-3-642-02230-2_42). URL: http://dx.doi.org/10.1007/978-3-642-02230-2_42.
- [76] C. Chen et al. "Constraint factor graph cut-based active contour method for automated cellular image segmentation in RNAi screening". In: *Journal of Microscopy* 230.2 (2008), pp. 177–191. ISSN: 1365-2818. DOI: [10.1111/j.1365-2818.2008.01974.x](https://doi.org/10.1111/j.1365-2818.2008.01974.x). URL: <http://dx.doi.org/10.1111/j.1365-2818.2008.01974.x>.
- [77] Y. Al-Kofahi et al. "Improved Automatic Detection and Segmentation of Cell Nuclei in Histopathology Images". In: *IEEE Transactions on Biomedical Engineering* 57.4 (2010), pp. 841–852. ISSN: 0018-9294. DOI: [10.1109/TBME.2009.2035102](https://doi.org/10.1109/TBME.2009.2035102).
- [78] H. Kong, M. Gurcan, and K. Belkacem-Boussaid. "Partitioning Histopathological Images: An Integrated Framework for Supervised Color-Texture Segmentation and Cell Splitting". In: *IEEE Transactions on Medical Imaging* 30.9 (2011), pp. 1661–1677. ISSN: 0278-0062. DOI: [10.1109/TMI.2011.2141674](https://doi.org/10.1109/TMI.2011.2141674).
- [79] Huei-Fang Yang and Yoonsuck Choe. "Cell tracking and segmentation in electron microscopy images using graph cuts". In: *2009 IEEE International Symposium on Biomedical Imaging: From Nano to Macro*. 2009, pp. 306–309. DOI: [10.1109/ISBI.2009.5193045](https://doi.org/10.1109/ISBI.2009.5193045).
- [80] L. Zhang et al. "Automated segmentation of abnormal cervical cells using global and local graph cuts". In: *2014 IEEE 11th International Symposium on Biomedical Imaging (ISBI)*. 2014, pp. 485–488. DOI: [10.1109/ISBI.2014.6867914](https://doi.org/10.1109/ISBI.2014.6867914).
- [81] Lu Liu et al. "Interactive Separation of Segmented Bones in CT Volumes Using Graph Cut". In: *Medical Image Computing and Computer-Assisted Intervention – MICCAI 2008: 11th International Conference, New York, NY, USA, September 6-10, 2008, Proceedings, Part I*. Ed. by Dimitris Metaxas et al. Berlin, Heidelberg: Springer Berlin Heidelberg, 2008, pp. 296–304. ISBN: 978-3-540-85988-8. DOI: [10.1007/978-3-540-85988-8_36](https://doi.org/10.1007/978-3-540-85988-8_36). URL: http://dx.doi.org/10.1007/978-3-540-85988-8_36.
- [82] Nhat Vu and B.S. Manjunath. "Graph cut segmentation of neuronal structures from transmission electron micrographs". In: *IEEE International Conference on Image Processing* (2008).
- [83] H. P. Ng et al. "Medical Image Segmentation Using K-Means Clustering and Improved Watershed Algorithm". In: *2006 IEEE Southwest Symposium on Image Analysis and Interpretation*. 2006, pp. 61–65. DOI: [10.1109/SSIAI.2006.1633722](https://doi.org/10.1109/SSIAI.2006.1633722).
- [84] Kalpana Shrivastava, Neelesh Gupta, and Neetu Sharma. "Medical Image Segmentation using Modified K Means Clustering". In: *International Journal of Computer Applications* 103.16 (2014), pp. 12–16. ISSN: 0975-8887. DOI: [10.1109/TMI.2011.2141674](https://doi.org/10.1109/TMI.2011.2141674).
- [85] Nameirakpam Dhanachandra, Khumanthem Manglem, and Yambem Jina Chanu. "Image Segmentation Using K -means Clustering Algorithm and Subtractive Clustering Algorithm". In: *Procedia Computer Science* 54 (2015), pp. 764–771. ISSN: 1877-0509. DOI: [10.1016/j.procs.2015.06.090](https://doi.org/10.1016/j.procs.2015.06.090). URL: <http://www.sciencedirect.com/science/article/pii/S1877050915014143>.

- [86] Xiaowei Chen, Xiaobo Zhou, and S.T.C. Wong. "Automated segmentation, classification, and tracking of cancer cell nuclei in time-lapse microscopy". In: *IEEE Transactions on Biomedical Engineering* 53.4 (2006), pp. 762–766. ISSN: 0018-9294. DOI: [10.1109/TBME.2006.870201](https://doi.org/10.1109/TBME.2006.870201).
- [87] Jihong Liu, Weina Ma, and Soo-Young Lee. "A Segmentation Method Based on Dynamic Programming for Breast Mass in MRI Images". In: *Medical Biometrics: First International Conference, ICMB 2008, Hong Kong, China, January 4-5, 2008. Proceedings*. Ed. by David Zhang. Berlin, Heidelberg: Springer Berlin Heidelberg, 2007, pp. 307–313. ISBN: 978-3-540-77413-6. DOI: [10.1007/978-3-540-77413-6_39](https://doi.org/10.1007/978-3-540-77413-6_39). URL: http://dx.doi.org/10.1007/978-3-540-77413-6_39.
- [88] Y. Zhang, B. J. Matuszewski, and L. K. Shark. "A Novel Medical Image Segmentation Method using Dynamic Programming". In: *Medical Information Visualisation - BioMedical Visualisation, 2007. MediVis 2007. International Conference on*. 2007, pp. 69–74.
- [89] R. Cardenes et al. "K-Voronoi diagrams computing in arbitrary domains". In: *Image Processing, 2003. ICIP 2003. Proceedings. 2003 International Conference on*. Vol. 2. 2003, pp. 941–944. DOI: [10.1109/ICIP.2003.1246838](https://doi.org/10.1109/ICIP.2003.1246838).
- [90] Chunyan Jiang, Xinhua Zhang, and Christoph Meinel. "Hybrid Framework for Medical Image Segmentation". In: *Computer Analysis of Images and Patterns: 11th International Conference, CAIP 2005, Versailles, France, September 5-8, 2005. Proceedings*. Ed. by André Gagolowicz and Wilfried Philips. Berlin, Heidelberg: "Springer Berlin Heidelberg, 2005, pp. 264–271. ISBN: 978-3-540-32011-1. DOI: [10.1007/11556121_33](https://doi.org/10.1007/11556121_33). URL: http://dx.doi.org/10.1007/11556121_33.
- [91] G. Li et al. "Segmentation of Touching Cells Using Gradient Flow Tracking". In: *2007 4th IEEE International Symposium on Biomedical Imaging: From Nano to Macro*. 2007, pp. 77–80. DOI: [10.1109/ISBI.2007.356792](https://doi.org/10.1109/ISBI.2007.356792).
- [92] Fatima A. Merchant, Shishir K. Shah, and Kenneth R. Castleman. "Object Measurement". In: *Microscope Image Processing*. USA: Elsevier Inc, 2008, pp. 195–219. ISBN: 978-0-12-372578-3.
- [93] Charlotte Giesen et al. "Highly multiplexed imaging of tumor tissues with subcellular resolution by mass cytometry". In: *Nature Methods* 11.4 (2014), pp. 417–422. DOI: [10.1038/nmeth.2869](https://doi.org/10.1038/nmeth.2869). URL: <http://dx.doi.org/10.1038/nmeth.2869>.
- [94] Xaosong Yuan et al. "MDL Constrained 3-D Grayscale Skeletonization Algorithm for Automated Extraction of Dendrites and Spines from Fluorescence Confocal Images". In: *Neuroinformatics* 7.4 (2009), pp. 213–232. ISSN: 1559-0089. DOI: [10.1007/s12021-009-9057-y](https://doi.org/10.1007/s12021-009-9057-y). URL: <http://dx.doi.org/10.1007/s12021-009-9057-y>.
- [95] Michal Kozubek and Pavel Matula. "An efficient algorithm for measurement and correction of chromatic aberrations in fluorescence microscopy". In: *Journal of Microscopy* 200.3 (2000), pp. 206–217. ISSN: 1365-2818. DOI: [10.1046/j.1365-2818.2000.00754.x](https://doi.org/10.1046/j.1365-2818.2000.00754.x). URL: <http://dx.doi.org/10.1046/j.1365-2818.2000.00754.x>.
- [96] Dominique Attali and Annick Montanvert. "Computing and Simplifying 2D and 3D Continuous Skeletons". In: *Elsevier Computer Vision and Image Understanding* 67.3 (1997), pp. 261–273. ISSN: 1365-2818. DOI: [10.1006/cviu.1997.0536](https://doi.org/10.1006/cviu.1997.0536). URL: <http://dx.doi.org/10.1006/cviu.1997.0536>.

- [97] Andrew P. French et al. "Colocalization of fluorescent markers in confocal microscope images of plant cells". In: *Nat. Protocols* 3 (4 2008), pp. 619–628. ISSN: 1754-2189. DOI: [10.1038/nprot.2008.31](https://doi.org/10.1038/nprot.2008.31). URL: <http://dx.doi.org/10.1038/nprot.2008.31>.
- [98] Vadim Zinchuk, Olga Zinchuk, and Teruhiko Okada. "Quantitative Colocalization Analysis of Multicolor Confocal Immunofluorescence Microscopy Images: Pushing Pixels to Explore Biological Phenomena". In: *ACTA HISTOCHEMICA ET CYTOCHEMICA* 40.4 (2007), pp. 101–111. DOI: [10.1267/ahc.07002](https://doi.org/10.1267/ahc.07002).
- [99] D. Pinkel, T. Straume, and J.W. Gray. "Cytogenetic analysis using quantitative, high-sensitivity, fluorescence hybridization". In: *Proceedings of the National Academy of Sciences* 83.9 (1986), pp. 2934–2938. eprint: <http://www.pnas.org/content/83/9/2934.full.pdf>. URL: <http://www.pnas.org/content/83/9/2934.abstract>.
- [100] M. Loferer-Krößbacher, J. Klima, and R. Psenner. "Determination of Bacterial Cell Dry Mass by Transmission Electron Microscopy and Densitometric Image Analysis". In: *Appl. Environ. Microbiol.* 64 (2 1998), pp. 688–694. DOI: [10.1038/nmeth929](https://doi.org/10.1038/nmeth929). URL: <http://dx.doi.org/10.1038/nmeth929>.
- [101] N. Watanabe et al. "Motility of bile canaliculi in the living animal: implications for bile flow." In: *The Journal of Cell Biology* 113.5 (1991), pp. 1069–1080. DOI: [10.1083/jcb.113.5.1069](https://doi.org/10.1083/jcb.113.5.1069). eprint: <http://jcb.rupress.org/content/113/5/1069.full.pdf+html>. URL: <http://jcb.rupress.org/content/113/5/1069.abstract>.
- [102] Michael J. Rust, Mark Bates, and Xiaowei Zhuang. "Sub-diffraction-limit imaging by stochastic optical reconstruction microscopy (STORM)". In: *Nat Meth* 3 (10 2006), pp. 793–796. DOI: [10.1038/nmeth929](https://doi.org/10.1038/nmeth929). URL: <http://dx.doi.org/10.1038/nmeth929>.
- [103] Michael V. Boland and Robert F. Murphy. "A neural network classifier capable of recognizing the patterns of all major subcellular structures in fluorescence microscope images of HeLa cells". In: *Bioinformatics* 17.12 (2001), pp. 1213–1223. DOI: [10.1093/bioinformatics/17.12.1213](https://doi.org/10.1093/bioinformatics/17.12.1213). eprint: <http://bioinformatics.oxfordjournals.org/content/17/12/1213.full.pdf+html>. URL: <http://bioinformatics.oxfordjournals.org/content/17/12/1213.abstract>.
- [104] R.O. Duda, P.E. Hart, and D.G. Stork. *Pattern Classification*. John Wiley & Sons, 2001.
- [105] V. Atlamazoglou et al. "Texture analysis of fluorescence microscopic images of colonic tissue sections". In: *Medical and Biological Engineering and Computing* 39.2 (2001), pp. 145–151. ISSN: 1741-0444. DOI: [10.1007/BF02344796](https://doi.org/10.1007/BF02344796). URL: <http://dx.doi.org/10.1007/BF02344796>.
- [106] Riccardo Cicchi et al. "Scoring of collagen organization in healthy and diseased human dermis by multiphoton microscopy". In: *Journal of Biophotonics* 3.1-2 (2010), pp. 34–43. ISSN: 1864-0648. DOI: [10.1002/jbio.200910062](https://doi.org/10.1002/jbio.200910062). URL: <http://dx.doi.org/10.1002/jbio.200910062>.
- [107] Erik J. Sánchez, Lukas Novotny, and Xie Sunney. "Near-Field Fluorescence Microscopy Based on Two-Photon Excitation with Metal Tips". In: *Phys. Rev. Lett.* 82 (20 1999), pp. 4014–4017. DOI: [10.1103/PhysRevLett.82.4014](https://doi.org/10.1103/PhysRevLett.82.4014). URL: <http://link.aps.org/doi/10.1103/PhysRevLett.82.4014>.

- [108] C. Xu et al. "Multiphoton fluorescence excitation: new spectral windows for biological nonlinear microscopy". In: *Proceedings of the National Academy of Sciences* 93.20 (1996), pp. 10763–10768. eprint: <http://www.pnas.org/content/93/20/10763.full.pdf>. URL: <http://www.pnas.org/content/93/20/10763.abstract>.
- [109] Rajesh Babu Sekar and Ammasi Periasamy. "Fluorescence resonance energy transfer (FRET) microscopy imaging of live cell protein localizations". In: *Journal of Cellular Biology* 160 (5 2004), pp. 629–633. DOI: [10.1083/jcb.200210140](https://doi.org/10.1083/jcb.200210140).
- [110] Mark J. Miller et al. "Two-Photon Imaging of Lymphocyte Motility and Antigen Response in Intact Lymph Node". In: *Science* 296.5574 (2002), pp. 1869–1873. ISSN: 0036-8075. DOI: [10.1126/science.1070051](https://doi.org/10.1126/science.1070051). eprint: <http://science.sciencemag.org/content/296/5574/1869.full.pdf>. URL: <http://science.sciencemag.org/content/296/5574/1869>.
- [111] Anshu Bagga Mathur, George A. Truskey, and W. Monty Reichert. "Atomic Force and Total Internal Reflection Fluorescence Microscopy for the Study of Force Transmission in Endothelial Cells". In: *Biophysical Journal* 78 (4 2000), pp. 1725–1735. DOI: [10.1016/S0006-3495\(00\)76724-5](https://doi.org/10.1016/S0006-3495(00)76724-5). URL: [http://dx.doi.org/10.1016/S0006-3495\(00\)76724-5](http://dx.doi.org/10.1016/S0006-3495(00)76724-5).
- [112] Tomaso Poggio, Vincent Torre, and Christof Koch. "Computational vision and regularization theory". In: *Nature* 317.6035 (1985), pp. 314–319. DOI: [10.1038/317314a0](https://doi.org/10.1038/317314a0). URL: <http://dx.doi.org/10.1038/317314a0>.
- [113] D. Terzopoulos. "Regularization of Inverse Visual Problems Involving Discontinuities". In: *IEEE Transactions on Pattern Analysis and Machine Intelligence* PAMI-8.4 (1986), pp. 413–424. ISSN: 0162-8828. DOI: [10.1109/TPAMI.1986.4767807](https://doi.org/10.1109/TPAMI.1986.4767807).
- [114] S.I. Kabanikhin. "Definitions and examples of inverse and ill-posed problems". In: *J. Inv. Ill-Posed Problems* 16 (2008), pp. 317–357. ISSN: 0162-8828. DOI: [10.1515/JIIP.2008.069](https://doi.org/10.1515/JIIP.2008.069).
- [115] Albert Tarantola. *Inverse Problem Theory and Methods and Models for Parameter Estimation*. Philadelphia, PA, USA: Society for Industrial and Applied Mathematics, 2005, pp. 1–37. ISBN: 0-89871-572-5.
- [116] Mario Bertero and Patrizia Boccacci. *Introduction to Inverse Problems in Imaging*. Bath, UK: IOP Publishing Ltd, 1998, pp. 1–37. ISBN: 0 7503 0439 1.
- [117] M. Bertero and M. Piana. "Inverse problems in biomedical imaging: modeling and methods of solution". In: *Complex Systems in Biomedicine*. Ed. by Alfio Quarteroni, Luca Formaggia, and Alessandro Veneziani. Milano: Springer Milan, 2006, pp. 1–33. ISBN: 978-88-470-0396-5. DOI: [10.1007/88-470-0396-2_1](https://doi.org/10.1007/88-470-0396-2_1). URL: http://dx.doi.org/10.1007/88-470-0396-2_1.
- [118] Andrew Thomas Delong. "Advances in Graph-Cut Optimization: Multi-Surface Models, Label Costs, and Hierarchical Costs [online]". Doctoral theses, Dissertations. The University of Western Ontario, London Ontario, Canada, 2011 [cit. 2016-09-19]. URL: <http://www.psi.toronto.edu/~andrew/papers/thesis.pdf>.
- [119] David Waltz. "Understanding Line Drawings of Scenes with Shadows". In: *The Psychology of Computer Vision*. McGraw-Hill, 1975, pp. 19–91.
- [120] Azriel Rosenfeld, Robert A. Hummel, and Steven W. Zucker. "Definitions and examples of inverse and ill-posed problems". In: *IEEE Transactions on Systems, MAN, and Cybernetics* 6.6 (1976), pp. 420–433.

- [121] Katsuhiko Sakaue, Akira Amano, and Naokazu Yokoya. "Optimization Approaches in Computer Vision and Image Processing". In: *IEECE Trans. Inf. & Syst.* E82.3 (1999), pp. 534–547.
- [122] Yuri Boykov, Olga Veksler, and Ramin Zabih. "Fast Approximate Energy Minimization via Graph Cuts". In: *IEEE Trans. Pattern Anal. Mach. Intell.* 23.11 (2001), pp. 1222–1239. ISSN: 0162-8828. DOI: [10.1109/34.969114](https://doi.org/10.1109/34.969114). URL: <http://dx.doi.org/10.1109/34.969114>.
- [123] Vladimir Kolmogorov. "Convergent Tree-Reweighted Message Passing for Energy Minimization". In: *Proc. Int'l Workshop Artificial Intelligence and Statistics*. 2005.
- [124] David Mumford. "Optimal approximation by piecewise smooth functions and associated variational problems". In: *Commun. Pure Applied Mathematics* (1989), pp. 577–685.
- [125] Jianbo Shi and Jitendra Malik. "Normalized Cuts and Image Segmentation". In: *IEEE Transactions on Pattern Analysis and Machine Intelligence* 22 (1997), pp. 888–905.
- [126] T. Athanasiadis et al. "Semantic Image Segmentation and Object Labeling". In: *IEEE Transactions on Circuits and Systems for Video Technology* 17.3 (2007), pp. 298–312. ISSN: 1051-8215. DOI: [10.1109/TCSVT.2007.890636](https://doi.org/10.1109/TCSVT.2007.890636).
- [127] Robert J. Adler and Jonathan E. Taylor. *Random fields and geometry*. Springer monographs in mathematics. New York: Springer, 2007. ISBN: 978-0-387-48112-8. URL: <http://opac.inria.fr/record=b1123290>.
- [128] Anatoly V. Skorokhod Iosif I. Gikhman. *Introduction to the Theory of Random Processes*. Dover Books on Mathematics. Dover Publications, 1996. ISBN: 0486693872.
- [129] Matthew Brett, Will Penny, and Stefan Kiebel. *An Introduction to Random Field Theory*. MRC Cognition and Brain Sciences Unit, Cambridge UK, 2003.
- [130] Richard L. Smith. "Introduction to Besag (1974) Spatial Interaction and the Statistical Analysis of Lattice Systems". In: *Breakthroughs in Statistics*. Ed. by Samuel Kotz and Norman L. Johnson. New York, NY: Springer New York, 1997, pp. 285–323. ISBN: 978-1-4612-0667-5. DOI: [10.1007/978-1-4612-0667-5_13](https://doi.org/10.1007/978-1-4612-0667-5_13). URL: http://dx.doi.org/10.1007/978-1-4612-0667-5_13.
- [131] Stuart Geman and Donald Geman. "Stochastic Relaxation, Gibbs Distributions, and the Bayesian Restoration of Images". In: *IEEE Trans. Pattern Anal. Mach. Intell.* 6.6 (1984), pp. 721–741. ISSN: 0162-8828. DOI: [10.1109/TPAMI.1984.4767596](https://doi.org/10.1109/TPAMI.1984.4767596). URL: <http://dx.doi.org/10.1109/TPAMI.1984.4767596>.
- [132] Julian Besag. "On the statistical analysis of dirty pictures". In: *Journal of the Royal Statistical Society B* 48.3 (1986), pp. 48–259.
- [133] John Lafferty. "Conditional random fields: Probabilistic models for segmenting and labeling sequence data". In: Morgan Kaufmann, 2001, pp. 282–289.
- [134] J. M. Hammersley and P. E. Clifford. "Markov random fields on finite graphs and lattices". In: Unpublished manuscript (1971).
- [135] Gerhard Winkler. *Image Analysis, Random Fields and Markov Chain Monte Carlo Methods: A Mathematical Introduction (Stochastic Modelling and Applied Probability)*. Secaucus, NJ, USA: Springer-Verlag New York, Inc., 2006. ISBN: 3540442138.
- [136] Cyril Cassisa. "Local Vs Global Energy Minimization Methods: Application to Stereo Matching". In: *IEEE* (2010), pp. 678–683. ISSN: 978-1-4244-6789-1.

- [137] Olga Veksler. "Efficient Graph-based Energy Minimisation Methods in Computer Vision [online]". Doctoral theses, Dissertations. Cornell University, 1999 [cit. 2016-09-20]. URL: <http://www.csd.uwo.ca/faculty/olga/Papers/thesis.pdf>.
- [138] V. Černý. "Thermodynamical approach to the traveling salesman problem: An efficient simulation algorithm". In: *Journal of Optimization Theory and Applications* 45.1 (1985), pp. 41–51. ISSN: 1573-2878. DOI: [10.1007/BF00940812](https://doi.org/10.1007/BF00940812). URL: <http://dx.doi.org/10.1007/BF00940812>.
- [139] S. Kirkpatrick, C. D. Gelatt, and M. P. Vecchi. "Optimization by simulated annealing". In: *SCIENCE* 220.4598 (1983), pp. 671–680.
- [140] L. A. MacEachern and T. Manku. "Genetic algorithms for active contour optimization". In: *Circuits and Systems, 1998. ISCAS '98. Proceedings of the 1998 IEEE International Symposium on*. Vol. 4. 1998, pp. 229–232. DOI: [10.1109/ISCAS.1998.698801](https://doi.org/10.1109/ISCAS.1998.698801).
- [141] Lucia Ballerini. "Genetic Snakes for Medical Images Segmentation". In: *Evolutionary Image Analysis, Signal Processing and Telecommunications: First European Workshops, EvoIASP'99 and EuroEcTel'99, Göteborg, Sweden, May 26-27, 1999. Proceedings*. Ed. by Riccardo Poli et al. Berlin, Heidelberg: Springer Berlin Heidelberg, 1999, pp. 59–73. ISBN: 978-3-540-48917-7. DOI: [10.1007/10704703_5](https://doi.org/10.1007/10704703_5). URL: http://dx.doi.org/10.1007/10704703_5.
- [142] Lucia Ballerini. "Genetic Snakes for Color Images Segmentation". In: *Applications of Evolutionary Computing: EvoWorkshops 2001: EvoCOP, EvoFlight, EvoIASP, EvoLearn, and EvoSTIM Como, Italy, April 18–20, 2001 Proceedings*. Ed. by Egbert J. W. Boers. Berlin, Heidelberg: Springer Berlin Heidelberg, 2001, pp. 268–277. ISBN: 978-3-540-45365-9. DOI: [10.1007/3-540-45365-2_28](https://doi.org/10.1007/3-540-45365-2_28). URL: http://dx.doi.org/10.1007/3-540-45365-2_28.
- [143] Reinhard Möller and Rene Zeipelt. "Automatic Segmentation of 3D-MRI Data Using a Genetic Algorithm". In: *Medical Imaging and Augmented Reality: First International Workshop, MIAR 2001, Hong Kong, China, June 10–12, 2001. Proceedings*. 2001, pp. 278–281. DOI: [10.1109/MIAR.2001.930303](https://doi.org/10.1109/MIAR.2001.930303). URL: <http://dx.doi.org/10.1109/MIAR.2001.930303>.
- [144] O. Ibáñez et al. "Genetic approaches for topological active nets optimization". In: *Pattern Recognition* 42.5 (2009), pp. 907–917. ISSN: 0031-3203. DOI: [http://dx.doi.org/10.1016/j.patcog.2008.09.005](https://doi.org/10.1016/j.patcog.2008.09.005). URL: <http://www.sciencedirect.com/science/article/pii/S0031320308003762>.
- [145] Chris McIntosh and Ghassan Hamarneh. "Medical Image Segmentation: Energy Minimization and Deformable Models (Chapter 23)". In: *Medical Imaging: Technology and Applications* (2013). Ed. by T. Farncombe and K. Iniewski, pp. 661–692. URL: <http://www.cs.sfu.ca/~hamarneh/ecopy/crc2013a.pdf>.
- [146] D. Terzopoulos. "On matching deformable models to images". In: *Optical Society of America, Topical Meeting on Machine Vision*. Provided by the SAO/NASA Astrophysics Data System. 1987. URL: <http://adsabs.harvard.edu/abs/1980osa..meet..160T>.
- [147] T. F. Chan and L. A. Vese. "Active Contours Without Edges". In: *Trans. Img. Proc.* 10.2 (2001), pp. 266–277. ISSN: 1057-7149. DOI: [10.1109/83.902291](https://doi.org/10.1109/83.902291). URL: <http://dx.doi.org/10.1109/83.902291>.

- [148] Judea Pearl. *Probabilistic Reasoning in Intelligent Systems: Networks of Plausible Inference*. San Francisco, CA, USA: Morgan Kaufmann Publishers Inc., 1988. ISBN: 0-934613-73-7.
- [149] Brendan Frey and David MacKay. "A Revolution: Belief Propagation in Graphs With Cycles". In: *In Neural Information Processing Systems*. MIT Press, 1998, pp. 479–485.
- [150] William T. Freeman, Egon C. Pasztor, and Owen T. Carmichael. "Learning Low-Level Vision". In: *Int. J. Comput. Vision* 40.1 (2000), pp. 25–47. ISSN: 0920-5691. DOI: [10.1023/A:1026501619075](https://doi.org/10.1023/A:1026501619075). URL: <http://dx.doi.org/10.1023/A:1026501619075>.
- [151] Vladimir Kolmogorov and Ramin Zabih. "What energy functions can be minimized via graph cuts?" In: *IEEE Transactions on Pattern Analysis and Machine Intelligence* 26.2 (2004), pp. 65–81.
- [152] Y. Boykov and M.P. Jolly. "Interactive graph cuts for optimal boundary and region segmentation of objects in N-D images". In: *Proc. IEEE Int'l Conf. on Computer Vision* 1 (2001), pp. 105–112.
- [153] Yuri Boykov and Vladimir Kolmogorov. "An Experimental Comparison of Min-Cut/Max-Flow Algorithms for Energy Minimization in Vision". In: *IEEE Transactions on Pattern Analysis and Machine Intelligence* 26 (2001), pp. 359–374.
- [154] Vladimir Kolmogorov et al. "A Comparative Study of Energy Minimization Methods for Markov Random Fields with Smoothness-Based Priors". In: *IEEE Transactions on Pattern Analysis & Machine Intelligence* 30.undefined (2007), pp. 1068–1080. ISSN: 0162-8828. DOI: doi.ieee.org/10.1109/TPAMI.2007.70844.
- [155] P. Kohli, M. Pawan Kumar, and P. H. S. Torr. "P³ & Beyond: Move Making Algorithms for Solving Higher Order Functions". In: *IEEE Transactions on Pattern Analysis and Machine Intelligence* 31.9 (2009), pp. 1645–1656. ISSN: 0162-8828. DOI: [10.1109/TPAMI.2008.217](https://doi.ieee.org/10.1109/TPAMI.2008.217).
- [156] Nikos Komodakis, Georgios Tziritas, and Nikos Paragios. "Fast, Approximately Optimal Solutions for Single and Dynamic MRFs". In: *CVPR*. IEEE Computer Society, 2007. ISBN: 1-4244-1179-3. URL: <http://dblp.uni-trier.de/db/conf/cvpr/cvpr2007.html#KomodakisTP07>.
- [157] M. Pawan Kumar and Daphne Koller. "MAP Estimation of Semi-metric MRFs via Hierarchical Graph Cuts". In: *Proceedings of the Twenty-Fifth Conference on Uncertainty in Artificial Intelligence*. UAI '09. Arlington, Virginia, United States: AUAI Press, 2009, pp. 313–320. ISBN: 978-0-9749039-5-8. URL: <http://dl.acm.org/citation.cfm?id=1795114.1795151>.
- [158] D. M. Greig, B. T. Porteous, and A. H. Seheult. "Exact Maximum A Posteriori Estimation for Binary Images". In: *Journal of the Royal Statistical Society. Series B (Methodological)* 51.2 (1989), pp. 271–279. ISSN: 00359246. URL: <http://www.jstor.org/stable/2345609>.
- [159] Sébastien Roy and Ingemar Johansson Cox. "A maximum-flow formulation of the n-camera stereo correspondence problem". In: *Computer Vision, 1998. Sixth International Conference on*. 1998, pp. 492–499.
- [160] Yuri Boykov, Olga Veksler, and Ramin Zabih. "Markov Random Fields with Efficient Approximations." In: *CVPR*. IEEE Computer Society, 1998, pp. 648–655. ISBN: 0-8186-8497-6. URL: <http://dblp.uni-trier.de/db/conf/cvpr/cvpr1998.html#BoykovVZ98>.

- [161] L. R. Ford and D. R. Fulkerson. "Maximal Flow through a Network". In: *Canadian Journal of Mathematics* 8 (1956), pp. 399–404. URL: <http://www.rand.org/pubs/papers/P605/>.
- [162] E.A. Dinic. "Algorithm for solution of a problem of maximum flow in a network with power estimation". In: *Soviet Math* 11 (1970), pp. 1277–1280.
- [163] Jack Edmonds and Richard M. Karp. "Theoretical Improvements in Algorithmic Efficiency for Network Flow Problems". In: *J. ACM* 19.2 (1972), pp. 248–264. ISSN: 0004-5411. DOI: [10.1145/321694.321699](https://doi.acm.org/10.1145/321694.321699). URL: <http://doi.acm.org/10.1145/321694.321699>.
- [164] Andrew V. Goldberg and Robert E. Tarjan. "A New Approach to the Maximum-flow Problem". In: *J. ACM* 35.4 (1988), pp. 921–940. ISSN: 0004-5411. DOI: [10.1145/48014.61051](https://doi.acm.org/10.1145/48014.61051). URL: <http://doi.acm.org/10.1145/48014.61051>.
- [165] Narsingh Deo. *Graph Theory with Applications to Engineering and Computer Science (Prentice Hall Series in Automatic Computation)*. Upper Saddle River, NJ, USA: Prentice-Hall, Inc., 1974. ISBN: 0133634736.
- [166] John Adrian Bondy. *Graph Theory With Applications*. Oxford, UK, UK: Elsevier Science Ltd., 1976. ISBN: 0444194517.
- [167] Maarten van Steen. *Graph theory and complex networks : An introduction*. Lexington: Maarten van Steen, 2010. ISBN: 978-90-815406-1-2. URL: <http://opac.inria.fr/record=b1130915>.
- [168] Mark Newman. *Networks: An Introduction*. 1st edition. Oxford University Press, 2010. ISBN: 0199206651.
- [169] Eugene Lawler. "4.5. Combinatorial Implications of Max-Flow Min-Cut Theorem, 4.6. Linear Programming Interpretation of Max-Flow Min-Cut Theorem". In: *Combinatorial Optimization: Networks and Matroids*. Ed. by Eugene Lawler. Dover, 2001, pp. 117–120. ISBN: 0-486-41453-1.
- [170] Solomon Eyal Shimony. "Finding MAPs for belief networks is NP-hard". In: *Artificial Intelligence* 68.2 (1994), pp. 399–410. ISSN: 0004-3702. DOI: [http://dx.doi.org/10.1016/0004-3702\(94\)90072-8](http://dx.doi.org/10.1016/0004-3702(94)90072-8). URL: <http://www.sciencedirect.com/science/article/pii/0004370294900728>.
- [171] Thomas H. Cormen et al. *Introduction to Algorithms, Third Edition*. 3rd. The MIT Press, 2009. ISBN: 0262033844, 9780262033848.
- [172] V. B. Cherkassky and V. A. Goldberg. "On Implementing the Push—Relabel Method for the Maximum Flow Problem". In: *Algorithmica* 19.4 (19), pp. 390–410. ISSN: 1432-0541. DOI: [10.1007/PL00009180](https://doi.org/10.1007/PL00009180). URL: <http://dx.doi.org/10.1007/PL00009180>.
- [173] R. Szeliski et al. "A Comparative Study of Energy Minimization Methods for Markov Random Fields with Smoothness-Based Priors". In: *IEEE Transactions on Pattern Analysis and Machine Intelligence* 30.6 (2008), pp. 1068–1080. ISSN: 0162-8828. DOI: [10.1109/TPAMI.2007.70844](https://doi.org/10.1109/TPAMI.2007.70844).
- [174] Nhat Bao Sinh Vu. "Image Segmentation with Semantic Priors: A Graph Cut Approach [online]". Doctoral theses, Dissertations. University of California, Santa Barbara, 2008 [cit. 2016-10-03]. URL: <https://vision.ece.ucsb.edu/sites/vision.ece.ucsb.edu/files/publications/NhatsThesis.pdf>.

- [175] Noha El Zehiry et al. "Graph Cut Optimization for the Mumford-Shah Model". In: *The Seventh IASTED International Conference on Visualization, Imaging and Image Processing*. VIIP '07. Palma de Mallorca, Spain: ACTA Press, 2007, pp. 182–187. ISBN: 978-0-88986-692-8. URL: <http://dl.acm.org/citation.cfm?id=1659167.1659203>.
- [176] Vladimir Kolmogorov and Yuri Boykov. "What Metrics Can Be Approximated by Geo-Cuts, Or Global Optimization of Length/Area and Flux." In: *ICCV*. IEEE Computer Society, 2005, pp. 564–571. ISBN: 0-7695-2334-X. URL: <http://dblp.uni-trier.de/db/conf/iccv/iccv2005-1.html#KolmogorovB05>.
- [177] Yuri Boykov. "Computing geodesics and minimal surfaces via graph cuts". In: *in International Conference on Computer Vision*. 2003, pp. 26–33.
- [178] Martin Maska et al. "Segmentation and Shape Tracking of Whole Fluorescent Cells Based on the Chan-Vese Model". In: *IEEE Trans. Medical Imaging* 32.6 (2013), pp. 995–1006.
- [179] S. Huang et al. *CIL* 9233. Picture. (accessed July 6, 2015). URL: <http://www.cellimage-library.org/images/9233>.
- [180] R. Mejia. *CIL* 11996. Picture. <http://www.cellimagelibrary.org/images/11996>. (accessed July 6, 2015).
- [181] E. Morselli. *CIL* 13902. Picture. <http://www.cellimagelibrary.org/images/13902>. (accessed July 6, 2015).
- [182] E. Morselli. *CIL* 13903. Picture. <http://www.cellimagelibrary.org/images/13903>. (accessed July 6, 2015).
- [183] E. Morselli. *CIL* 13904. Picture. <http://www.cellimagelibrary.org/images/13904>. (accessed July 6, 2015).
- [184] Prue Talbot. *CIL* 12627. Picture. (accessed October 21, 2016). URL: <http://www.cellimagelibrary.org/images/12627>.
- [185] Eugenia Morselli et al. *CIL* 13899. Picture. (accessed October 21, 2016). URL: <http://www.cellimagelibrary.org/images/13899>.
- [186] Eugenia Morselli et al. *CIL* 13901. Picture. (accessed October 21, 2016). URL: <http://www.cellimagelibrary.org/images/13901>.
- [187] Weimiao Yu et al. *CIL* 40217. Picture. (accessed October 21, 2016). URL: <http://www.cellimagelibrary.org/images/40217>.
- [188] Linda Parysek. *CIL* 195. Picture. (accessed October 21, 2016). URL: <http://www.cellimagelibrary.org/images/195>.
- [189] Allen Liu and Sandra L. Schmid. *CIL* 10102. Picture. (accessed October 21, 2016). URL: <http://www.cellimagelibrary.org/images/10102>.
- [190] Allen Liu and Sandra L. Schmid. *CIL* 10104. Picture. (accessed October 21, 2016). URL: <http://www.cellimagelibrary.org/images/10104>.
- [191] Azusa Hotta et al. *CIL* 12294. Picture. (accessed October 21, 2016). URL: <http://www.cellimagelibrary.org/images/12294>.
- [192] Anne Carpenter. *CIL* 21749. Picture. (accessed October 21, 2016). URL: <http://www.cellimagelibrary.org/images/21749>.
- [193] Anne Carpenter. *CIL* 21759. Picture. (accessed October 21, 2016). URL: <http://www.cellimagelibrary.org/images/21759>.

- [194] M. Deshmukh et al. *CIL* 41066. Picture. (accessed October 21, 2016). URL: <http://www.cellimagelibrary.org/images/41066>.
- [195] Olga Pontes and Craig Pikaard. *CIL* 188. Picture. (accessed October 21, 2016). URL: <http://www.cellimagelibrary.org/images/188>.
- [196] R.I. Kumaran, Z. Lazar, and David L. Spector. *CIL* 10093. Picture. (accessed October 21, 2016). URL: <http://www.cellimagelibrary.org/images/10093>.
- [197] Anne Carpenter. *CIL* 32140. Picture. (accessed October 21, 2016). URL: <http://www.cellimagelibrary.org/images/32140>.
- [198] Nikita Orlov, Wendy Iser, and Cathy Wolkow. *CIL* 1057. Picture. (accessed October 21, 2016). URL: <http://www.cellimagelibrary.org/images/1057>.
- [199] Nikita Orlov, Wendy Iser, and Cathy Wolkow. *CIL* 1265. Picture. (accessed October 21, 2016). URL: <http://www.cellimagelibrary.org/images/1265>.
- [200] Michael Cammer and Phyllis Novikoff. *CIL* 35278. Picture. (accessed October 21, 2016). URL: <http://www.cellimagelibrary.org/images/35278>.
- [201] Kate Nobes and Mark Shipman. *CIL* 38974. Picture. (accessed October 21, 2016). URL: <http://www.cellimagelibrary.org/images/38974>.
- [202] Hesed Padilla-Nash and Thomas Ried. *CIL* 228. Picture. (accessed October 21, 2016). URL: <http://www.cellimagelibrary.org/images/228>.
- [203] Jr. Arturo Orjalo, Sally Coassir, and Hans Johansson. *CIL* 41066. Picture. (accessed October 21, 2016). URL: <http://www.cellimagelibrary.org/images/41066>.
- [204] Yi-Chun Maria Chen. *CIL* 37338. Picture. (accessed October 21, 2016). URL: <http://www.cellimagelibrary.org/images/37338>.
- [205] Yi-Chun Maria Chen. *CIL* 37339. Picture. (accessed October 21, 2016). URL: <http://www.cellimagelibrary.org/images/37339>.
- [206] Karen Meaburn et al. *CIL* 13432. Picture. (accessed October 21, 2016). URL: <http://www.cellimagelibrary.org/images/13432>.
- [207] Karen Meaburn et al. *CIL* 13438. Picture. (accessed October 21, 2016). URL: <http://www.cellimagelibrary.org/images/13438>.